Channel modelling and smart antenna performance analysis for UMTS

Channel modelling and smart antenna performance analysis for UMTS

PROEFSCHRIFT

ter verkrijging van de graad van doctor aan de
Technische Universiteit Eindhoven,
op gezag van de Rector Magnificus, prof.dr.ir. C.J. van Duijn,
voor een commissie aangewezen door het College voor
Promoties in het openbaar te verdedigen op
donderdag 13 oktober 2005 om 16.00 uur

door

Marija Jevrosimović

geboren te Belgrado, Servië en Montenegro

Dit proefschrift is goedgekeurd door de promotoren:

prof.dr.ir. E.R. Fledderus
en
prof.dr.ir. G. Brussaard

Copromotor:

dr.ir. M.H.A.J. Herben

CIP-DATA LIBRARY TECHNISCHE UNIVERSITEIT EINDHOVEN

Jevrosimović, Marija.

Channel modelling and smart antenna performance analysis for UMTS/ by Marija Jevrosimović. – Eindhoven : Technische Universiteit Eindhoven, 2005.
Proefschrift. – ISBN 90-386-2301-1
NUR 959
Trefw.: mobiele telecommunicatie / radiogolfvoortplanting / antennestelsels.
Subject headings: 3G mobile communication / radiowave propagation / antenna arrays.

mojim roditeljima
to my parents

Eerste promotor:	prof.dr.ir. E.R. Fledderus
Tweede promotor:	prof.dr.ir. G. Brussard
Copromotor:	dr.ir. M.H.A.J. Herben

Kerncommissie:

prof.Dr.-Ing. T. Kürner
prof.dr.ir. L.P. Ligthart
dr.ir. P.C.W. Sommen

The work presented in the thesis was performed in the faculty of Electrical Engineering of the Eindhoven University of Technology, and was partly financially supported by the Dutch Ministry of Economic affairs in the BTS project Broadband Radio@Hand within the BraBantBreedBand (B4) programme.

Contents

Summary

The effect of realistic propagation on smart antenna performance for UMTS in an urban micro-cell environment is presented in the thesis. The main issues addressed include looking into channel modelling requirements necessary for the smart antenna performance analysis and identifying the system and propagation factors that have the most dominant contribution to the results.

A novel result regarding the difference between deterministic and stochastic propagation modelling for smart antenna performance prediction is presented. It is shown that stochastic models do not include correlation between users in the antenna array space properly, which can have significant influence on the accuracy of the results, especially for the UMTS uplink.

A novel modelling method that incorporates simplified aspects of UMTS on the basis of deterministic propagation data is proposed. The benefit of using smart antenna in the power controlled environment regarding the number of users that can be sustained and optimum transmit powers is analysed. A novel analysis on establishing propagation factors in a micro-cell environment that pose main limitations to the system performance for two representative antenna processing schemes, optimum combining and maximum ratio combining, is presented.

The main advantage of using optimum combining over maximum ratio combining is a larger number of users that can be accommodated in the system and better coverage improvement properties. Significant transmit power reduction can also be achieved, but it is limited by the type of local scattering at the base station in a particular environment. Fast fading is found critical for low to moderate speeds at the UMTS frequency of 2GHz, where the angular spread at the side of the mobile station is the most influential propagation parameter related to this system aspect. For moderate angular spreads, the fast fading effects are manifested by a significant increase in optimum transmitted power level with the mobile terminal speed and more pronounced difference in the channel tracking ability between the two antenna processing schemes.

Finally, a novel method to minimise deterministic data necessary for the system performance analysis is presented. The core of the method consists in computation of the channel composition for the center of the pixel directly from the deterministic model and characterising the channel for any point

within the pixel on the basis of the information. The main idea is to reduce computational burden along a trajectory by the resolution corresponding to the size of the pixel. The problem of finding the optimum pixel size at a sufficient accuracy from the system point of view is addressed. The main limitations of the proposed method are analysed with respect to spatial changes in propagation conditions. The obtained pixel size result shows that it is possible to significantly decrease the computational time needed for deterministic models.

Acronyms and Symbols

BER	Bit Error Rate
BLER	Block Error Rate
BPSK	Binary Phase Shift Keying
BS	Base Station
CIR	Complex Impulse Response
FDD	Frequency Division Duplex
GBSBEM	Geometrically Based Single-Bounce Elliptical Model
3GPP	Third Generation Partnership Project
LOS	Line-of-Sight
MAI	Multiple Access Interference
MIMO	Multiple Input-Multiple Output
MRC	Maximum Ratio Combining
MS	Mobile Station
NLOS	Non Line-of-Sight
OC	Optimum Combining
PN	Pseudo-Noise
SINR	Signal over Interference+Noise Ratio
TDD	Time Division Duplex
UMTS	Universal Mobile Communication System
WCDMA	Wideband Code Division Multiple Access
WDCM	Wideband Directional Channel Model
WSSUS	Wide-Sense Stationary Uncorrelated-Scattering

$\mathbf{a}(\varphi)$	antenna array steering vector in the direction φ
$a_m(\varphi)$	m-th element of the antenna steering vector in the direction φ
$\alpha_{q,i}$	i-th user amplitude for the q-th multipath
b_i	i-th user data bit sequence
c	speed of light: $3 \cdot 10^8$ m/s
c_i	i-th user CDMA code sequence
d	spacing between two adjacent antenna elements
D, $\bar{D}$	the size of a pixel: general, average
f_c	carrier frequency
f_{pc}	fast power control frequency
$\phi_{q,i}$	i-th user phase for the q-th multipath
$\mathbf{G}$	gain matrix
G_{ji}	the total gain in the direction of the j-th user ($j \neq i$) when the antenna pattern is optimised for the i-th user
G_{ii}	the total gain in the direction of the i-th user when the antenna pattern is optimised for that user
$\gamma_{l,i}$	i-th user SINR for the l-th Rake finger
γ_0, $\gamma_0^{'}$	SINR: target, approximate
$\mathbf{h}_{l,i}$, $\mathbf{h}_{l,i}^{'}$	i-th user spatial signature for the l-th Rake finger: general, approximate
$h_{l,i}^{rake}$	i-th user signal for the l-th Rake finger received on one antenna
h_i^{ref}	i-th user signal for a single Rake finger received on one antenna
$\mathbf{I}_K$	$K \times K$ identity matrix
$I_{l,i,j}$	interfering signal from the j-th user at the l-th Rake finger after applying antenna weights optimised for the i-th user
$I_{i,j}$	interfering signal from the j-th user after summation over Rake fingers
K	number of users in the system
L	number of Rake fingers
λ	eigenvalue
λ_c	free-space carrier frequency wavelength
λ_{max}	spectral radius of a matrix
Λ	rms angular spread
M	number of antenna array elements
N	the ratio between the symbol and chip duration
N_{dB}	the processing gain (expressed in dB)
N_0	spectral noise density
$\mathbf{n}$	thermal noise vector

$\mathbf{p}$, $\mathbf{p}_{opt}$	transmit power vector: general, optimum
P_i, $P_i^{'}$	i-th user transmit power: general, approximate
P_i^r	i-th user received power
Q	total number of dominant multipath components
R	circular antenna array radius
R_c	chip rate
R_d	data rate
$R_{j,i}$, $\hat{R}_{j,i}$	partial cross-correlation between PN sequences belonging to i-th and j-th user ($i \neq j$)
$R_s(\cdot)$	autocorrelation function of the PN sequence
$\mathbf{R}_{in,i}$, $\mathbf{R}_{in,i}^{'}$	i-th user interference+noise correlation matrix: general, approximate
$\mathbf{r}_{l,i}$	i-th user signal vector at the l-th Rake finger after correlation with the local PN sequence
$S_{l,i}$	i-th user desired signal at the l-th Rake finger after applying antenna weights
S_i	i-th user desired signal after summation over Rake fingers
σ^2	thermal noise power at the receiver input
$\sigma_{l,i}^2$	thermal noise power for the l-th Rake finger after applying antenna weights optimised for the i-th user
σ_i^2	i-th user thermal noise power after summation over Rake fingers
σ_τ	rms delay spread
$\varsigma_i(\varphi)$	the gain of antenna pattern optimised for the i-th user in the direction φ
t_{pc}	frame slot duration
T_c	CDMA code chip duration
T_s	data symbol duration
$\tau_{q,i}$	i-th user time delay for the q-th multipath
$\tau_{l,i}$	i-th user time delay for the l-th Rake finger
$\tau_{0,i}$	i-th user time delay of the first incoming multipath
θ_i	phase of the i-th user modulator
u_i	i-th user transmit signal
v	MS velocity
v_{12}	angle between two spatial signature vectors
$\varphi_{q,i}$	i-th user angle-of-arrival for the q-th multipath
$\mathbf{w}_{l,i}$	i-th user antenna weight vector for the l-th Rake finger
$\mathbf{y}_i$	i-th user input signal vector at the receiver
$z_{l,i}$	i-th user signal for the l-th Rake finger after applying antenna weights
Z_i	i-th user output signal after summation over Rake fingers

1

Introduction

Cellular communication is one of the fastest growing fields in the world of telecommunications [1]. First generation (1G) cellular systems, that appeared in the eighties, supported analog voice-only service. After one decade, the second generation (2G) systems came into wide public use, which marks the beginning of digital communication in mobile radio. Wireless voice service, text messaging and access to low rate data were included in 2G. Third generation (3G) systems have emerged, as a need to create a global single multimedia mobile radio standard, allowing images and video transfer and access to networks by the higher data rates. Universal Mobile Telecommunication System (UMTS) is one of the 3G systems which has been agreed on by the 3G partnership groups, 3GPP and 3GPP2 [2].

The main feature of UMTS is that users transmit data simultaneously at the same frequency. Users are separated on the basis of different coding sequences, the technique being called Wideband Code Division Multiple Access (WCDMA). Although seen as a spectrally efficient method, the system suffers from multiple access interference (MAI). Antenna array processing is considered to have great potential in dealing with the interference problem. In UMTS, the radio channel has very pronounced multipath and fast fading effects. In order to analyse the benefit of using antenna arrays under such complex conditions, a model that describes in detail the variability of signals in both delay and angular domain is required.

In this thesis, the main focus is on a micro-cell environment, where the changes in the channel are subject to many location-specific propagation mechanisms. In the uplink, i.e. signal is transmitted from the mobile station (MS) to the base station (BS), the propagation channel belonging to different users is, generally, not the same. This is in contrast with the downlink,

where the signals intended for interfering users are received via the same channel together with the desired signal at the MS. This makes uplink particularly critical for adequate modelling of interference and in turn, channel modelling requirements. One of the focal points of the thesis is to analyse how important an accurate prediction about interference is for the smart antenna performance analysis in the uplink. The main goals of the thesis are given, as follows:

- determine what is lacking in the current standard propagation models regarding smart antenna analysis for UMTS and motivate the necessity for using deterministic models for prediction in urban micro-cells

- analyse smart antenna performance in power-controlled UMTS for different system settings and propagation conditions using the deterministic model (μFipre) developed at the Eindhoven University of Technology (TU/e); investigate how system parameters and realistic propagation factors correlate with respect to results for two representative types of smart antenna algorithms, optimum combining (OC) and maximum ratio combining (MRC).

- introduce the concept of a *pixel* in order to spatially characterise the channel with sufficient accuracy from the system point of view, using minimum amount of deterministic data; the aim of this analysis is to reduce the computational burden of the ray-tracing model μFipre

The rest of the chapter elaborates on the description and modelling of UMTS aspects in Section 1.1, followed by the overview of current trends, as well as novel issues featured in the thesis, regarding channel modelling in Section 1.2 and smart antenna analysis in Section 1.3.

1.1 UMTS: description and modelling

In order to identify the aspects of the system that are relevant for the purpose of this study, the most important characteristics of UMTS are given in Section 1.1.1. In the modelling approach proposed in this thesis, the complexity of the system is reduced to include only those aspects that have the greatest influence on the performance. The aspects included in the system modelling will be described in Section 1.1.2.

1.1.1 Description of UMTS

The description of UMTS is divided into two main parts. The first part outlines the basic principle of the data transmission specific for UMTS, while the second part focuses on the WCDMA radio interface.

The principle of the spread-spectrum CDMA and uplink data transmission

The main characteristic of WCDMA is the use of quasi-random bits, derived from CDMA spreading codes, in order to enable separation between signals belonging to different sources that are simultaneously transmitted at the same frequency. These quasi-random bits are called chips and are transmitted at the rate of R_c=3.84 Mcps. User data bits are multiplied with the CDMA quasi-random code, most commonly referred to as a pseudonoise (PN) sequence, which results in the increase of the transmitted signal bandwidth. The carrier bandwidth is 5 MHz for the chip rate of R_c=3.84 Mcps, including guard bands between adjacent spectrum slots. The spectrum of the signal after the spreading operation is well below the noise floor of the receiver [3]. This makes the signal difficult to detect without the knowledge of the corresponding CDMA code.

The basic principle of the spreading process is shown in the upper part of Fig. 1.1 [4], where the user data is a BPSK modulated sequence of rate R_d with the bits having values ± 1 and the number of chips in the spreading sequence is N. The term N is also referred to as the length of the PN sequence and is equal to: $N = T_s/T_c$, where T_s represents the duration of the data symbol and T_c stands for the chip duration. The resulting data rate is $R_d = N \cdot R_c$. This increase in the data rate corresponds to the widening of the bandwidth of the data signal. At the receiver the operation of despreading is performed by multiplication of the received signal with the same PN sequence, followed by integration over the symbol duration. This represents a classical matched filtering process.

The middle part of Fig. 1.1 shows that in the process of despreading, the signal is restored to the original rate R_d, assuming perfect synchronisation of the local PN sequence at the receiver with the sequence of the corresponding user. The lower part of the figure shows the effect of multiplying the PN sequence, assigned to the desired user, with the received signal belonging to an interfering user. After despreading the value of an interfering signal slightly fluctuates around zero. The spreading and despreading concept in the spectral domain is shown in Fig. 1.2. The bandwidth of the original

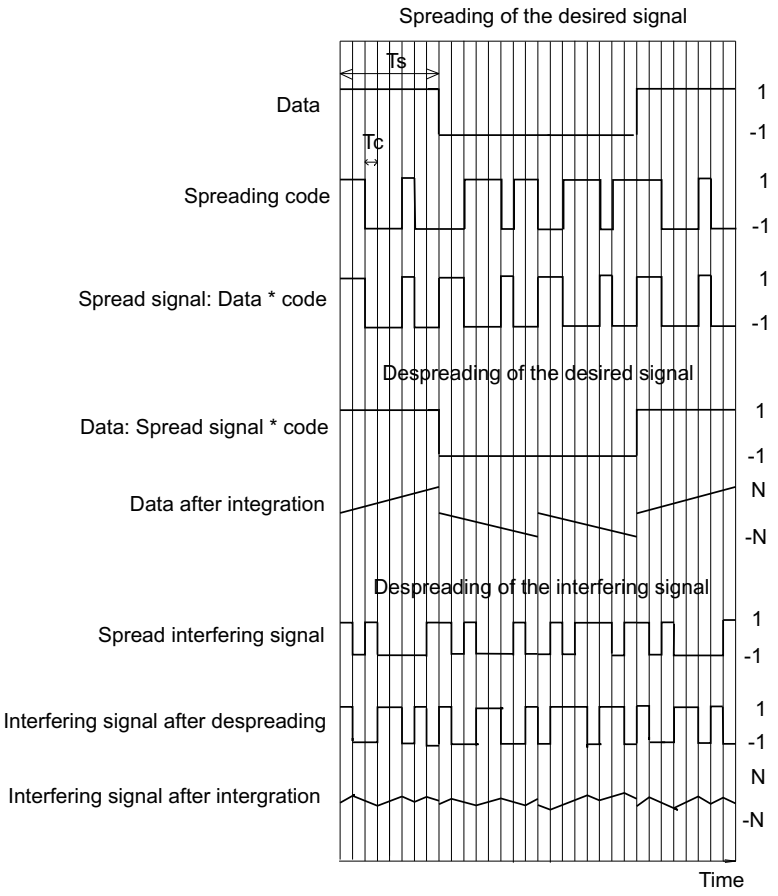

Figure 1.1: The principle of spreading in CDMA

transmitted signal B_n is increased by the factor of N, resulting in a larger signal bandwidth B_w. The signal at the receiver is the summation of the desired signal and interfering signals coming from other users, which are also wide-band. The multiplication of the spread signal, immersed into multi-user interference, with the local PN sequence restores the received signal to the original bandwidth. The despreading operation only further randomises interference, but it remains spread over the same frequency band. After narrow-band filtering at the receiver with a bandpass filter, its bandwidth being equal to that of the original signal, only a small fraction of the interfering signal power will pass through the filter, whereas the power of the desired signal will be $N = B_w/B_n$ times larger than that of the interference.

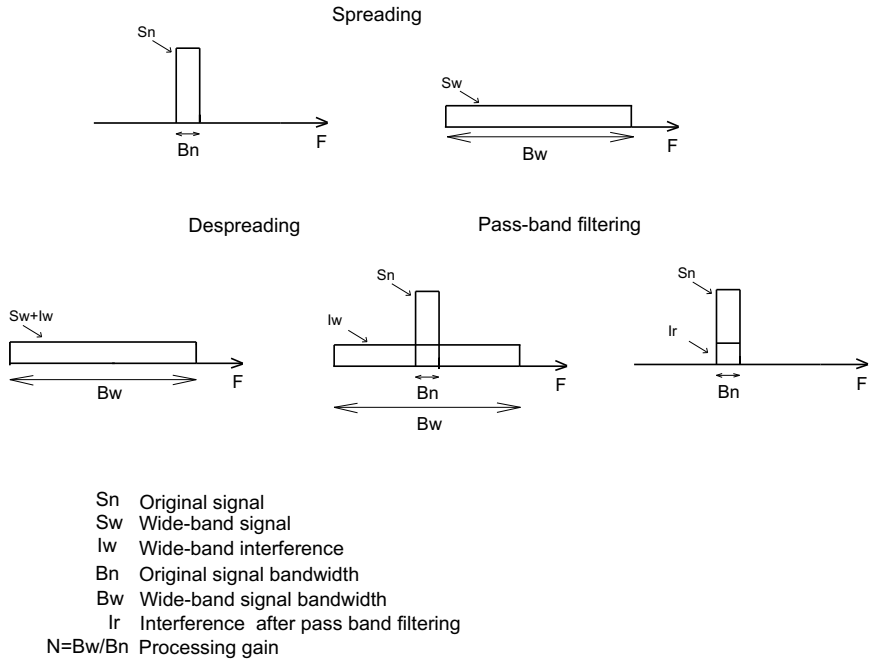

Figure 1.2: Spreading in spectral domain

This phenomenon is referred to as the *processing gain* and represents the fundamental feature of CDMA systems.

In UMTS, the transmission is carried out in frames of 10 ms duration, during which the data rate is constant. The user data transmission in the uplink is carried out on two channels: the dedicated physical data channel (DPDCH) and dedicated physical control channel (DPCCH). As the names imply, the data bits are carried by the DPDCH, while the DPCCH carries control signals. The uplink DPCCH uses a slot structure with 15 slots over 10 ms radio frame, as shown in Fig. 1.3 [4]. This results in a slot duration of t_{pc}=0.666 μs, which corresponds to 2560 chips. Each slot has four fields. The complete description of the function of the four fields can be found in [4]. Only two of them are mentioned here, being of primary importance for the system aspects modelling: the field used for channel estimation consisting of pilot bits and TPC field for the power control process, carrying commands for update of power levels (power control will be detailed later).

The multiplexing of the DPDCH and DPCCH is also shown in Fig. 1.3. The two channels are separated by two orthogonal channelisation codes C_d

and C_c, after which the combined signals are scrambled by a complex spreading sequence $C_i + jC_q$. Scrambling follows the operation of spreading and is used to separate different mobile terminals from each other without changing the signal bandwidth. In the uplink, there are two options for scrambling codes: short and long scrambling codes. The short scrambling code length is 256 chips. Short codes are used when the advanced receiver techniques such as multiuser detection are applied. Long codes are used if the base station has a Rake receiver and are truncated to a 10ms frame length. The long codes are so-called Gold codes [1], [3]. Since there are millions of scrambling codes available, there is no need for code planning in the uplink.

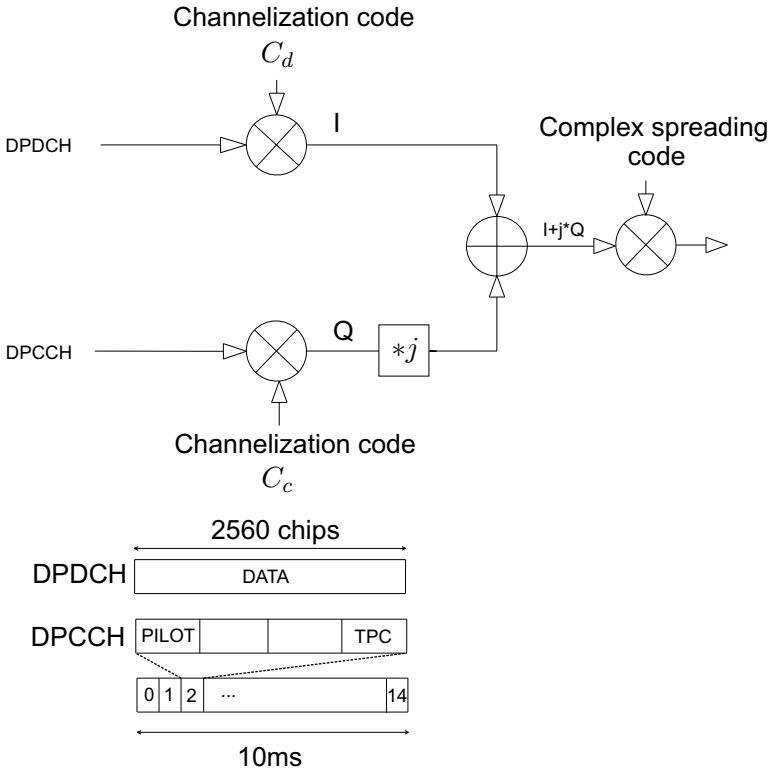

Figure 1.3: I-Q/code multiplexing with complex scrambling

Basic characteristics of WCDMA interface

There are two basic modes of operation in UMTS: Frequency Division Duplex (FDD mode) and Time Division Duplex (TDD mode). Two 2x60 MHz

frequency bands are allocated for the FDD mode, 1920-1980 MHz plus 2110-2170 MHz, for Europe and most of Asia. The band of 25 MHz is available for TDD mode in the 1900-1920 MHz and 2010-2025 MHz band [4]. Separate 5 MHz carrier frequencies are used for uplink and downlink in FDD mode, whereas in TDD mode only one 5 MHz carrier is used for both uplink and downlink on the basis of time-sharing.

The UMTS radio channel has very pronounced multipath propagation and fast fading effects for the chip duration of T_c=0.26 μs and operating frequency of around 2 GHz. There are many multipath waves coming from different directions, especially in an urban micro-cell environment, due to various propagation mechanisms such as: reflections, diffractions and scatterings from trees and buildings. The WCDMA receiver can not separate multipath signal components that fall within one chip bin, i.e. the delay difference between them being lower than the duration of one chip. At the frequency of 2 GHz, the paths with half the wavelength difference, i.e. 7 cm, arrive at almost the same time as compared to the duration of a single chip, which corresponds to a path of 78 m [4]. This means that fast fading is quite critical for 2 GHz because signal cancellation due to summation of signals with various phases occurs when MS moves over very short distances.

The fact that many users share the same channel with severe fast fading calls for a strict power control, which is another important aspect of WCDMA. Power control primarily solves the so-called "near-far" problem. This is related to a large difference in distance with respect to the BS between users. Without power control, a mobile that is very close to the BS can block other mobiles that are located at larger distances. Another type of problem, related to fast fading, occurs when a mobile is in a deep fade with respect to another one, so that the blocking of one user by another can happen even when the difference in the distance is not very large. This is why *fast* power control is essential in UMTS.

There are two modes in the power control process: *fast closed-loop power control* and *slow outer-loop power control*. In the uplink fast power control process, the base station performs signal-over-interference+noise ratio (SINR) estimation and compares it to the desired value for SINR, referred to as a *target SINR*. In case the measured SINR is higher than the target value, the base station will send the command to the mobile terminal to reduce the transmit power level by a certain step-size, otherwise, the mobile will be commanded to increase the transmit power, also by the same value. The SINR estimation and power update is executed at the frequency of $f_{pc} = 1500$Hz, i.e. for each time slot, which is fast enough to combat fast fading for low to moderate speeds of the mobile. Apart from solving the

above mentioned problems, power control also plays an important role in achieving the maximum possible capacity. The target SINR is set according to minimum requirements for a particular service and power levels should not be much higher than what is necessary to meet these requirements. In this way, MAI coming from other users is kept as low as possible which allows maximum achievable capacity for a certain coverage or maximum coverage for a certain number of users [4]. Another slower power control mode (outer-loop power control), plays the role of adjusting the target SINR according to the requirements of an individual radio link, defined in terms of a target bit error rate (BER) or block error rate (BLER) that specify the desired quality of service. The outer-loop power control is based on error rate measurements. The system is designed to tolerate errors to a certain extent and with this mechanism it is ensured that it is always within a tolerable range. If the error rate is too high, the target SINR is increased and if it is too low, it is decreased. The target SINR floats around some minimum value that satisfies the desired quality of service, changing slowly as the MS speed and propagation environment changes.

Another aspect, typical for CDMA systems, is the so-called *soft handover*, which occurs when a MS is in an overlapping region of two cells. The main feature of the soft handover is that the MS maintains communication with two base stations, until one of them becomes significantly stronger. This can be seen as some sort of macro-diversity obtained via communication over independent channels due to the dual BS capabilities. The diversity gain permits the decrease in transmit power when the mobile station is near the edge of a cell, which significantly reduces other-cell interference.

The WCDMA air interface can support advanced CDMA reception techniques such as adaptive antennas and multiuser detection. The thesis deals with analysing performance of antenna array processing, commonly referred to as *smart antenna*, in a realistic environment. In order to include detailed information from a concrete environment, the modelling of complex system aspects has to be simplified. The accuracy of modelling should be at the level which is sufficient to obtain good insight into the influence of the propagation and identification of the most dominant factors on the system performance. The general description of modelling the most important aspect of the system and simplifications assumed in this study will be given in Section 1.1.2.

1.1.2 Modelling aspects of UMTS

The classical analysis of the physical layer performance of a system involves extensive link-level simulations, while using a simple stochastic channel model [5],[6]. The main output of such simulations is the BER and BLER, which can be used to compare different transmitter-receiver techniques. The novel approach, proposed in this study, differs in the way the system analysis is performed and the way the propagation data is utilised for that purpose. The deterministic ray-tracing channel model μFipre [7] is used, whose output is not so easily integrated in a link-level simulator and is much more spatially dependent on the local characteristics of the environment.

The output of the ray-tracing model is the complete composition of waves in terms of amplitude, delay, phase and angle-of-arrival for the given MS and BS coordinates. The parameters describing the composition of the waves will be referred to as *ray parameters* and are further detailed in Chapter 2. The analysis of smart antenna in this study is based on performance indicators such as the achieved SINR, as well as transmit mobile powers for any position of the desired user on a given trajectory and given locations of interfering users in the system. The main pros and cons using deterministic models are as follows:

- Deterministic models include detailed propagation data which gives good insight into the relationship between realistic propagation and the system performance.
- The main drawback is the complexity of the site-specific input data that has to be acquired from a concrete environment and of the output data that has to be subsequently processed.

The advantages and disadvantages of stochastic models can be summarised as below:

- Stochastic models do not include very accurate propagation data, reflecting only the most general channel characteristics; they usually comprise a large number of different propagation scenarios in the form of an average power delay-angular distribution
- Stochastic models are more flexible for the analysis of various advanced processing techniques, which can be readily compared without the need to include very accurate and detailed propagation data.

The lower flexibility of using the ray-tracing model for complex system modelling is compensated by a considerable insight into the effects of the concrete propagation phenomena to the system performance.

The main simplification assumed in the system modelling is the availability of a perfect channel knowledge, i.e. the realistic channel estimation process is not simulated. In reality, channel estimation is performed for every slot per frame [8] and, in addition to that, the processing gain of the pilot signal is very high for all types of transmitted data, so it is valid to assume that reliable channel information is at all times available at the receiver. The main conclusions in this thesis are made on the basis of the comparison between either different channel models, different antenna processing schemes or different types of environment, with which primarily fundamental restrictions imposed by propagation are analysed. It is, therefore, valid to assume perfect channel estimation, taking into account that the results are associated with the upper bound of the system performance. For similar reasons, the analysis involves a single cell case. This also excludes the soft handover, being significant only for simulation of a multiple-cell situation.

Another simplification concerns implementation of different PN sequences in the receiver model. PN sequences are assumed to be the composite result of both spreading and scrambling processes. In order to avoid using explicit PN codes, the sequences are assumed to be random binary sequences. The results in this thesis are based on averaged powers of the desired and interfering users. This allows including the effect of cross-correlation between different PN sequences as a constant factor, assigned to all interfering signals. This factor is obtained as an average result over all possible PN sequences. More details about this will be given in Chapter 2. On the whole, the most dominant effect of CDMA coding is included as a basic gain of the desired user power over the total interference power, which is independent of the additional gains due to antenna array processing in spatial domain. The gain that stems from the selective properties of CDMA codes is actually the processing gain already introduced in Section 1.1.1.

The effects of the fast closed-loop power control are modelled in two ways: the first, referred to as "perfect power control", represents the case when the power control is assumed instantaneous and the achieved SINR is equal to the specified desired target value for all users; in the second, referred to as "imperfect power control", the power update process is performed at the frequency of $f_{pc} = 1500$Hz and with ± 1dB power level change. This approach is closer to the realistic situation in UMTS [9]. According to the first approach, optimum transmit powers are obtained that give equal target SINR at the BS for all users. The aim is to identify the basic influence of the system factors, like processing gain, antenna array size and target SINR on the smart antenna performance. In the second approach, finite-time effects are modelled by performing the power update for positions spaced at

$d_{pc} = vt_{pc}$ on a trajectory where the user moves. Here $t_{pc} = 6.66 \cdot 10^{-4}$ s represents the time allocated for the power update and v represents the speed of the mobile. The second approach gives a more realistic insight in the comparison between different antenna processing schemes and also introduces the speed of the mobile as a new parameter. This analysis also shows the influence of the fast fading in a realistic power control process. The carrier frequency at which the channel will be simulated is f_c=1.9 GHz, which falls in the range of frequencies allocated for UMTS uplink.

Different types of services will be included, such as, voice service, real-time and non-real time data service. With the type of service, a specific value for the processing gain is associated. The target SINR, that is set during the outer-loop power control process, is assumed fixed. To a certain extent, this approach has elements of the link budget calculation when certain representative target SINR values with the corresponding processing gains are assumed [4]. The service types considered, together with the associated processing gains and target SINR values used in this thesis, are given in the table 1.1.

type of service	processing gain	target SINR
voice	25dB	5dB
real time data	15dB	1dB
non-real time data	10dB	1dB

Tabel 1.1: Processing gains and target SINR values for the corresponding type of service

1.2 Channel modelling: state of the art and motivation focus

System performance analyses have been performed largely by using models that are based on the statistical channel description. The models accepted within 3GPP framework represent a step further from pure stochastic tapped delay line models, as described in [10]. Those models include the channel description in the angular domain, as well, and also attempt to reproduce a more realistic correlation between the delay and angular domain [11]. There are three main implementations of the stochastic channel models developed for the analysis of 3G systems: parametric, geometry-based and correlation-based models [12].

Parametric models directly describe channel signals as a superposition of waves. The model described in [13] is an example of a parametric model which assumes multiple antenna elements at both the transmitter and the receiver side. The model has the form of a tapped delay line, where each tap reflects a propagation path. If the number of resolvable taps is denoted by L, the time delay associated with the l-th path and (i,j)-th transmitter-receiver antenna pair as $\tau_{l,i,j}$, while $\delta(t)$ denotes the dirac function, the impulse response between the i-th transmitting and j-th receiving antenna $h_{i,j}$ is defined as follows:

$$h_{i,j}(t,\tau) = \sum_{l=1}^{L} c_{l,i,j}(t)\delta(\tau - \tau_{l,i,j}) \tag{1.1}$$

The Virtual Ray Model (VRM) [14] introduces an additional feature: resolvable multipath components are represented as superposition of waves that fall into one delay bin. This model has been proposed as a system-level model for 3GPP. Here, the channel coefficients $c_{l,i,j}$, defined for the l-th resolvable path and (i,j)-th antenna pair, include the path loss PL, the shadow fading σ_f and space-time fading $\beta_{l,i,j}$ and are given by:

$$c_{l,i,j} = PL\sigma_f\beta_{l,i,j}(t) \tag{1.2}$$

Space-time fading effects are included in terms of a coefficient $\beta_{l,i,j}(t)$, given as a sum of waves within the l-th delay bin, where Q_l is a number of contributing waves:

$$\begin{aligned}\beta_{l,i,j}(t) = \quad & \tfrac{1}{\sqrt{Q_l}} \textstyle\sum_{q=1}^{Q_l} \quad \{\alpha_{l,q}\exp(\jmath 2\pi f_c\cos(\phi_{l,q}))\cdot \\ & \cdot a_i(\varphi_{Tx}^{l,q})a_j(\varphi_{Rx}^{l,q})\exp(\jmath 2\pi f_c t\cos(\varphi_{Tx}^{l,q}))\}\end{aligned} \tag{1.3}$$

The term $a_i, i = 1,...M$, associated with i-th antenna element in an M-dimensional antenna array, reflects the phase change of a certain multipath component due to spatial disposition of the i-th antenna element. It is defined in terms of the angle-of-arrival $\varphi_{Rx}^{l,q}$ impinging on the BS antenna array and is also dependent on the antenna array configuration. Similarly, the term $\exp(\jmath 2\pi f_c t\cos(\varphi_{Tx}^{l,q}))$ denotes the phase change of a multipath component due to a mobile movement (Doppler shift) and is expressed in terms of the angle-of-arrival at the MS side.

This approach is similar to the modelling method used in this study. The channel parameters, given for the q-th wave in the l-th delay bin, like amplitude $\alpha_{l,q}$, phase $\phi_{l,q}$, angle-of-arrival at the BS (receiver) $\varphi_{Rx}^{l,q}$ and

angle-of-arrival at the MS (transmitter) $\varphi_{Tx}^{l,q}$ are analogous to the *ray parameters* obtained from the ray-tracing model. In parametric models, however, the channel parameters are taken from a given power delay-angular distribution which is common to all channel impulse response realisations. The power delay-angular distribution statistically describes the dispersion of power in delay and angular domain and is commonly referred to as *power delay-angular profile*. The term $\alpha_{l,q}$ in Eq. 1.3 represents the relative attenuation of the q-th wave in the l-th bin, which is directly defined by the power profile curve. In this thesis, the path-loss, shadow fading and small-scale fading are not treated as separate concepts, described in terms of statistics, as is commonly the case with statistical modelling [15], but the amplitude of a certain ray is the result of signal attenuation at each scattering point as the ray propagates from the MS to BS. The amplitude of each ray, obtained by a deterministic model represents the composite result of all these phenomena and is associated deterministically with the given position in the environment, instead of being derived from a statistical distribution.

Geometry-based models assume a certain probability density associated with the distribution of scatterers in the area around the BS and MS. One of the representatives is a Wideband Directional Channel Model (WDCM), developed for micro-cells [16],[17]. Scatterers are grouped in clusters which emulates a more realistic situation where multipath waves arrive in groups only from specific angles, instead of being uniformly distributed in all directions. The channel composition in terms of *ray parameters* is, then, obtained by tracing rays via scatterers' points, once the scatterers get generated according to the specified distribution. The distribution of scatterers can be related to a certain power delay-angular distribution, which provides the main link between the parametric and geometry-based modelling.

Correlation based models describe the channel in terms of spatial correlation between antenna elements. The underlying reason for this is that these kind of models are basically developed for multiple input-multiple output (MIMO) systems, where the performance is largely dependant on this parameter. The complex channel coefficients are assumed to be Gaussian distributed which enables MIMO modelling based on the second order statistics. The 3GPP narrow-band MIMO correlation-based model is described in [18]. When extended to a wide-band version with L resolvable paths and $\Delta\tau$ delay resolution, the channel coefficient matrix is given as:

$$\mathbf{H}(\tau) = \sum_{l=1}^{L}((\mathbf{R}_{Rx}^{l})^{1/2}\mathbf{A}^{l}(\mathbf{R}_{Tx}^{l})^{1/2})\delta[\tau - (l-1)\Delta\tau] \tag{1.4}$$

where $\mathbf{R}_{Rx}^{l}$ and $\mathbf{R}_{Tx}^{l}$ represent spatial correlation matrices of the l-th tap at the transmitter and receiver respectively, while the matrix $\mathbf{A}^{l}$ has entries in the form of mutually independent, circularly symmetric complex Gaussian random variables. The spatial correlation matrices $\mathbf{R}_{Rx}^{l}$ and $\mathbf{R}_{Tx}^{l}$ reflect spatial correlation properties at the transmitter and receiver, assumed independent of each other.

The main feature of correlation-based models is that the channel characterisation is not done in terms of superposition of waves, which corresponds to a physical channel modelling. Specific values for the spatial correlation may correspond to different channel realisations, but which give the same performance measure for MIMO systems. This is why it is no longer possible to provide the link from a correlation-based model to a physical model. The other way around is, naturally, feasible; spatial correlation can be obtained from a specified power angular profile [19]. Furthermore, the angular spread has been found to be the most dominant channel parameter for the value of the spatial correlation [20], which means that the channel for MIMO systems analysis can be characterised predominantly on the basis of one parameter only.

The most comprehensive stochastic model has been developed within the COST 259 project [21]. This model plays an important role for testing the 3G and 4G systems. Different cell types, macro-, micro- and pico-cell, are included. It is a geometry-based model characterised by the clustering of multipath components. The components of a cluster exhibit the same large-scale behaviour, while the large-scale behaviour of distinct clusters is independent. A statistical description of the propagation conditions is defined for every type of environment within a particular cell and includes the description of the waves spreading within a cluster, as well as the distribution of clusters. Small-scale fluctuations are the result of phase variations of the impinging waves assuming that the MS is moving over a sufficiently small local area (not larger than some tens of a wavelength). Large-scale fluctuations are the result of the MS movement over larger areas. These are modelled by means of an "appearing" and "disappearing" of multipath components, described by specified transition functions.

The common feature of the stochastic models described above is the fact the channel description, given in the form of a power delay-angular profile, comprises a larger number of different propagation conditions. In the COST 259 model, the representative types of environment and the associated power profiles are identified within each cell type. In an urban micro-cellular environment, where the BS is located below the average rooftop level, the channel conditions are subject to diverse propagation mechanisms, specific

to a local building and vegetation structure around the BS. This is the reason why the changes in the channel are frequent and abrupt even within a small area. In such an environment, users can have quite different angular profiles as seen from the BS, depending on their specific location. For the analysis of smart antenna, which performs spatial filtering of interference, inadequate modelling of the spatial correlation between users in the antenna array space can influence the result significantly. In stochastic models, this information is lost due to the fact that the power delay-angular profile represents an average over different propagation scenarios associated with one type of environment. Smart antenna results can be sensitive to the loss of the spatial structure of interference for urban micro-cellular environments. The current stochastic models for micro-cells do not reproduce accurately this kind of relationship between users. More details regarding the comparison between a deterministic and a stochastic channel modelling approach are shown in Chapter 3, where the motivation for deterministic modelling is clearly outlined. The concept of spatial correlation of users in the antenna array space and spatial structure of interference is explained in Chapter 2.

In this work, where the results are based on a deterministic model, the power delay-angular description is specific to every user location. The variation of the channel in time, which is commonly reproduced via a Doppler shift in a stochastic model, is replaced by the concept of the purely spatial channel model, as will be described in Chapter 2. One of the novel results in the thesis regarding channel modelling is the comparison between the stochastic and deterministic modelling and establishing what is fundamentally lacking in stochastic models for accurate prediction of smart antenna performance. Another novelty concerns proposing a method to restrict necessary deterministic data to a minimum, while maintaining sufficient accuracy of the system performance prediction. Using deterministic channel information enables proper analysis of the influence of the spatial structure of MAI on smart antenna performance. The basic concepts related to antenna array analysis will be introduced in Section 1.3.

1.3 Antenna array processing: state of the art and motivation focus

Antenna array processing is seen as having a great potential in performance enhancement for third generation CDMA systems [22],[23] due to good signal over interference enhancement properties. Fast power control already plays quite a significant role in controlling interference by adjusting trans-

mit powers to achieve a certain signal level over MAI for all users in the system. The main benefit of using antenna array processing, as an additional mechanism to reduce interference, is that transmit powers can be further reduced. This, in turn, gives 'room' for more users in the system, resulting in the capacity improvement. The gain in power reduction can also be utilised to improve coverage, since in the uplink transmission the main restriction on the coverage is imposed by the maximum transmit power of a mobile. Improved coverage can reduce the density of base stations in a certain area which significantly reduces equipement-related costs. Another advantage is the extension of the battery life-time of mobile terminals.

Antenna array performance analyses for CDMA channels were largely based on a typical assumption that interference can be modelled as spatially-white, which has been considered acceptable assuming a large number of users in a cell [24], [25]. For this reason, it has been considered in quite a number of analyses [26], [27], [28] that antenna algorithms need not necessarily utilise the information about the spatial structure of interference, especially since these type of algorithms are proved to be more complex than those that are based on the channel information of the desired user only. One of the aims of this study is to analyse the benefit of algorithms that use the information about the spatial structure of interference in an urban micro-cell without making *a priori* assumption about spatial whiteness.

Generally speaking, all antenna array processing schemes tend to optimise antenna pattern in order to provide a maximum gain towards the desired user and steer nulls or side-lobes towards interferers. In [29], [30] a comprehensive summary of antenna array processing schemes is given. Regardless of their complexity and implementation aspects, all antenna array processing schemes can be roughly classified into a group of algorithms that utilise information about interference in the process of optimisation and those that use the information of the desired user only.

Optimum Combining and Maximum Ratio Combining are two representative algorithms where the former makes use of the information about the spatial structure of interference in order to find optimum antenna weights that give maximum SINR and the latter ignores the information about interference and maximises the signal towards the desired user. In Fig. 1.4, the basic principle of the two algorithms is shown. MRC is equivalent to a plain beamforming, when all degrees of freedom are used to steer a beam towards the desired user, while in case of OC, the antenna pattern is formed to place "nulls" or "side-lobes" towards interfering users. OC resorts to MRC, if the structure of interference is not influential for the result, which from the statistical point of view has been referred to as a *spatially-white* interference.

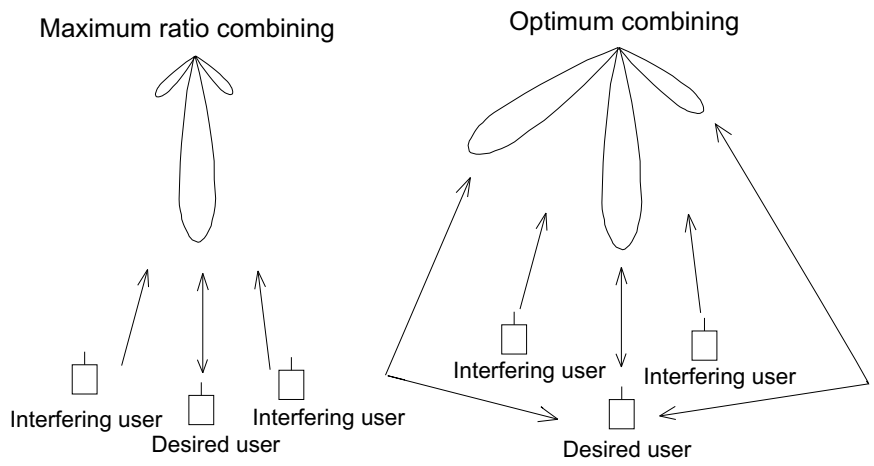

Figure 1.4: The principle of MRC and OC

This means that for these cases OC yields the same performance as MRC.

In this thesis, the spatial structure of interference is taken deterministically i.e. OC resorts to MRC only if signals from interfering users correlate in angular domain with the signal of the desired user in such a way that there is no significant difference in the performance. More details will be given in the following chapters and especially Chapter 4. For the time being, it should be clear that, using this approach, the influence of the spatial structure will not depend so much on the number of users, but on the actual power angular characterisation, specific to each user. The statistical concept of *spatial whiteness* is abandoned in this study and the significance of the spatial structure of interference on the system performance is analysed by comparing OC with MRC scheme. Generally, if the spatial structure has a significant influence, the benefit of OC over MRC in terms of reduction in the transmit power can be substantial. There are several aspects, however, that make this comparison not trivial, because the result will not depend solely on the propagation factors that determine the distribution of angles-of-arrival, but also on the certain system characteristics. There are aspects where OC can obviously be favoured over MRC, but there are also those that reduce the benefit of OC.

On one hand, OC can effectively use the available degrees of freedom offered by an antenna array to directly suppress interference, which makes it generally more advantageous than MRC. On the other hand, in a power-controlled system antenna processing will not make maximal use of available

degrees of freedom for each user, because the level of MAI suppression is balanced with the required quality of performance in terms of the specified SINR for all users. This generally reduces the benefit of OC over MRC. On top of that, interference suppression properties of MRC can be improved by simply increasing the antenna array size, because the beam formed towards the desired user becomes narrower.

The multipath environment, however, imposes some restrictions to applicability of MRC. The signal belonging to one user consists of multipaths that arrive from different angles and also have various phases, which can lead to signal cancellation in the directions from which multipath components with opposite or almost opposite phases arrive. Using OC, the antenna pattern can be 'cleverly' formed to steer nulls towards the most dominant interfering components that do not automatically cancel. The advantage of OC is larger, as the directions from which components arrive are more separated in angle. It has been reported that a significant level of interference suppression is achievable even if the mean angles of the desired and interfering user coincide, provided that the angular spread is large [31].

It is clear that the benefit of OC over MRC will depend on the composite contribution of the factors like the antenna array size, propagation aspects, target SINR, ... Regarding smart antenna performance in general, novel results are presented about identifying the most dominant system and propagation factors and analysing their level of influence with respect to number of users that can be sustained and optimum transmit powers for these two processing schemes.

1.4 Overview of chapters

The modelling of UMTS aspects using deterministic channel information, given in terms of *ray parameters*, is described in Chapter 2. The main signal and receiver model includes combined Rake-antenna processing for asynchronous uplink transmission. The mathematical basis for obtaining simulation results presented throughout the thesis is explained.

In Chapter 3, the comparison of the smart antenna performance using a deterministic ray-tracing model and a stochastic geometry-based model is presented to motivate the necessity of using more deterministic channel information than what is included in the current stochastic models. The analysis is based on a simple interference scenario in a non power-controlled environment. The aim is to indicate that stochastic models do not reflect the spatial correlation between users properly, which can significantly influence

the prediction of the smart antenna performance.

Chapter 4 is focused on smart antenna performance under power control. The analysis is based on simulation results obtained from the ray-tracing model, where a specific type of an urban environment, represented by the TU/e university campus, is used as an input. Basic trends regarding the dependance of optimum powers on system parameters like the processing gain, target SINR, the antenna array size and number of users are established for OC and MRC algorithms. This chapter also elaborates on the influence of spatial structure of interference by comparing the results of the two antenna processing schemes.

In Chapter 5, a method to minimise the amount of deterministic data needed for proper system performance analysis is proposed. The concept of a *pixel* is considered with the idea to reduce the channel prediction burden along a trajectory by the resolution corresponding to the size of the pixel. The exact channel composition is obtained for the center of the pixel only and is assumed unchanging for any other point within the pixel. The problem of finding the optimum pixel size at a sufficient accuracy from the system point of view is addressed. One of the main benefits of obtaining the channel composition for one point per pixel is decreasing the computational burden of deterministic models.

In Chapter 6, a different type of an urban micro-cell environment, represented by the city center of the Hague, is introduced for the comparison with the university campus environment. The main motivation is to find out more about the influence of realistic propagation factors on smart antenna analysis on one hand and to check the consistency of the pixel size result on a different type of environment, on the other. Summary, conclusions and recommendations are given in Chapter 7.

2

System and channel modelling

2.1 Introduction

In this chapter, a novel modelling method that incorporates simplified aspects of UMTS using deterministic channel information given in terms of *ray parameters* is proposed. The introductory sections, Section 2.2 and Section 2.3, outline the basic, well-known principle of the Rake receiver and antenna array processing. Novel contributions are presented in the following sections. In Section 2.4, a simplified signal and receiver model in a multiuser environment is described, on the basis of which the deterministic spatial channel model is proposed in Section 2.5. The model proposed can be used to calculate global channel parameters, such as the delay and angular spread, and average powers of the desired and interfering signals for arbitrary locations in the environment. The derivation of SINR achieved using a Rake receiver combined with MRC and OC antenna array processing schemes represents the background for the simulation results in further chapters.

2.2 Rake receiver

Wideband CDMA signals are frequency selective in a multipath environment. More precisely, a channel is frequency selective if the delay spread is larger than the UMTS chip duration T_c=260 ns. Frequency selective channels are generally represented as tapped delayed line models [10]. Multipath signals that are delayed by more than one chip duration are not correlated, and therefore, those multipaths are treated as resolvable paths. A Rake receiver represents an optimum receiver for multipath channels in a Gaussian

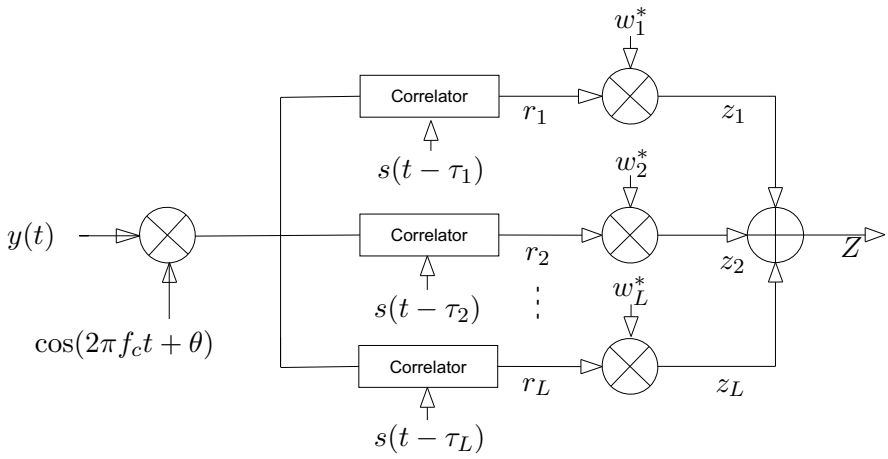

Figure 2.1: Rake receiver

noise [32]. The Rake receiver, represented in Fig. 2.1, consists of a bank of correlators. The function of the bank of correlators is to detect L strongest resolvable multipaths. These correlators are called fingers and each of them is equivalent to a filter matched to a shifted version of the transmitted PN sequence $s(t-\tau_l)$, where $\tau_l = (l-1)T_c+\tau_0, l = 1,...L$ represents the delay of components captured by the l-th Rake finger and τ_0 is the delay of the first received multipath component. A simplified receiver model, represented in Fig. 2.1, assumes the presence of a desired signal only and shows the basic principle of the Rake combining. The desired signal at the receiver input $y(t)$ is BPSK modulated with the carrier frequency of f_c and modulating phase of θ. After demodulation and correlation with the delayed PN sequence, the signals on each finger are multiplied with the complex conjugate of the corresponding tap coefficient. In this way, the signals on all fingers are made equal in phase, after which the summation over Rake fingers is performed. The signal at the l-th Rake finger r_l obtained as a result of correlation and demodulation can be written as:

$$r_l = \sqrt{2P}\int_{\tau_l}^{\tau_l+T_s} y(t)s^*(t-\tau_l)\cos(2\pi f_c t+\theta)dt = \sqrt{\frac{P}{2}}b_0 h_l \qquad (2.1)$$

Here, T_s represents the duration of the transmit data symbol, P is the average transmit power, b_0 is the data symbol and h_l represents the complex channel coefficient for the l-th path (tap coefficient). The operator $(\cdot)^*$ denotes a complex conjugate. In order to obtain Rake finger weights $w_l, l = 1,...L$, the

estimation of L channel coefficients is needed. These can be obtained from the pilot signal. The finger weights are, therefore, defined as: $w_l = h_l$, and the signal at each Rake finger becomes:

$$z_l = w_l^* r_l \tag{2.2}$$

The final output signal Z, obtained after the summation over L Rake fingers, can be written as:

$$Z = \sum_{l=1}^{L} z_l \tag{2.3}$$

This is a typical diversity receiver in the delay domain and the presence of MAI is ignored. This receiver is most optimal if MAI can be considered to be Gaussian.

2.3 Rake-antenna processing

When multiple antenna elements are included in combination with Rake combining, a simultaneous space-delay processing is performed, as shown in Fig. 2.2. Antenna array processing can further enhance the desired signal, but also directly suppress interference. As already explained, two antenna processing algorithms will be considered: maximum ratio combining and optimum combining.

In a wide-band channel, the antenna pattern is optimised for each resolvable multipath, i.e. each Rake finger [33]. If $\mathbf{y}(t)$ is the desired input signal vector received by M antenna elements, the signal vector after correlation and demodulation for the l-th Rake finger, $\mathbf{r}_l$, is:

$$\mathbf{r}_l = \sqrt{2P} \int_{\tau_l}^{\tau_l + T_s} \mathbf{y}(t) s^*(t - \tau_l) \cos(2\pi f_c t + \theta) dt = \sqrt{\frac{P}{2}} b_0 \mathbf{h}_l \tag{2.4}$$

The term $\mathbf{h}_l$ represents an M-dimensional signal vector for the l-th resolvable path. After applying antenna weights for each finger $\mathbf{w}_l$, the following is obtained:

$$z_l = \mathbf{w}_l^H \mathbf{r}_l \tag{2.5}$$

where $(.)^H$ operator represents a Hermitian transpose. This can be rewritten as a summation over antenna elements as:

$$z_l = \sum_{m=1}^{M} w_{l,m}^* r_{l,m} \tag{2.6}$$

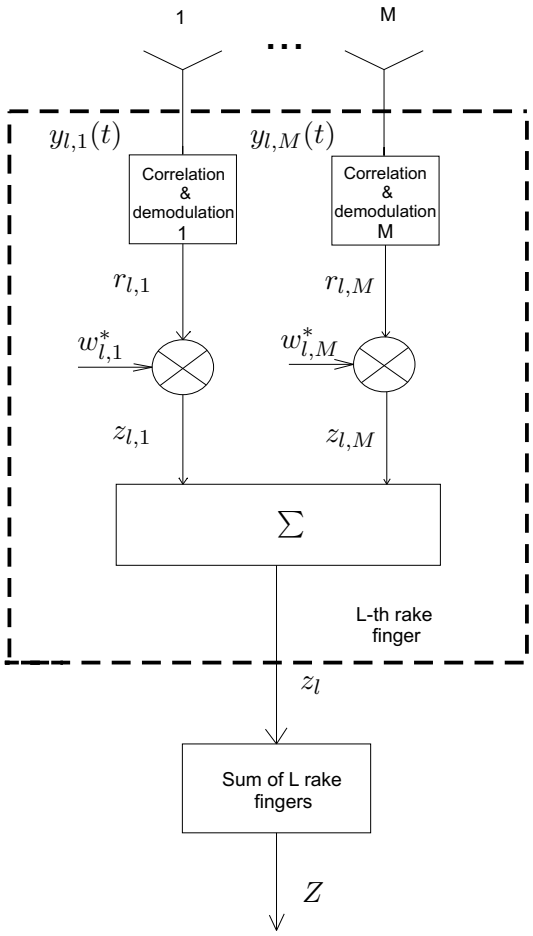

Figure 2.2: Rake-antenna processing

---

where index m associates the corresponding vector element with the m-th antenna. In case of MRC processing, the antenna weights are defined as:

$$\mathbf{w}_l = \mathbf{h}_l \tag{2.7}$$

There is an obvious analogy to the Rake receiver with a single antenna. If MRC is applied, the receiver operates as a two-dimensional Rake receiver in delay and space domain, where the total number of fingers is $L \cdot M$. The final signal is obtained as the summation of all signals on L Rake fingers and

M antenna elements:

$$Z = \sum_{l=1}^{L} z_l = \sum_{l=1}^{L} \sum_{m=1}^{M} w_{l,m}^{*} r_{l,m} \tag{2.8}$$

This receiver is optimum only for a spatially-white interference. If the spatial structure of MAI is significant, OC represents the most optimal processing technique. Let $\mathbf{h}_j, j = 1, ...K$ be signal vectors of $K-1$ independent interfering sources, with the corresponding transmit powers P_j (assuming the total number of users K). The SINR for each Rake finger γ_l can be written as:

$$\gamma_l = \frac{P|\mathbf{w}_l^H \mathbf{h}_l|^2}{\sum_{j=1}^{K-1} P_j|\mathbf{w}_l^H \mathbf{h}_j|^2 + \sigma^2|\mathbf{w}_l|^2} \tag{2.9}$$

According to the spatial filter Wiener solution [34], the antenna weight vector that maximises SINR, given by Eq. 2.9, is a function of the spatial signature of the desired user $\mathbf{h}_l$ and the spatial correlation matrix of interference $\mathbf{R}_{in}$, given as:

$$\mathbf{R}_{in} = \sum_{j=1}^{K-1} \frac{P_j}{P} \mathbf{h}_j \mathbf{h}_j^H + \frac{\sigma^2}{P} \mathbf{I}_M \tag{2.10}$$

where $\mathbf{I}_M$ represents an $M \times M$ identity matrix and σ^2 is the power of the thermal noise. Optimum weight vector $\mathbf{w}_l$ that maximises γ_l is defined as:

$$\mathbf{w}_l = \mathbf{R}_{in}^{-1} \mathbf{h}_l \tag{2.11}$$

The derivation of Eq. 2.11 is given in Appendix A. As a result, the maximum SINR can be written in the following compact form:

$$\gamma_l = \mathbf{h}_l^H \mathbf{R}_{in}^{-1} \mathbf{h}_l \tag{2.12}$$

2.4 Signal and receiver model

Now that the basic principle of Rake-antenna processing is explained, a simplified signal and receiver model for UMTS can be derived. The transmit signal for the i-th user, with the corresponding transmit power P_i, can be represented as:

$$u_i(t) = \sqrt{2P_i} b_i(t) \cdot s_i(t) \cos(2\pi f_c t + \theta_i) \tag{2.13}$$

where $b_i(t)$ is a bipolar information bearing signal (data bit, with T_s symbol duration), $s_i(t)$ is a spreading waveform (pseudo-random sequence with T_c

chip duration), f_c is the carrier frequency and θ_i represents the random phase of the i-th user modulator. The data signal and the spreading sequence are defined as follows:

$$b_i(t) = \sum_{n=-\infty}^{\infty} b_{i,n} p_b(t - nT_s), b_{i,n} = \pm 1 \tag{2.14}$$

$$s_i(t) = \sum_{n=-\infty}^{\infty} s_{i,n} p_s(t - nT_c), s_{i,n} = \pm 1 \tag{2.15}$$

Here $p_b(t)$ and $p_s(t)$ represent rectangular pulses of unit height and duration of T_s and T_c respectively. The UMTS pulse shaping filter, a root-raised cosine [35], was not included in the modelling. The signal for the i-th user at the input of the receiver, after being transmitted via a multipath propagation channel, can be written in terms of *ray parameters* as follows:

$$\mathbf{y}_i(t) = \sum_{q=1}^{Q_i} \alpha_{q,i} \exp(j\phi_{q,i}) \mathbf{a}(\varphi_{q,i}) u_i(t - \tau_{q,i}) \tag{2.16}$$

where $\alpha_{q,i}$, $\phi_{q,i}$, $\tau_{q,i}$, $\varphi_{q,i}$, represent i-th user amplitude, phase, time delay and angle-of-arrival for the q-th propagation path, respectively, and Q_i is the total number of dominant multipaths. The term $\mathbf{a}(\varphi) = [a_1(\varphi), a_2(\varphi), ..., a_M(\varphi)]$ represents an M-dimensional antenna steering vector, with elements defined in case of a linear array, as:

$$a_m(\varphi) = \exp(-\jmath \frac{2\pi}{\lambda_c}(m-1) d \sin\varphi) \tag{2.17}$$

where d is the spacing between adjacent antenna array elements and λ_c denotes the carrier wavelength. For a circular array, the elements of the antenna steering vector are defined as:

$$\begin{aligned} a_m(\varphi) \quad = \quad & \exp(-\jmath \frac{2\pi}{\lambda_c} \{ R \cos((m-1)\frac{2\pi}{M}) \cos(\varphi) + \\ & R \sin((m-1)\frac{2\pi}{M}) \sin(\varphi) \}) \end{aligned} \tag{2.18}$$

where R represents the radius of the array. The separation between two antenna elements used in the thesis is $d = \lambda_c/2$. This assures high correlation between signals on an antenna array, which is necessary to optimise the antenna pattern in favour of the desired user and against interference (unlike diversity cases when larger spacing between antenna elements is needed in

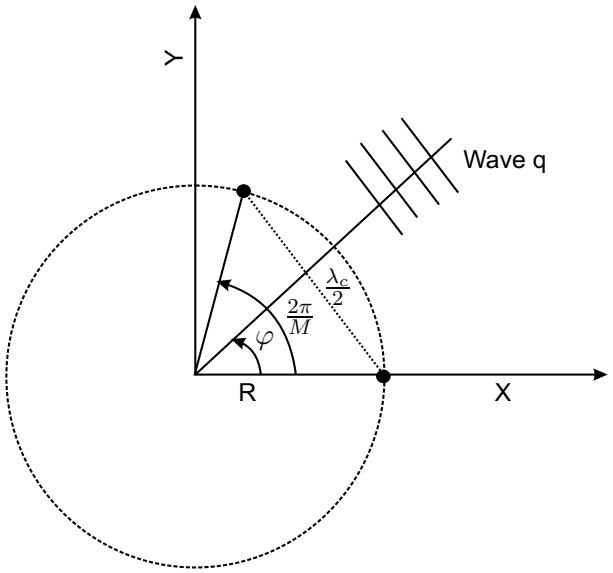

Figure 2.3: Antenna array configuration

order to obtain independent fading signals for any angular distribution). In [36], a half-wavelength antenna spacing was found optimum in case of simple beamforming and for a uniform spatial distribution of interfering sources. The antenna array radius is, then, given as:

$$R = \frac{\lambda_c}{4\sin(\pi/M)} \tag{2.19}$$

In the simulations performed in this study, a circular antenna array is assumed in order to circumvent sensitivity to antenna array orientation. The configuration of a circular array with parameters defined as above and for an arbitrary q-th multipath component (with the corresponding angle-of-arrival φ), impinging on the array, is shown in Fig. 2.3. Only two antenna elements are depicted in the figure to allow for the general case description with an arbitrary number M of antenna elements. The waves arriving in the horizontal plane are considered in the antenna array model.

In a system with K users, the total received signal is given as follows:

$$\mathbf{y}(t) = \mathbf{y}_i(t) + \sum_{j=1, j\neq i}^{K} \mathbf{y}_j(t) + \mathbf{n}(t) \tag{2.20}$$

where $\mathbf{y}_i(t)$ represents the desired signal, $\mathbf{y}_j(t)$ is the received signal belonging to the j-th interfering user ($j \neq i, j = 1, ...K$) and $\mathbf{n}(t)$ represents the thermal noise vector. The desired user signal received at the l-th Rake finger $\mathbf{r}_{l,i}$, subsequent to despreading and demodulation (with perfect synchronisation assumed) is given as follows:

$$\mathbf{r}_{l,i} = \sqrt{2P_i} \int_{\tau_{l,i}}^{\tau_{l,i}+T_s} \mathbf{y}_i(t) s_i^*(t - \tau_{l,i}) \cos(2\pi f_c t + \theta_i) dt = \sqrt{\frac{P_i}{2}} b_0 \mathbf{h}_{l,i} \quad (2.21)$$

The term $\mathbf{h}_{l,i}$ represents an overlay of multipath signals received by an M-dimensional antenna array, which fall into the l-th delay bin, where $\tau_{l,i} = (l-1)T_c + \tau_{0,i}$. It will be referred to as i-th user *spatial signature* for the l-th Rake finger and is defined as:

$$\mathbf{h}_{l,i} = \sum_{q=1}^{Q_i} \alpha_{q,i} \exp(\jmath\phi_{q,i}) \mathbf{a}(\varphi_{q,i}) R_s(\tau_{q,i} - \tau_{l,i}) \quad (2.22)$$

Here, $R_s(.)$ represents the autocorrelation of the PN sequence. The autocorrelation is ideally assumed to have a triangular shape with the base equal to $2T_c$, as given by:

$$R_s(\tau_{q,i} - \tau_{l,i}) = \begin{cases} 1 - |\frac{\tau_{q,i} - \tau_{l,i}}{2T_c}|, & |\frac{\tau_{q,i} - \tau_{l,i}}{2T_c}| < 1 \\ 0 & \text{otherwise} \end{cases} \quad (2.23)$$

The transmit signal for the j-th user ($j \neq i$) can be written, analogous to Eq. 2.16, as:

$$\mathbf{y}_j(t) = \sum_{q=1}^{Q_j} \alpha_{q,j} \exp(\jmath\phi_{q,j}) \mathbf{a}(\varphi_{q,j}) u_j(t - \tau_{q,j}) \quad (2.24)$$

The signal corresponding to the j-th user generates interference at the l-th Rake finger after cross-correlation with the PN sequence of the desired signal. If the term $\alpha_{q,j} \exp(\jmath\phi_{q,j}) \mathbf{a}(\varphi_{q,j})$ in Eq. 2.24, which is a function of the *ray parameters* and is associated with the q-th multipath component, is conveniently separated from the time-dependent term $u_j(t - \tau_{q,j})$ by replacing it with a single factor $\mathbf{F}_{q,j}$ in further representation, the input interfering signal at the receiver becomes:

$$\mathbf{y}_j(t) = \sum_{q=1}^{Q_j} \mathbf{F}_{q,j} u(t - \tau_{q,j}) \quad (2.25)$$

The interference generated at the l-th Rake finger after cross-correlation can be written as [37]:

$$\mathbf{r}_{l,j} = \sqrt{\frac{P_j}{2}} \sum_{q=1}^{Q_j} \{b_{j,-1} R_{j,i}(\tau_{q,j} - \tau_{l,i}) + b_{j,0} \hat{R}_{j,i}(\tau_{q,j} - \tau_{l,i})\} \mathbf{F}_{q,j} \tag{2.26}$$

The signal of the j-th interfering user is dependent on partial cross-correlations $R_{j,i}$ and $\hat{R}_{j,i}$ between PN sequences belonging to the i-th and j-th user and adjacent data bits $b_{j,-1}$ and $b_{j,0}$. The partial cross-correlations are defined as follows:

$$R_{j,i}(\tau) = \int_0^{\tau} s_j(t-\tau) s_i(t) dt \tag{2.27}$$

$$\hat{R}_{j,i}(\tau) = \int_{\tau}^{T_s} s_j(t-\tau) s_i(t) dt \tag{2.28}$$

The i-th user desired signal for the l-th Rake finger, after applying antenna weights for MRC and OC, can be written as:

$$S_{l,i}^{mrc} = (\mathbf{w}_{l,i}^{mrc})^H \mathbf{r}_{l,i} \tag{2.29}$$

$$S_{l,i}^{oc} = (\mathbf{w}_{l,i}^{oc})^H \mathbf{r}_{l,i} \tag{2.30}$$

Similarly, the i-th user interfering signal coming from the j-th user at the l-th Rake finger can be written for MRC and OC as:

$$I_{l,i,j}^{mrc} = (\mathbf{w}_{l,i}^{mrc})^H \mathbf{r}_{l,j} \tag{2.31}$$

$$I_{l,i,j}^{oc} = (\mathbf{w}_{l,i}^{oc})^H \mathbf{r}_{l,j} \tag{2.32}$$

2.5 Spatial channel model

A signal model for the Rake-antenna array receiver has been derived. For the calculation of the average powers on the basis of *ray parameters*, a spatial model will be proposed. Global channel parameters like delay and angular spread are initially defined in Section 2.5.1, the derivation of average powers of the desired and interfering signals is shown in Section 2.5.2, followed by derivation of SINR for the Rake-antenna processing in Section 2.5.3.

2.5.1 Channel parameters

The rms delay spread σ_τ is defined as the square root of the second moment of the power dispersion in delay domain [15]. Expressed in terms of the deterministic *ray parameters*, i.e. amplitude α_q and delay τ_q for each contributing wave $q, q = 1, ..Q$, it can be written as follows:

$$\sigma_\tau = \sqrt{\bar{\tau}^2 - (\tau_m)^2} \tag{2.33}$$

$$\bar{\tau}^2 = \frac{\sum_{q=1}^{Q} \alpha_q^2 \tau_q^2}{\sum_{q=1}^{Q} \alpha_q^2} \tag{2.34}$$

$$\tau_m = \frac{\sum_{q=1}^{Q} \alpha_q^2 \tau_q}{\sum_{q=1}^{Q} \alpha_q^2} \tag{2.35}$$

The rms angular spread Λ is defined as the root mean square of the power dispersion in angular domain. The angular spread is defined on the basis of *ray parameters*, i.e. amplitude α_q and angle-of-arrival φ_q for each wave $q, q = 1, ...Q$, as follows:

$$\Lambda = \sqrt{\frac{\sum_{i=q}^{Q} \alpha_q^2 (\varphi_q - \bar{\varphi})^2}{\sum_{q=1}^{Q} \alpha_q^2}} \tag{2.36}$$

Here $\bar{\varphi}$ represents the mean angle in the direction of the centre of gravity, defined as:

$$\bar{\varphi} = arctan(\frac{\sum_{q=1}^{Q} \alpha_q^2 cos(\varphi_q)}{\sum_{q=1}^{Q} \alpha_q^2 sin(\varphi_q)}) \tag{2.37}$$

2.5.2 Average powers of the desired and interfering signal

The signal model has been derived assuming that the complete composition of waves, i.e. *ray parameters*, is known for a certain position of the MS. Interference caused by the j-th user at the l-th Rake finger $\mathbf{r}_{l,j}$ includes a factor $F_{q,j} = \alpha_{q,j} \exp(j\phi_{q,j})\mathbf{a}(\varphi_{q,j})$ for each multipath wave q, which is purely deterministic, and a factor that represents the cross-correlation between PN sequences belonging to different users (see Eq. 2.26), which is stochastic.

The cross-correlation factor, associated with PN sequences belonging to the i-th and j-th user, is written again for convenience and is termed as C_{ij}:

$$C_{ij} = b_{j,-1} R_{j,i}(\tau_{q,j} - \tau_{l,i}) + b_{j,0} \hat{R}_{j,i}(\tau_{q,j} - \tau_{l,i}) \tag{2.38}$$

$$C_{ij} = b_{j,-1}R_{j,i}(\tau_{q,j} - (l-1)T_c - \tau_{0,i}) + b_{j,0}\hat{R}_{j,i}(\tau_{q,j} - (l-1)T_c - \tau_{0,i}) \quad (2.39)$$

The term $\tau_{0,i}$, representing the delay of the first incoming ray for the i-th user, is assumed to be a uniform distributed random variable in the interval $[0, T_s]$ for asynchronous uplink transmission. PN sequences are assumed to be random binary sequences, similarly to the approach given in [37], where the effect of cross-correlation is modelled as an average value, which is common to all pairs of sequences. The factor C_{ij} is statistical and since ultimate results in this thesis are based on average powers of interfering users, it is necessary to include the influence of the average squared factor $E\{C_{ij}^2\}$. The result, representing an average over different PN sequences and over $\tau_{0,i}$ is given as [38], [39]:

$$E\{C_{ij}^2\} = E\{[b_{j,-1}R_{j,i}(\tau_{q,j} - \tau_{l,i}) + b_{j,0}\hat{R}_{j,i}(\tau_{q,j} - \tau_{l,i})]^2\} = \frac{2}{3N} \quad (2.40)$$

This average value is not specific to any pair of PN sequences and is a function of the PN sequence length N only. In the following analysis, the effect of the correlation parameter on the modelling of interfering signals will be shown.

The ultimate parameter of interest, i-th user SINR at the l-th Rake finger, is defined on the basis of average powers of the desired and interfering users as:

$$\gamma_{l,i}^{mrc|oc} = \frac{|S_{l,i}^{mrc|oc}|^2}{E\{\sum_{j=1,j\neq i}^{K} |I_{l,i,j}^{mrc|oc}|^2\} + (\sigma_{l,i}^{mrc|oc})^2} \quad (2.41)$$

The average power of the total contribution of all interfering users equals the summation of average powers belonging to each interfering user. This is valid under the assumption that data bits for different users are mutually uncorrelated. The average power of the j-th interfering user can be written as:

$$E\{|I_{l,i,j}^{mrc|oc}|^2\} = E\{|(\mathbf{w}_{l,i}^{mrc|oc})^H \mathbf{r}_{l,j}^{mrc|oc}|^2\} \quad (2.42)$$

In case of MRC, antenna combining weights are defined as:

$$\mathbf{w}_{l,i}^{mrc} = \mathbf{h}_{l,i} \quad (2.43)$$

which results in the following expression for the interference power:

$$E\{|I_{l,i,j}^{mrc}|^2\} = E\{|\mathbf{h}_{l,i}^H \mathbf{r}_{l,j}^{mrc}|^2\} \quad (2.44)$$

$$E\{|I_{l,i,j}^{mrc}|^2\} = \frac{P_j}{2N}|\mathbf{h}_{l,i}^H \mathbf{h}_j|^2 \quad (2.45)$$

The term $\mathbf{h}_j$ will be referred to as spatial signature of the interfering signal and is defined as:

$$\mathbf{h}_j = \sum_{q=1}^{Q_j} \sqrt{\frac{2}{3}} \alpha_{q,j} \exp(\jmath\phi_{q,j}) \mathbf{a}(\varphi_{q,j}) \tag{2.46}$$

The last expression gives an insight into the modelling of interfering signals on the basis of *ray parameters*. The amplitude of each multipath wave, composing the spatial signature of the interfering signal, is scaled by the coefficient $\sqrt{2/3}$ (see Eq. 2.40). The dependence on a specific Rake finger is excluded, i.e. all interfering multipath components contribute by the scaling coefficient of $\sqrt{2/3}$ for each Rake finger. The factor N refers to the effective increase in the received desired signal power over the total interference. This is the processing gain, which is already introduced as a factor that indicates the level of separation between users in the code domain. In the further annotation, processing gain N will be included with the desired signal, as a multiplicative factor. The power of interference coming from the thermal noise can be written as:

$$(\sigma_{l,i}^{mrc|oc})^2 = \sigma^2 |\mathbf{w}_{l,i}^{mrc|oc}|^2 \tag{2.47}$$

where σ^2 represents the power of the thermal noise at the receiver input, which is defined as:

$$\sigma^2 = \frac{N_0}{T_c} \tag{2.48}$$

Here, N_0 represents the spectral density of the thermal noise at the BS. The power of the desired signal for MRC can be written as:

$$|S_{l,i}^{mrc}|^2 = N \frac{P_i}{2} |\mathbf{h}_{l,i}|^4 \tag{2.49}$$

In the case of OC the antenna weight vector $\mathbf{w}_{l,i}^{oc}$, which maximises SINR, will be given as (see Eq. 2.10 and Eq. 2.11):

$$\mathbf{w}_{l,i}^{oc} = \mathbf{R}_{in,i}^{-1} \mathbf{h}_{l,i} \tag{2.50}$$

$$\mathbf{R}_{in,i} = \sum_{j=1, j\neq i}^{K} \frac{P_j}{P_i} \mathbf{h}_j \mathbf{h}_j^H + \sigma^2 \mathbf{I}_M \tag{2.51}$$

The power of the i-th desired and j-th interfering signal at the l-th Rake finger are, respectively, given as:

$$|S_{l,i}^{oc}|^2 = N \frac{P_i}{2} |(\mathbf{R}_{in,i}^{-1} \mathbf{h}_{l,i})^H \mathbf{h}_{l,i}|^2 \tag{2.52}$$

$$E\{|I_{l,i,j}^{oc}|^2\} = \frac{P_j}{2}(|\mathbf{R}_{in,i}^{-1}\mathbf{h}_{l,i})^H\mathbf{h}_j|^2 \tag{2.53}$$

Pure Rake combining involves maximum ratio combining in the delay domain. In that case, the concept of the *spatial signature* is replaced by a one-dimensional (1-D) signature $h_{l,i}^{rake}$, which represents the signal received by one antenna only. It is defined in terms of the *ray parameters*, as follows:

$$h_{l,i}^{rake} = \sum_{q=1}^{Q_i} \alpha_{q,i} \exp(\jmath\phi_{q,i}) R_s(\tau_{q,i} - \tau_{l,i}) a_1(\varphi_{q,i}) \tag{2.54}$$

Similarly, the 1-D signature of the j-th interfering user will be given as:

$$h_j^{rake} = \sum_{q=1}^{Q_j} \sqrt{\frac{2}{3}} \alpha_{q,i} \exp(\jmath\phi_{q,i}) a_1(\varphi_{q,i}) \tag{2.55}$$

Since Rake finger weights $w_{l,i}^{rake}$ are defined as $w_{l,i}^{rake} = h_{l,i}^{rake}$, the corresponding powers of the i-th desired, j-th interfering user and thermal noise for the single antenna case are, respectively, given as (analogous to MRC in the space domain):

$$|S_{l,i}^{rake}|^2 = NP_i|h_{l,i}^{rake}|^4 \tag{2.56}$$

$$E\{|I_{l,i,j}^{rake}|^2\} = P_j|(h_{l,i}^{rake})^* h_j^{rake}|^2 \tag{2.57}$$

$$(\sigma_{l,i}^{rake})^2 = \sigma^2|w_{l,i}^{rake}|^2 \tag{2.58}$$

2.5.3 SINR calculation

In Section 2.5.2, the powers of the desired and interfering users have been derived on the basis of the *ray parameters*. It is now possible to calculate the total SINR for a single antenna case, MRC and OC. The total signal for the i-th user and l-th Rake finger, including the three cases, will be:

$$z_{l,i}^{rake|mrc|oc} = S_{l,i}^{rake|mrc|oc} + \sum_{j=1,j\neq i}^{K} I_{l,i,j}^{rake|mrc|oc} + n_{l,i}^{rake|mrc|oc} \tag{2.59}$$

Assuming that data bits belonging to different users are mutually independent, the total interference power coming from $K-1$ users is equal to the power sum over all interfering users. SINR for the i-th user and l-th finger $\gamma_{l,i}$ is, then, given by:

$$\gamma_{l,i}^{rake|mrc|oc} = \frac{|S_{l,i}^{rake|mrc|oc}|^2}{\sum_{j=1,j\neq i}^{K} E\{|I_{l,i,j}^{rake|mrc|oc}\}|^2 + (\sigma_{l,i}^{rake|mrc|oc})^2} \tag{2.60}$$

The SINR for the flat-fading channel, i.e. only one Rake finger is active, will be treated first, followed by the case featuring multiple Rake fingers.

SINR for the flat-fading channel

In the following derivations, the index designating a Rake finger will be omitted from the variables representing the spatial signature, antenna weight vector and the achieved SINR, assuming that corresponding definitions hold for the first Rake finger, i.e. $l = 1$. The processing involving a single Rake finger and a single antenna will be treated as a *reference* case.

Referring to the theory given in Section 2.5.2, the i-th user SINR for a single antenna case γ_i^{ref} will be given as:

$$\gamma_i^{ref} = \frac{|S_{1,i}^{ref}|^2}{|I_{1,i}^{ref}|^2 + (\sigma_{1,i}^{ref})^2} = N\frac{|(w_i^{ref})^H h_i^{ref}|^2}{\sum_{j=1,j\neq i}^{K} |(w_i^{ref})^H h_j^{ref}|^2 + \sigma^2 |w_i^{ref}|^2} \tag{2.61}$$

$$\gamma_i^{ref} = N\frac{P_i |h_i^{ref}|^4}{\sum_{j=1,j\neq i}^{K} P_j |(h_i^{ref})^H h_j^{ref}|^2 + \sigma^2 |h_i^{ref}|^2} \tag{2.62}$$

The Rake receiver is optimal in Gaussian noise only. In that case, the achieved SINR reduces to the following expression:

$$\gamma_i^{ref} = N\frac{P_i |h_i^{ref}|^2}{\sigma^2} \tag{2.63}$$

The i-th user SINR in case of MRC γ_i^{mrc} is given as:

$$\gamma_i^{mrc} = \frac{|S_{1,i}^{mrc}|^2}{|I_{1,i}^{mrc}|^2 + (\sigma_{1,i}^{mrc})^2} = N\frac{|(\mathbf{w}_i^{mrc})^H \mathbf{h}_i|^2}{|(\mathbf{w}_i^{mrc})^H \mathbf{h}_j|^2 + \sigma^2 |\mathbf{w}_i^{mrc}|^2} \tag{2.64}$$

$$\gamma_i^{mrc} = N\frac{P_i |\mathbf{h}_i|^4}{\sum_{j=1,j\neq i}^{K} P_j |(\mathbf{h}_i)^H \mathbf{h}_j|^2 + \sigma^2 |\mathbf{h}_i|^2} \tag{2.65}$$

MRC processing is also optimal in a Gaussian or spatially-white noise. Analogous to the results for the pure Rake processing in delay domain, the i-th user SINR in a Gaussian noise becomes:

$$\gamma_i^{mrc} = N\frac{P_i |\mathbf{h}_i|^2}{\sigma^2} \tag{2.66}$$

Finally, the i-th user SINR in case of OC is given as:

$$\gamma_i^{oc} = \frac{|S_{1,i}^{oc}|^2}{|I_{1,i}^{oc}|^2 + (\sigma_{1,i}^{oc})^2} = N\frac{|(\mathbf{w}_i^{oc})^H \mathbf{h}_i|^2}{|(\mathbf{w}_i^{oc})^H \mathbf{h}_j|^2 + \sigma^2 |\mathbf{w}_i^{oc}|^2} \tag{2.67}$$

The last equation resorts to a compact form when antenna weights are defined by Eq. 2.50, as shown in Section 2.3:

$$\gamma_i^{oc} = N\mathbf{h}_i^H \mathbf{R}_{in,i}^{-1} \mathbf{h}_i \tag{2.68}$$

$$\mathbf{R}_{in,i} = \sum_{j=1, j\neq i}^{K} \frac{P_j}{P_i} \mathbf{h}_j \mathbf{h}_j^H + \sigma^2 \mathbf{I}_M \tag{2.69}$$

In this study, antenna processing is analysed using deterministic data. The statistics originating from asynchronous transmission and different PN sequences is included in terms of an average factor, as shown by Eq. 2.40, while the rest is treated deterministically. In previous studies, the term *spatially-white* has been used strictly from the statistical point of view. Channel realisations are generated from a certain power delay-angular distribution and the spatial correlation matrix of interference is calculated by averaging over a certain time period. In the current approach, every spatial position is characterised by a concrete channel composition. Spatial signatures can be determined using *ray parameters* and in turn average SINR, related to the location of the desired user and for arbitrary locations of interferers. From the strictly statistical point of view, the term *spatially- white* indicates that the normalised correlation matrix of interference is equal to an identity matrix. In that case, OC performs equally to MRC, as as can be directly seen from Eq. 2.66 and Eq. 2.68.

Instead of using the term *spatially-white* to indicate that interfering users may correlate with the desired one in the same way as a Gaussian noise, one can say that the *spatial structure* of interfering users is not influential to the OC versus MRC result. This represents one of the novel features of the modelling approach presented in this thesis. The term *spatial structure* refers to the relation among vector spaces defined by spatial signatures of the desired and interfering users, which are established deterministically. Basically MRC gives similar results as OC in the following cases:

- The received powers of interferers is negligible compared to the power of the desired signal. In that case the only noise "seen" by an antenna array is the thermal Gaussian noise. The received powers of interferers depend on the transmit powers and power loss due to propagation effects in an urban environment, like direct path-loss and shadowing. The influence of the transmit power will be more clear in Chapter 4, when the effect of the power control process is included.

- In case the received powers of interfering users and the desired one are comparable, the spatial structure will become important. However, if

the following relationship is true, the spatial structure of interference can be treated as not influential to the OC versus MRC result:

$$\mathbf{R}_{in,i}^{-1}\mathbf{h}_i = \mathbf{h}_i \tag{2.70}$$

This condition is, actually, equal to the statement that the antenna weight vector for OC and MRC is the same: $\mathbf{w}_i^{mrc} = \mathbf{w}_i^{oc}$. From the studies involving a statistical approach, the expression *spatially-white* interference means that the autocorrelation matrix $\mathbf{R}_{in,i}$ is equal to the identity matrix. The condition, given by Eq. 2.70, implies a wider-sense situation: the spatial signature of the desired user is equal to the eigenvector, corresponding to the largest eigenvalue of the matrix $\mathbf{R}_{in,i}^{-1}$. In reality, the exact equality will never be fulfilled, but also in the case of an approximate equality, there will not be a significant gain of using OC over MRC. Assuming that the powers of interfering users are fixed (a non power-controlled situation), the condition given by Eq. 2.70 will result in the same i-th user SINR for given transmit powers of the desired P_i and interfering users $P_j, j \neq i, j = 1, ..K$, or the same transmit power of the i-th user for a given desired SINR.

- In a multi-user power-controlled environment, the conditions under which OC gives the same results as MRC in terms of optimum transmit power for the given target SINR, are even less strict than what is given by Eq. 2.70. More details will be given in Chapter 4

SINR for a frequency selective channel

In case there is more than one active Rake finger, the total output signal for pure Rake combining and MRC will be given as the sum of signals on all Rake fingers. Assuming there are L active Rake fingers, the i-th user signal is given as:

$$Z_i^{rake|mrc} = \sum_{l=1}^{L} z_{l,i}^{rake|mrc} \tag{2.71}$$

$$Z_i^{rake|mrc} = S_i^{rake|mrc} + \sum_{j=1,j\neq i}^{K-1} I_{i,j}^{rake|mrc} + n_i^{rake|mrc} \tag{2.72}$$

The total desired and interfering signal are, respectively, given as:

$$S_i^{rake|mrc} = \sum_{l=1}^{L} S_{l,i}^{rake|mrc} \tag{2.73}$$

$$I_{i,j}^{rake|mrc} = \sum_{l=1}^{L} I_{l,i,j}^{rake|mrc} \tag{2.74}$$

The total SINR after pure Rake combining/MRC $\gamma_i^{rake|mrc}$ can be written as:

$$\gamma_i^{rake|mrc} = \frac{|S_i^{rake|mrc}|^2}{\sum_{j=1,j\neq i}^{K} |I_{i,j}^{rake|mrc}|^2 + (\sigma_i^{rake|mrc})^2} \tag{2.75}$$

where $(\sigma_i^{rake/mrc})^2$ represents the total noise power as a result of Rake combining, and is defined as the summation of noise powers over Rake fingers as:

$$(\sigma_i^{rake/mrc})^2 = \sum_{l=1}^{L} (\sigma_{l,i}^{rake/mrc})^2 \tag{2.76}$$

The i-th user SINR for pure Rake combining and MRC is then:

$$\gamma_i^{rake} = N \frac{P_i (\sum_{l=1}^{L} |h_{l,i}^{rake}|^2)^2}{\sum_{j=1,j\neq i}^{K} P_j |\sum_{l=1}^{L} (h_{l,i}^{rake})^* h_j^{rake}|^2 + \sigma^2 \sum_{l=1}^{L} |h_{l,i}^{rake}|^2} \tag{2.77}$$

$$\gamma_i^{mrc} = N \frac{P_i (\sum_{l=1}^{L} |\mathbf{h}_{l,i}|^2)^2}{\sum_{j=1,j\neq i}^{K} P_j |\sum_{l=1}^{L} (\mathbf{h}_{l,i})^H \mathbf{h}_j|^2 + \sigma^2 \sum_{l=1}^{L} |\mathbf{h}_{l,i}|^2} \tag{2.78}$$

In case of OC, a simple summation of signals over Rake fingers after applying antenna weights (as is the case for pure Rake combining and MRC) is no longer valid. The signals on different Rake fingers $z_{l,i}^{oc}, l = 1, ...L$, obtained as a result of optimum combining, have to be equalised in phase first by applying coefficients equal to the complex conjugate of the desired signal, as:

$$Z_i^{oc} = \sum_{l=1}^{L} \zeta_{l,i}^* z_{l,i}^{oc} = \sum_{l=1}^{L} \zeta_{l,i}^* (S_{l,i}^{oc} + \sum_{j=1,j\neq i}^{K} I_{l,i,j}^{oc} + n_{l,i}^{oc}) \tag{2.79}$$

By applying the coefficient $\zeta_{l,i}^*$, signals from Rake fingers are coherently combined. It is equal to the complex desired signal obtained as a result of OC: $\zeta_{l,i} = S_{l,i}^{oc}$ (see also Eq. 2.30.). The resulting SINR γ_i^{oc} is given as:

$$\gamma_i^{oc} = \frac{(\sum_{l=1}^{L} |S_{l,i}^{oc}|)^2}{\sum_{j=1,j\neq i}^{K} |\sum_{l=1}^{L} (S_{l,i}^{oc})^* I_{l,i,j}^{oc}|^2 + \sum_{l=1}^{L} (\sigma_{l,i}^{oc})^2} \tag{2.80}$$

2.6 Conclusions

In this chapter, a novel method to incorporate simplified UMTS aspects using a deterministic channel model is proposed. Analytical formulas for calculating SINR for the pure Rake combining, MRC and OC at the UMTS base station receiver are given in terms of *ray parameters*. The simulation results in the following chapters are based on the theory presented here.

3

Comparison between a deterministic and a stochastic channel model

3.1 Introduction

As pointed out in Chapter 1, channel models can be roughly divided into those where the channel description is given in terms of statistics, i.e. stochastic models, and those that include concrete information about environment, i.e. deterministic models. Models based on the stochastic approach generally assume certain statistics related to global channel characteristics such as the dispersion of power in delay and angular domain, large-scale and small-scale fading. Deterministic models incorporate site-specific data, like buildings and vegetation information.

Models developed within the 3GPP framework for testing the performance of 3G systems are largely based on the statistical modelling approach, due to difficulties in including more deterministic data in a flexible way. However, it is important to study how accurate a channel model for 3G systems should be and wether it it necessary to include more deterministic data than what is included in the current stochastic models. In the light of this statement, the comparison of two models, the deterministic ray-tracing model μFipre and the stochastic Wideband Directional Channel Model (WDCM) [16] is dealt with in this chapter. The results of the comparison are given in terms of the achieved SINR for Rake-antenna processing for UMTS. The ray-tracing model is used as a benchmark, having been initially verified

through measurements. Diverse propagation mechanisms are included like: reflections from building walls, diffraction on building corners, transmission through buildings and scattering from vegetation. In the stochastic model, on the other hand, the propagation environment is defined in terms of a statistical spatial distribution of scatterers. The parameters that describe the spatial distribution of scatterers represent the input to the model. In order to allow for a fair comparison between the two models, the stochastic model has to be "tuned"to μFipre by determining input parameters that make WDCM reflect the propagation conditions from the ray-tracing model as best as possible.

In Section 3.2 and Section 3.3, a detailed description of the deterministic μFipre and the stochastic WDCM is, respectively, given. In Section 3.4, the procedure of tuning the stochastic model to μFipre on the basis of the delay and angular spread (the parameters representing global channel characteristics) is described and results compared in terms of the obtained SINR. The results of the tuning procedure on the basis of a different parameter, found very dominant for the achieved SINR result and referred to as a *spatial separation parameter*, are shown in Section 3.5. The conclusions are drawn in Section 3.6.

3.2 Ray-tracing model

The description of the ray-tracing model, in terms of the input data from a concrete environment and explanation of the ray tracing procedure, is given in Section 3.2.1. The verification of the model on the basis of measurements is presented in Section 3.2.2.

3.2.1 General description of the μFipre ray-tracing model

The earliest work in the field of deterministic modelling of radiowave propagation is represented in [40], where the main focus was on the planning for land mobile satellite systems. The result of this work, the three-dimensional software called *FiPre*, was later adapted for propagation prediction for terrestrial mobile communication systems [41]. The ray-tracing model μFipre, developed for the planning of urban micro-cells, makes use of a detailed information about buildings and vegetation in a given environment and also accounts for the transmission through buildings and scattering from trees in addition to standard propagation mechanisms like reflections and diffractions, already included in earlier ray-tracing versions. The ray-tracing model is two-dimensional (2-D), which is adequate for urban micro-cells where the

height of the BS antenna is much below the average rooftop level. The model neglects over-rooftop propagation and ground reflection. The following propagation mechanisms are modelled: direct wave or line-of-sight (LOS) propagation, reflection from building faces, transmission through buildings, diffraction by building corners (both internal and external) and scattering from trees.

The information about buildings that serves as an input to the model are databases containing 2-D coordinates of building corners, complex permitivities ε_r and specific attenuation coefficients α_b. The specific attenuation coefficient is important for modelling the transmission through buildings and accounts for the influence of a building interior. This parameter is taken to be α_b=2 dB/m, which is obtained empirically as a result of averaging over 22 different buildings [42]. Equal values for permitivities are used for all buildings in the environment, assuming a homogeneous building structure. The information about vegetation includes the heights of trees, tree canopy radii, as well as equivalent scattering amplitudes and cross sections per unit volume of the tree canopies (more details are given in [7]). Other parameters that can be specified as an input to the model are the frequency, location of the BS and maximum permitted ray order. The ray order determines the accuracy of the predictions, since it specifies the maximum number of successive interactions of the ray with the environment, while propagating from MS to the BS. Furthermore, it is possible to specify the ray order for the specific type of interaction.

The ray tracing procedure is based on the virtual sources concept. The real source, i.e. the MS, generates new virtual sources in the presence of scattering objects, like buildings and trees. These scattering objects act as real sources and generate new propagating waves, which in turn give rise to new virtual sources as a result of interaction with the environment. This is repeated until the specified maximum ray order is reached. The output of μFipre represents a detailed information about rays propagating from MS to the BS, including the coordinates of the virtual sources i.e. points of interactions. The output data, associated with each multipath component, includes the received power level, the length of the covered distance and phases. From the received power information, it is possible to calculate the amplitude of a given ray. The time delay of a certain multipath component is determined using information about the length of the covered distance, whereas angles-of-arrival at the side of the mobile and the base station can be calculated using the MS and BS coordinates in combination with the coordinates of the nearest points of interaction. In short, the ray-tracing model provides the information about the complete composition of waves,

i.e. *ray parameters* for the specified MS and BS locations in a concrete environment.

3.2.2 Verification of μFipre

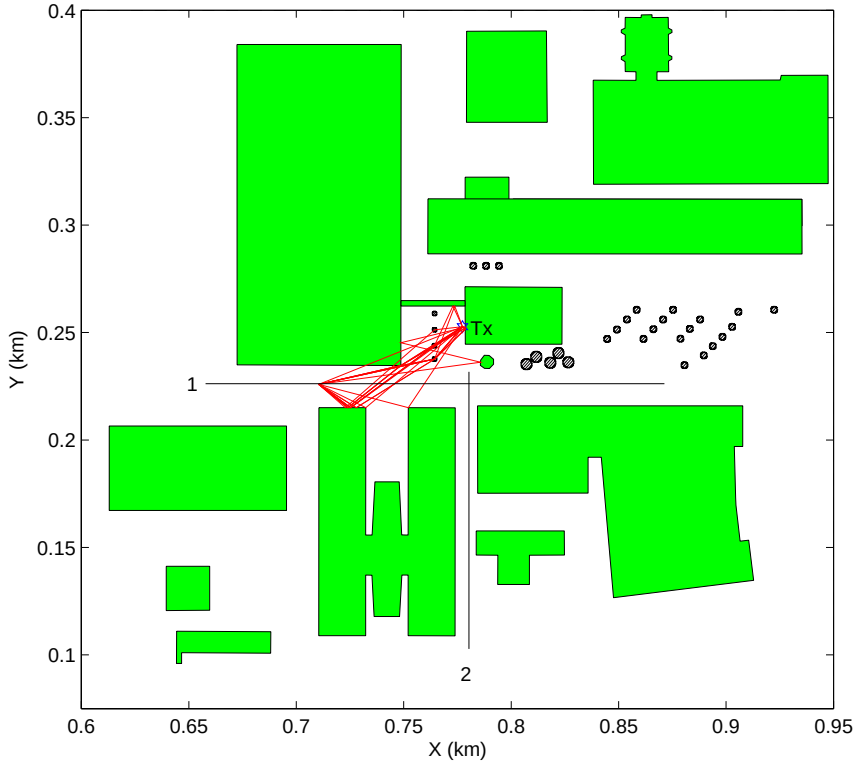

Figure 3.1: Measurement environment: part of TU/e campus; numbers 1-2 designate trajectories where the measurements were taken, Tx denotes the position of the transmitter; scattered dots stand for trees

The ray-tracing model is used as a benchmark for the comparison with the stochastic WDCM. Certain number of measurements have been conducted in order to verify the accuracy of the ray-tracing model. The channel sounder using a PN correlation method has been used for the complex impulse response (CIR) measurements. It was developed at the Communications Research Centre, Ottawa, Canada for the Eindhoven University of Technology. The CIR is measured by demodulating and correlating the received

signal with the locally generated sequence, which is shifting in time and has T_c=20 ns chip duration. This type of receiver is known as a sliding-correlator receiver. The effective sampling rate is 4 samples/chip. The output measurement files contain CIRs with the range of 10.22 μs i.e. 511 bits of 20 ns each.

The measurements were performed at the TU/e campus for several trajectories. Two of these trajectories are shown in Fig. 3.1. The receiver was mounted on the roof of a van and measurements were taken for different positions, spaced at the distance of 1 m. Antennas used were omnidirectional in the azimuth plane, with an antenna gain of G_a=2 dBi, both at the transmitter and receiver end. The transmit power was P=27 dBm, the transmitter and receiver cable losses were L_t=1.85 dB and L_r=4.74 dB, respectively, and the receiver noise floor was σ^2=-88 dBm. The frequency at which measurements were taken was f_m=2.256 GHz. The power delay profile was produced for each position on the trajectory. The evolution of the

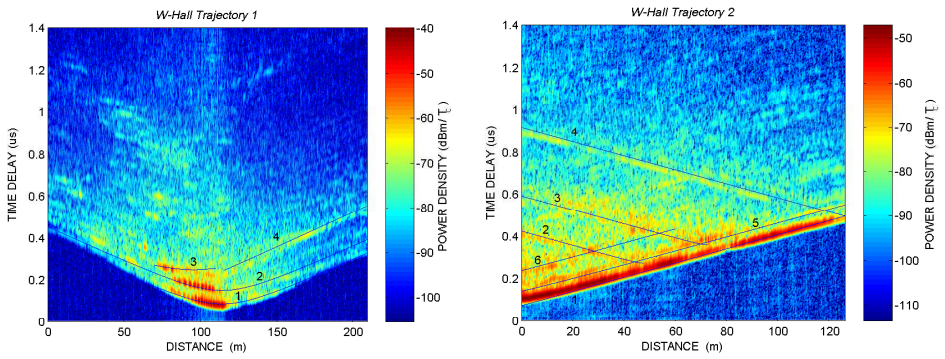

(a) (b)

Figure 3.2: Power delay profile obtained from measurements; numbered lines indicate multipath components identified by μFipre: (a) Trajectory 1; (b) Trajectory 2

power delay profile along trajectories designated with numbers 1 and 2 from Fig. 3.1 is shown in Fig. 3.2(a) and Fig. 3.2(b). The x-axis in the figures represents the distance covered during the measurements from the starting point. The high-coloured clusters represent the most dominant multipath components. The lines in the figures indicate multipath components that

were identified by μFipre. It is clear that the ray-tracing model is capable of predicting spatial evolution of dominant multipath components at the satisfactory accuracy. The results of the ray-tracing procedure, featuring 20 most dominant multipath components, for one specific location on the trajectory 1 are also shown in Fig. 3.1.

3.3 Stochastic channel model WDCM

The WDCM is a version of the Geometrically Based Single-Bounce Elliptical Model (GBSBEM) for micro-cells [43], developed for LOS scenarios, which assumes a uniform distribution of scatterers within an ellipse with the MS and BS placed in its foci. The ellipse represents the region of contributing scatterers, its size being related to the real width of the street. The scatterers are grouped in clusters which makes the model closer to more realistic scenarios, where the dispersion of waves is not continuous in delay and angle, as shown by Fig. 3.3 [44]. The model covers a variety of scenarios defi-

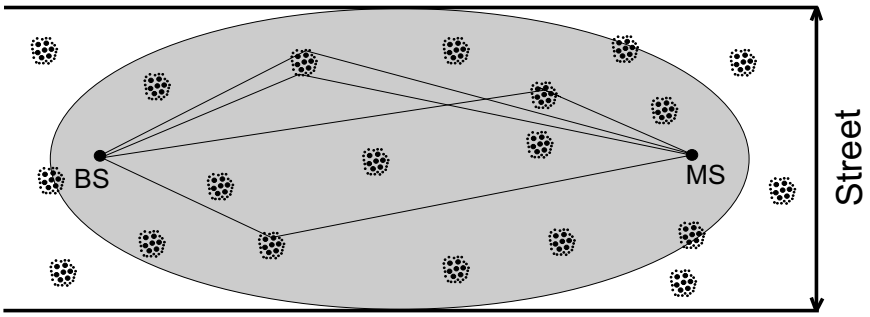

Figure 3.3: Modelling principle of WDCM

ned by input parameters that specify the spatial distribution of scatterers. The input parameters included in the model are the following: street width, effective street width ratio, cluster density, cluster standard deviation and average number of scatterers per cluster [44]. The effective street width ratio is a parameter used in combination with the real street width, which determines the size of the contributing scatterers' region. Only single scatterings are included in the model and the effective street width ratio is introduced to model the effect of the increased delay spread due to multiple reflections that exist in real scenarios. The actual width of the ellipse is determined by multiplication of the street width taken from a concrete environment with

the effective street width ratio. The cluster density determines the actual number of clusters given the size of the contributing scatterers' region. The distribution of clusters is uniform and scatterers within each cluster follow a Gaussian distribution, where the size of a cluster is specified by the cluster standard deviation. The number of scatterers per cluster is Poisson distributed. Each scatterer is assigned a random complex scattering coefficient with magnitudes and phases uniformly distributed within [0, 1] and [0, 2π] intervals, respectively.

Once the scatterers get generated according to the statistics given by the input parameters, rays are traced from the BS to the MS via a single scattering process within the ellipse. As a result, the output of the WDCM is also given in terms of *ray parameters*. The locations for which the *ray parameters* will be computed are given as an input to WDCM by specifying the corresponding distance from the BS on the LOS trajectory.

Unlike the ray-tracing model, WDCM does not include any concrete information from the environment, except the street width. Scatterers generated in WDCM cannot be differentiated with respect to concrete propagation mechanisms, like in μFipre. The stochastic model simply attempts to reproduce the average delay-angular wave dispersion that is typical for a micro-cell LOS situation on the basis of scatterers' distribution. The deterministic ray-tracing model produces one channel realisation for the specified input. This is in contrast with the stochastic WDCM that generates a variety of channel realisations on the basis of the same set of input parameters. For this reason, the channel parameters of interest in WDCM should be computed as average values over a large number of channel realisations (Monte Carlo method).

3.4 Comparing models on the basis of the delay and angular spread

The comparison of the two models will be initially done by tuning global channel parameters of the stochastic model, such as delay and angular spread, to μFipre. This procedure will be explained in Section 3.4.1. The empirical cumulative distribution functions on the basis of SINR values obtained for different positions of the MS on a trajectory in both models will be compared in Section 3.4.2 and the difference in the smart antenna performance will be explained in Section 3.4.3.

3.4.1 Description of the approach

The trajectory chosen as the input for the ray-tracing tool μFipre is the LOS street to allow a fair comparison with the WDCM. The simulation set-up is shown in Fig. 3.4. The desired user is moving on the LOS trajectory and

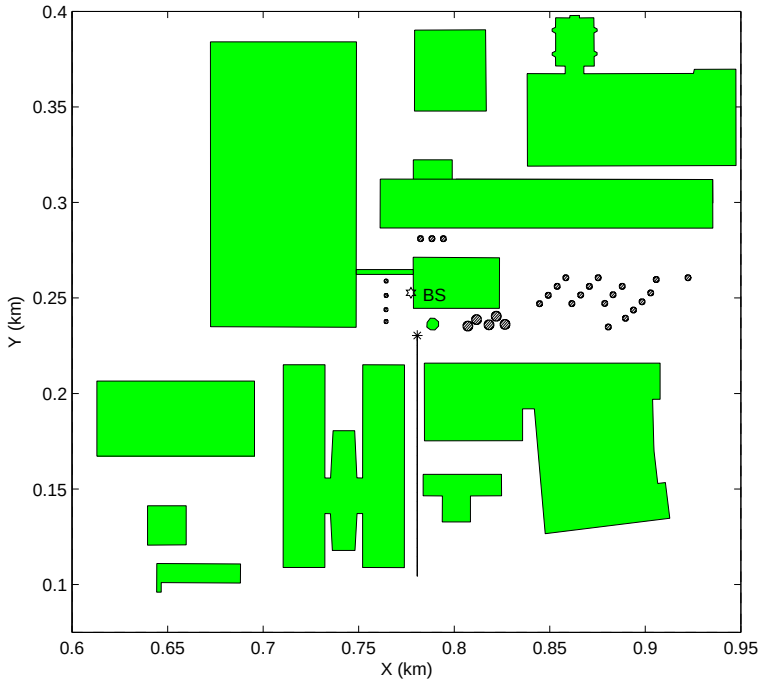

*Figure 3.4: Simulation environment with LOS street trajectory; BS indicates the position of the base station; * indicates the position of the interfering user*

there is one interfering user, located at the beginning of the same street. SINR values were calculated for the positions of the desired user MS, spaced at $\lambda_c/2$. According to [45], the correlation of the fading envelope is almost zero between half wavelength spaced samples for a uniform power angular distribution. The uniform distribution represents the most critical case regarding the envelope correlation between closely spaced samples. In a realistic micro-cellular environment, the angular distribution is usually confined to a narrower angular span, which results in an even larger correlation [46]. This implies that $\lambda_c/2$ sampling of SINR results is quite sufficient to include the small-scale effects in the channel.

The input parameters of the WDCM were found by matching the rms delay and angular spread for the points on the trajectory separated at $1m$. The delay and angular spread do not change significantly for distances smaller than 1m, since the channel preserves the wave composition over lengths smaller than 2m [47]. The delay and angular spread were parameters chosen for tuning the WDCM input, being the two most influential global channel characteristics on the space-time processing [48]. Rms delay and angular spread are defined using *ray parameters* as given by Eq. 2.33 and Eq. 2.36. The sensitivity of the delay and angular spread results to input parameters of WDCM were analysed in [44], where the effective street width ratio and cluster density were found as the most influential.

In the current analysis, the value for the effective street width ratio was varied in the range of 1-7 (with a step of 1) and the value for the cluster density in the range 0.0005 m^{-2}-0.004 m^{-2} (with a step of 0.001 m^{-2}). Since varying the cluster standard deviation and average number of scatterers per cluster does not produce significant differences for the delay and angular spread, these parameters were kept constant, their values chosen from [44] (1 for the cluster standard deviation and 20 for the average number of scatterers per cluster). The delay and angular spread from WDCM were calculated as average values on the basis of 100 channel realisations, the same being done in [44]. The matching criterion chosen was the minimum sum of relative differences between WDCM and μFipre results for the angular Δ_Λ and the delay spread Δ_τ, given by the minimising function Δ:

$$\Delta = \Delta_\tau + \Delta_\Lambda \tag{3.1}$$

where Δ_τ and Δ_Λ are defined as:

$$\Delta_\tau = \frac{1}{N_p} \sum_{i=1}^{N_p} \frac{|\sigma_\tau^{\mu Fipre} - \sigma_\tau^{WDCM}|}{\sigma_\tau^{\mu Fipre}} \tag{3.2}$$

$$\Delta_\Lambda = \frac{1}{N_p} \sum_{i=1}^{N_p} \frac{|\Lambda^{\mu Fipre} - \Lambda^{WDCM}|}{\Lambda^{\mu Fipre}} \tag{3.3}$$

Here, N_p represents the number of positions on the trajectory for which the delay and angular spread values were calculated. The input parameters for WDCM that meet the matching criterion best were as follows: the effective street width ratio of 6 and the cluster density of 0.001 m^{-2}. The dependence of the delay and angular spread on the LOS trajectory for μFipre and WDCM are shown in Fig. 3.5(a) and Fig. 3.5(b), respectively. It can be seen that the matching could not be entirely accurate. The delay and angular

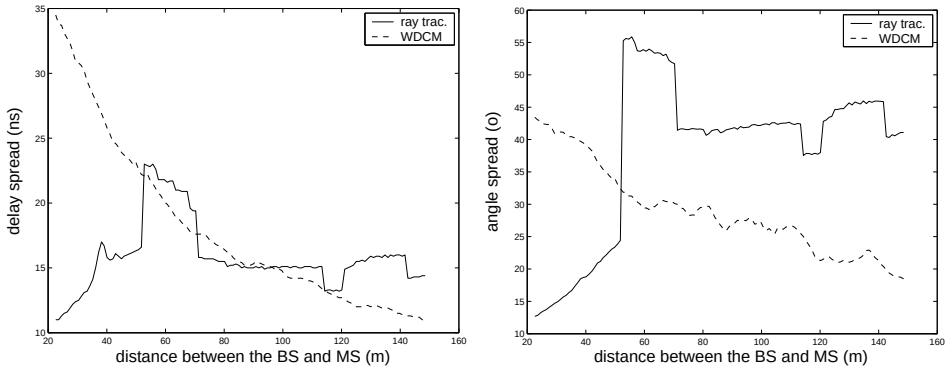

(a) (b)

Figure 3.5: (a) Delay spread obtained from μFipre and WDCM; (b) Angular spread obtained from μFipre and WDCM

---

spread results obtained from WDCM are decreasing with the distance from the BS, which is inherent to the model, whereas in the concrete situation, represented by μFipre results, the delay and angular spread exhibit more diverse behaviour along the trajectory. This is not particularly surprising for the following reasons. The delay and angular spread obtained from WDCM represent average results over a variety of LOS scenarios, decreasing with the distance from the BS (the ellipsoid region of contributing scatterers becomes narrower at the side of both MS and BS with a larger distance). On the other hand, the result from μFipre is associated with one site-specific situation, where the overall influence of the concrete propagation mechanisms causes different dependence of the delay and angular spread versus distance.

3.4.2 Simulation results

Once the input parameters for the stochastic model have been established, the antenna array processing results were produced on the basis of *ray parameters* in both models. The number of Rake fingers used was L=2 and the number of antenna elements M=3. The delay spread found for this LOS trajectory is considerably smaller than the UMTS chip length, see Fig. 3.5(a). For this reason, the results are expected to be influenced primarily by antenna array processing. Also, the inter-path or self-interference was considered

negligible due to a difference of around 20 dB between signal power on the two Rake fingers.

SINR values were calculated for the positions of the desired user MS spaced at $\lambda_c/2$ on the LOS trajectory. The interfering user is located at the distance of 22.68 m from the BS (the beginning of the trajectory, as shown in Fig. 3.4). Four different cases were analysed. Two cases correspond to results without the interfering user present. One of the cases represents the reference case, with a single Rake finger and a single antenna, and the other features two Rake fingers and three antenna elements. The other two cases deal with the influence of the interfering user, also comprising the reference case and processing with two Rake fingers and three-element antenna array. Spatial signatures for the desired and interfering user are calculated on the basis of *ray parameters*, obtained from both models for every position on the trajectory. SINR results for the reference case with the interfering user present were calculated using Eq. 2.62, while Eq. 2.63 was used when the thermal noise was the only interfering source. The SINR values obtained as a result of OC with the interfering user present, were calculated on the basis of Eq. 2.68. It has already been explained that OC reduces to MRC in a Gaussian noise. The SINR values obtained as a result of antenna array processing without the interfering user present, were calculated using Eq. 2.66, which represents the MRC scheme.

It is important to mention that all SINR results are normalised with respect to the processing gain. The processing gain does not affect the SINR distribution in this simple case without power control included (the transmit powers of the two users are assumed equal). The SINR results from μFipre for the four cases are shown in Fig. 3.6(a). The comparison of the two models was more feasible in terms of the statistics of the achieved SINR, than on the basis of single values for each position on the trajectory. For this reason, an empirical cumulative distribution function of SINR values over the whole trajectory was produced for each of the four cases, see Fig. 3.6(b).

The curves corresponding to the cases without the interfering user present are placed in a higher range of SINR values. A gain of around 4.7 dB using antenna array processing with respect to a single antenna case is obtained. This is in accordance with the theoretical results for antenna gain obtained using MRC in a Gaussian noise for a three-element antenna array (or $10\log M$ in the case of an arbitrary number of antenna elements M). The two curves placed in a lower range of SINR values in Fig. 3.6(b), correspond to the cases that include the influence of the interfering user. It can be seen that the gain is somewhat higher when the interfering user is present due to interference suppression and the compensation of fading.

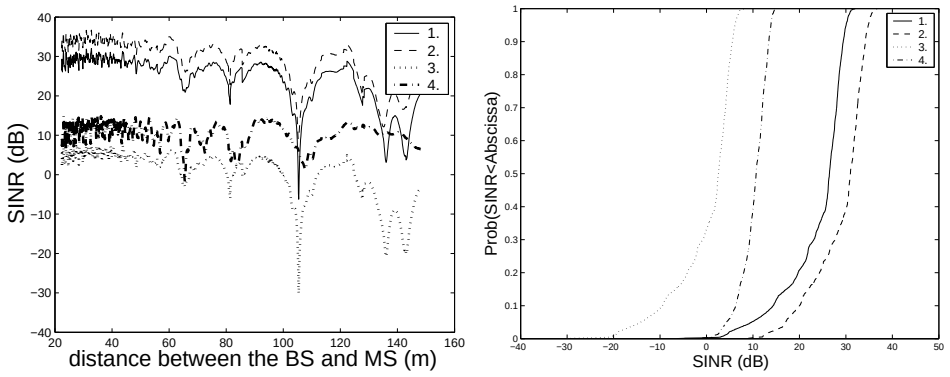

(a) (b)

Figure 3.6: μFipre results: (a) SINR versus BS-MS distance; 1: single antenna, interfering user not present; 2: MRC scheme; 3: single antenna, interfering user present; 4: OC scheme; (b) Cumulative distribution function of SINR; 1: single antenna, interfering user not present; 2: MRC scheme; 3: single antenna, interfering user present; 4: OC scheme

---

The SINR results in μFipre model were calculated on the basis of one deterministic channel realisation for each point on the trajectory. As already pointed out in Section 3.3, there are many channel realisations generated by WDCM according to the statistical distribution, defined by the input parameters. The SINR result for a single MS position in WDCM can be best characterised by a mean value with the upper and lower boundary. The mean values were obtained by averaging over 100 channel realisations and similar was done with the delay and angular spread calculation in Section 3.4.1. The upper and lower boundaries span the region of possible SINR values around the mean value. The shift of the upper and lower boundary from the average value is equal to the standard deviation σ_{dev}, also obtained as a result of averaging over 100 channel realisations. In short, the SINR value obtained for one position on the trajectory in the μFipre model corresponds to three values in WDCM (the mean value with the upper and lower boundary) for the same distance from the BS. For each case obtained from μFipre, the corresponding three curves were computed from WDCM on the basis of the mean SINR values and the two boundaries. The cumulative distribution functions of the achieved SINR in WDCM are shown in Fig. 3.7. The three

curves for each of the four cases define the range of expected values for SINR.

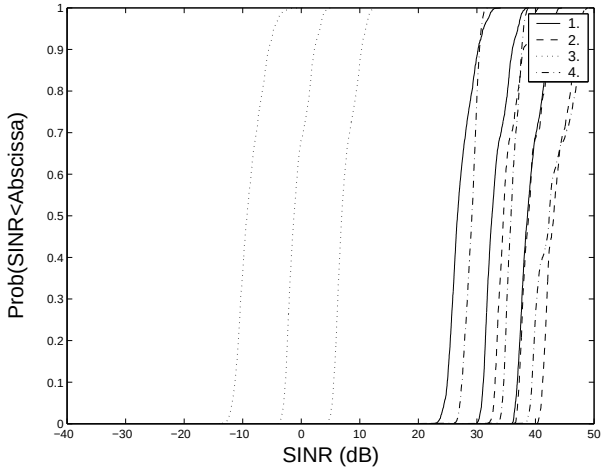

Figure 3.7: Cumulative distribution function of average SINR with upper and lower boundaries obtained from WDCM; 1: single antenna, interfering user not present; 2: MRC scheme; 3: single antenna, interfering user present; 4: OC scheme

The above given comparison represents a novel analysis that should establish what is lacking in the current stochastic models with respect to deterministic ones. The methodology regarding the comparison of the two models with disjoint approaches is new, including the interpretation of the results. The results obtained by the two models do not lend themselves to a trivial comparison. It is also difficult to give any concrete values for the gain in WDCM, due to a "spread" of SINR values for each case. What is obvious is that there is a clear distinction between the results obtained by OC and MRC in the ray-tracing model (see Fig. 3.6(b)), whereas the region of possible SINR values obtained by OC nearly overlap with the region corresponding to MRC results in the WDCM. This actually means that a much higher level of interference suppression was predicted by the WDCM. The interference suppression using OC was so effective that only the thermal noise was left and the results approach the MRC case.

3.4.3 Spatial separation parameter

Further analysis was made to explain the underlying cause of the mismatch in the performance prediction when the delay and the angular spread are used as tuning parameters. Let $\mathbf{h}_1$ and $\mathbf{h}_2$ represent spatial signatures for the desired and interfering user respectively, P the average transmit signal power and σ^2 the power of the thermal noise. Since only one Rake finger collects significant power, i.e. $L = 1$, the SINR as a result of OC can be written, using Eq. 2.68 for a flat-fading channel, as:

$$\gamma_1^{oc} = \mathbf{h}_1^H \mathbf{R}_{in,1}^{-1} \mathbf{h}_1 \tag{3.4}$$

where the spatial correlation matrix $\mathbf{R}_{in,1}^{-1}$ includes the effect of only one interfering user:

$$\mathbf{R}_{in,1} = \mathbf{h}_2 \mathbf{h}_2^H + \frac{\sigma^2}{P} \mathbf{I}_M \tag{3.5}$$

Using the matrix inversion lemma for an invertible matrix $\mathbf{A}$ and a vector $\mathbf{v}$, that states:

$$(\mathbf{A} + \mathbf{v}\mathbf{v}^H)^{-1} = \mathbf{A}^{-1} - \frac{\mathbf{A}^{-1}\mathbf{v}\mathbf{v}^H\mathbf{A}^{-1}}{1 + \mathbf{v}^H\mathbf{A}^{-1}\mathbf{v}} \tag{3.6}$$

the following result is obtained:

$$\mathbf{R}_{in,1}^{-1} = \frac{P}{\sigma^2}(\mathbf{I}_M - \frac{\mathbf{h}_2\mathbf{h}_2^H}{\sigma^2/P + \mathbf{h}_2^H\mathbf{h}_2}) \tag{3.7}$$

$$\gamma^{oc} = \frac{P}{\sigma^2}(|\mathbf{h}_1|^2 - \frac{|\mathbf{h}_1^H\mathbf{h}_2|^2}{\sigma^2/P + |\mathbf{h}_2|^2}) \tag{3.8}$$

In the presence of a dominant interferer ($|\mathbf{h}_2|^2 \gg \sigma^2$) Eq. 3.8 can be approximated to:

$$\gamma^{oc} = \frac{P}{\sigma^2}|\mathbf{h}_1|^2 \sin^2(v_{12}) \tag{3.9}$$

Where v_{12} is an indicator of the separation between the spatial signature of the desired user $\mathbf{h}_1$ and that of the interferer $\mathbf{h}_2$. It is defined as the angle between the spatial signatures of the desired and the interfering user, as given by:

$$\cos(v_{12}) = \frac{|\mathbf{h}_1^H\mathbf{h}_2|}{|\mathbf{h}_1||\mathbf{h}_2|} \tag{3.10}$$

The level of interference suppression is highly dependent on the level of separation between the spatial signatures of the desired user and the interferer [49]. The parameter $\cos(v_{12})$ will be referred to as the *spatial separation*

parameter further in the text. The cosinus of the angle v_{12} is more convenient for the representation of the separation between two spatial signatures, being in the range [0,1]. The maximum value is unity, which implies complete equality between spatial signatures.

The spatial separation parameter was calculated for both μFipre and WDCM. From Fig. 3.8, it can be seen that the difference between the models with respect to this parameter is very large. The reason for the near-overlap between the curves for the OC case when the interference is present and for the MRC case when the interference is not present in WDCM lies in the fact that the predicted $\cos(v_{12})$ is considerably smaller than what is obtained by the ray-tracing model. Tuning the model on the basis of global channel characteristics failed to reflect the correct relation between users' spatial signatures, leading to considerably different prediction of the antenna array performance. In the short analysis that follows, an attempt

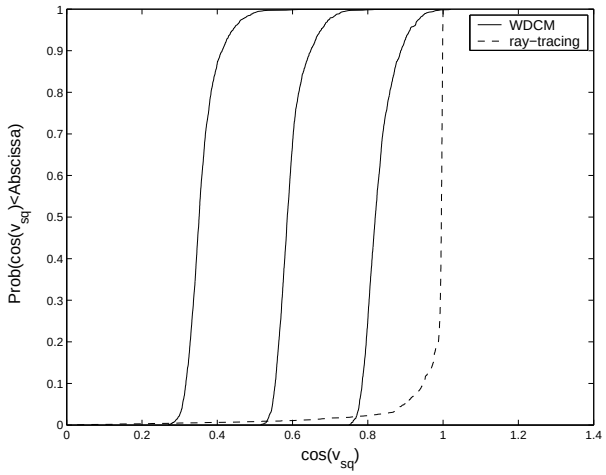

Figure 3.8: Cumulative distribution function of $\cos(v_{12})$*; average values with upper and lower boundaries obtained from WDCM and deterministic values obtained from* μ*Fipre*

has been made to give better insight into the relation between the spatial separation parameter and the angular spread. A simple signal model is assumed, where the power distribution in the angular domain is defined by specifying values for a mean angle-of-arrival and an angular spread. Let $\mathbf{h}_1$ and $\mathbf{h}_2$ be the spatial signatures belonging to two different users. The amplitudes of all multipath components for both users are assumed equal to

unity. The spatial signatures are defined as:

$$\mathbf{h}_i = \sum_{n_i=1}^{N_i} exp(\jmath\phi_{n_i})\mathbf{a}(\varphi_{n_i}) \tag{3.11}$$

where $N_i, \phi_{n_i}, \varphi_{n_i}, i = 1, 2$ represent the number of dominant multipath

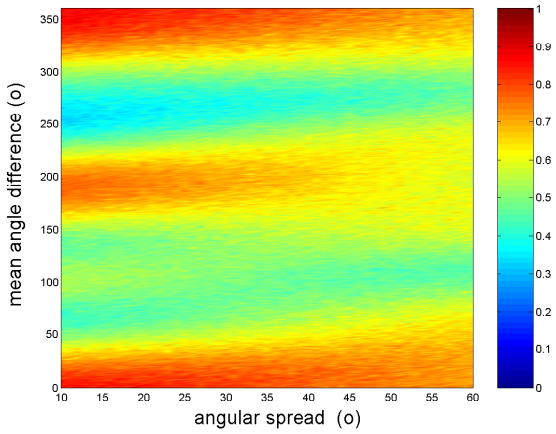

Figure 3.9: Spatial separation parameter

components, phases and angles-of-arrival, respectively. Angles-of-arrival are uniformly distributed round the mean angle $\varphi_i^0, i = 1, 2$ and within a certain angular range of $\Delta_i, i = 1, 2$. The mean angle and angular spread are kept constant for the user with a spatial signature designated as $\mathbf{h}_1$. The mean angle is $\varphi_1^0 = 0$, and the angular spread is $\Delta_1 = 30^o$. The mean angle of the second user φ_2^0 is varied in the range $[0^0, 360^o]$ with a step of 10^0 and the angular spread is varied in the range $[10^o, 60^o]$ with the step of 1^0. The values for the angular spread are chosen to simulate the situation similar to that obtained from μFipre and WDCM, see Fig. 3.5(b).

The phases of multipath signals for both users are assumed uniformly distributed within the range of $[0, 2\pi]$. The spatial separation parameter $\cos(v_{12})$ is calculated for every $[\varphi_2^0, \Delta_2]$ combination as an average over 100 signal realisations. The number of multipath components included is N_1=N_2=10. Owing to various propagation mechanisms in a typical microcell urban environment, the number of multipath components is usually much larger. However, the number of dominant components with comparable power levels is relatively small due to many successive interactions of the multi-

path waves with the environment. By including a small number of multipath components with equal power level, this situation becomes closer to reality.

The dependance of the average spatial separation parameter on the difference in the mean angle-of-arrival and the angular spread is shown in Fig. 3.9. It can be seen that very different levels of the spatial separation can be obtained around one concrete value for the angular spread, which highly depends on the difference between mean angles-of-arrival. This shows, that, indeed, it is not sufficient to describe channel characteristics in terms of global parameters in order to model the spatial correlation between users properly, but more detailed information about the concrete composition of waves is necessary.

3.5 Comparison of the models on the basis of the spatial separation parameter

Previous results motivate tuning the stochastic model input to μFipre scenario on the basis of the spatial separation parameter, since it was found to have quite a significant influence on the SINR result. The sensitivity of this parameter to input parameters of the stochastic model was analysed as an initial step in Section 3.5.1. The attempt to tune the stochastic model to μFipre by finding the street width that gives the best fit between empirical SINR cumulative functions from the stochastic and the ray-tracing model is described in Section 3.5.2. This was done for three different LOS streets to check the consistency of the model to physical reality.

3.5.1 Description of the approach

The influence of the WDCM input on the result for the spatial separation parameter $\cos(v_{12})$ was tested by varying one of the input parameters, while keeping the rest constant. The following figures, Fig. 3.10(a), Fig. 3.10(b), Fig. 3.10(c) and Fig. 3.10(d) show the dependence of the spatial separation parameter on the street width (varied in the range $[10, 40]$, with the step of 10), the cluster density (varied in the range [0.005 m^{-2},0.02 m^{-2}], with the step of 0.005 m^{-2}), the cluster diameter (varied in the range [0.5 m-2 m], with the step of 0.5 m) and average number of scatterers per cluster (varied in the range [10-40], with the step of 10), respectively. The results shown in the figures are obtained for the positions of the desired user on the trajectory, the interferer being located at the beginning of the street just like in the previous simulation set-up. High peaks in the curves, corresponding

to the location of the interfering user, reflect high correlation between the desired and the interfering user when their positions coincide. It is clear that

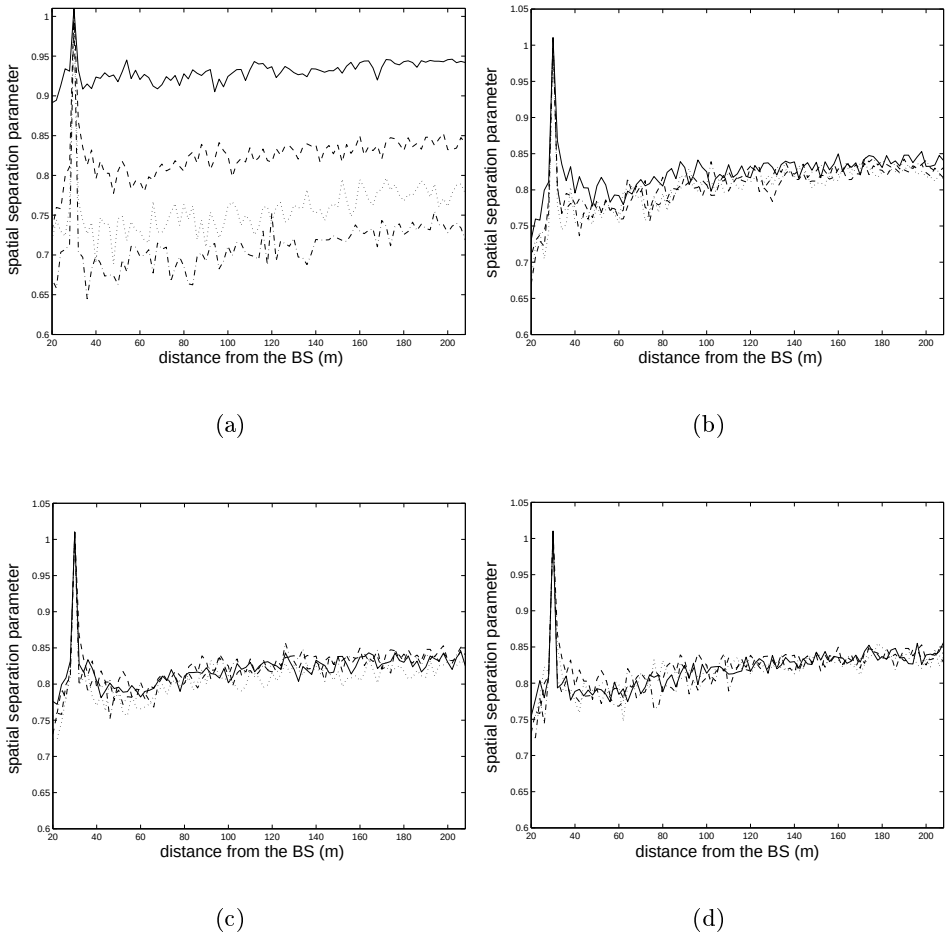

Figure 3.10: Sensitivity of the spatial separation parameter to WDCM input: (a) street width varies in the range $[10, 40]$*; (b) cluster density varies in the range [0.005* m^{-2}*,0.02* m^{-2}*]; (c) cluster standard deviation varies in the range* $[0.5, 2]$*; (d) average number of scatterers per cluster varies in the range* $[10, 40]$

the street width is the only input parameter with a significant influence on the value of the spatial separation parameter. The conclusion is that the

tuning of WDCM to μFipre is most effectively done by varying the street width. It is important to point out, once again, that the term *street width*, when applied to the WDCM context, represents the result of multiplication of the street width from the concrete environment with the effective street width ratio. As already explained in Section 3.3, the effective street width ratio is used to model the effect of multiple scatterings that has considerable influence on the result for the delay spread, since single scattering alone (as included in the WDCM) is not sufficient. The effective street width ratio should, on average, be the same for the three LOS situations analysed. Once the street width that gives the best fit between the models is found for different LOS cases, the obtained values for the effective street width ratio can be used to check the consistency of the results.

This approach differs from the previous analysis in several points. Three LOS streets of different widths from the μFipre scenario, including the one used in the previous analysis, have been chosen for the analysis (each with one interfering user located at the beginning of the trajectory) and SINR values calculated for all three cases. In order to find the WDCM input that gives the best match for each of the μFipre trajectories in terms of the achieved SINR, the street width has been varied. Other parameters were assigned the following fixed values: 0.005 m^{-2} for the cluster density, 1 for the cluster standard deviation and 20 for the average number of scatterers. In Section 3.4.2, the motivation for comparing the achieved SINR in terms of empirical cumulative distribution function was given. The striking difference between the two models (seen from Fig. 3.6(b) and Fig. 3.7) was manifested by the shift in the SINR cumulative function, obtained as a result of OC, with respect to the SINR curve corresponding to the MRC result. Since the analysis featured in Section 3.4.2 was rather new, the most important was to find the underlying cause for the striking difference between results obtained from the two models, while defining precisely the criterion for the comparison was not so feasible. In the following section the attempt is made to find input parameters that give the best fit between cumulative distribution functions of SINR obtained from μFipre and WDCM.

3.5.2 Simulation results

One of the ways to compare two empirical cumulative distribution functions is to use some of the known procedures that test the statistical similarity of two independent data sets. The Cramer-von Mises test was initially applied on the SINR results obtained by μFipre and WDCM. The test can be used to check whether two independent sets of data have identical distributions by

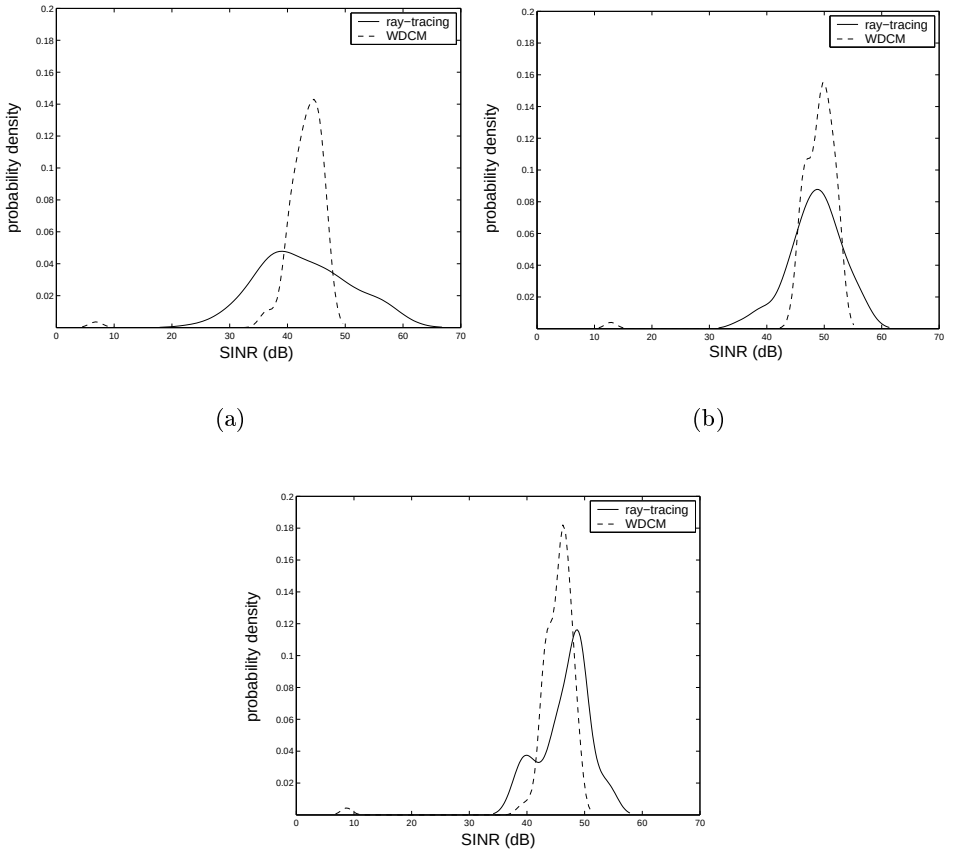

Figure 3.11: Probability density functions obtained from μFipre and WDCM (a) μFipre street width=20m, WDCM street width=7m; (b) μFipre street width=14m, WDCM street width=9m; (c) μFipre street width=10m, WDCM street width=8m

comparing their cumulative distribution functions [50]. If $S_1(x)$ and $S_2(y)$ represent cumulative functions belonging to the two data sets for arbitrary samples x and y, the test statistics is directly related to the sum of squares S_d of the differences between the two functions $S_1(x) - S_2(y)$ at all sample

μFipre	*WDCM*
10m	8m
14m	9m
20m	7m

Tabel 3.1: street width: μFipre versus WDCM

points. The test statistics T is defined as:

$$T = \frac{mn}{(m+n)^2} S_d^2 \tag{3.12}$$

where m and n represent the number of samples in the two data sets (m=n in this analysis) and S_d is defined as:

$$S_d = \sum_{m,n} (S1(x_m) - S2(y_n))^2 \tag{3.13}$$

The m-th sample in the first data set is denoted as x_m and n-th sample from the second data set as y_n. If the value of the test statics T exceeds the critical value of 0.461 for the 5% significance level, the two data sets can not be considered to have identical distributions.

For the three LOS cases, the street width in WDCM was varied and Cramer-von Mises test applied on the SINR results. It was actually not possible to find the street width that would give the positive result of the statistical test, i.e. the test statistics T would always exceed the critical value. As a consequence, another approach was taken, where the criterion for the fit between the two distributions was relaxed, without necessitating that the two cumulative functions reflect the same distribution. The alternative matching criterion chosen was the minimum error between mean SINR values from WDCM and μFipre. Empirical probability density functions of SINR values that meet the required criterion, obtained from both models, are shown in Fig. 3.11(a), Fig. 3.11(b) and Fig. 3.11(c). Minimising the error between mean SINR values gives the maximum overlap between these functions.

In table 3.1, the results of the street width values in the WDCM that give the best fit in terms of mean SINR are given with the corresponding real street width values in μFipre. If the model is consistent to physical reality, the same street width ratio should be found for all LOS cases. However, it can be seen from the values given in the table 3.1, that the consistency is not fulfilled and there is no clear relation between the WDCM input and real physical conditions.

3.6 Summary and conclusions

The novel comparison between a stochastic and a deterministic model has been presented on the basis of two different approaches. The two approaches differ in the way the input for the stochastic WDCM was tuned to a concrete scenario, featured in the deterministic model μFipre. The deterministic model was used as a benchmark.

According to the first approach, the model was tuned to global channel characteristics, like the delay and angular spread, by varying the street width ratio and cluster density (as the most influential parameters). This gave a significant mismatch in the system performance prediction of the antenna array processing due to differently predicted levels of separation between spatial signatures of the desired and interfering user. The parameter, referred to as a *spatial separation parameter*, was identified to have a significant influence on the result for the achieved SINR when OC is applied.

In the second approach, the stochastic model was tuned on the basis of the spatial separation parameter, also including more LOS scenarios to check the consistency of the model. The sensitivity of this parameter to WDCM input was initially tested and it was found that only the street width has a significant influence on the value for this parameter. This reduced the number of input parameters for WDCM that need to be varied in order to find the best fit with the results obtained by μFipre. Since Cramer von Mises test was found to be too strict for the comparison between SINR obtained from the two models, the criterion that minimised the error between mean SINR values was eventually chosen. The values for the street width that meet the criterion in question for each of the three LOS cases, show that the model does not incorporate real physical conditions in a consistent way.

Obviously the prediction of interference suppression using antenna array requires more details about the structure of interference, especially in case it can not be considered spatially-white. WDCM can not be used for the antenna array analysis for urban micro-cells, since it does not reflect the correlation in the antenna array space between users properly. For this reason, the deterministic model μFipre will be used for further smart antenna analysis.

4

Antenna array processing with power control

4.1 Introduction

One of the most important issues about employing antenna array processing for interference-limited 3G mobile communication systems is the increase in the number of users that can be simultaneously sustained and the reduction in the limited uplink transmit power. In UMTS, the role of the fast power control is to adjust transmit powers for each user in order to achieve a certain SINR based on a BLER or BER target. With the antenna array processing, the desired target SINR can be achieved for the lower transmit power.

The CDMA system performance improvement by employing antenna arrays is reported in [28]. The analysis was based on the statistical channel model and the assumption that the interference from other users is spatially-white. In Chapter 3 and in [51], it was shown that stochastic models do not predict the performance of antenna processing adequately, due to improper modelling of the correlation between users' spatial signatures. In the present analysis, the deterministic ray-tracing model, introduced in Chapter 3, is used. Since the locations of users in a concrete environment are accurately included, their mutual correlation in the antenna array space is adequately reflected. This approach is, also, not limited to any specific assumption about the statistics of interference structure, like *spatially-white interference*.

In the analysis to follow, a flat fading channel is assumed (only one Rake finger is active), since the delay spread over trajectories in the environment used as an input to the ray-tracing model is much lower than the UMTS chip

length, as was also indicated in Chapter 3. The analysis will consequently resort to pure antenna array processing. This is also convenient for the simplicity of the analysis which aims to show the trends of the sensitivity of optimum transmit powers to system and propagation parameters from the angular point of view. The case of a frequency selective channel, where more than one Rake finger is active, will be analysed in Chapter 6.

The system and propagation parameters that are most dominant for the optimum transmit powers result will be identified for two antenna processing algorithms: optimum combining and maximal ratio combining, introduced in Chapter 1 and Chapter 2. In a non power-controlled environment, i.e. the power of interference is constant without being adapted by any specific mechanism, OC has significant advantages over MRC regarding interference suppression [52]. In that case, if a certain level of SINR has to be achieved for one user, the transmit power obtained using OC can be considerably lower for many different scenarios than that obtained by MRC. The power control, on the other hand, controls interference on a basic level by achieving the same signal level over the total interference for all users. In that case, the results for optimum powers are less sensitive to the spatial distribution of users and are more dependent on the processing gain and antenna array size, as will be further shown. Comparative analysis of MRC and OC will be conducted in order to establish the benefits of OC over MRC for the given system parameters, such as the processing gain, antenna array size and number of users.

In Section 4.2, a mathematical model for the combined power control and antenna array processing is described. The perfect power control case is dealt with in Section 4.3, with the aim to identify the most dominant system parameters to the optimum transmit power result for both OC and MRC. The theoretical analysis is given first, followed by simulation results. In Section 4.4, a more realistic power control process is modelled, taking into account the finite time available for power updates and also the step size of 1 dB in the power update process. In this analysis, the MS speed is introduced as a new parameter. The chapter ends with conclusions, given in Section 4.5.

4.2 Mathematical formulation of the power control with antenna array processing

In a cell of K mobile users, there are K links that need to satisfy the minimum quality, specified by the target SINR. SINR achieved for the i-th user

γ_i can be expressed in terms of the i-th user received power P_i^r and received powers P_j^r belonging to interfering users $j \neq i, j = 1, ...K$:

$$\gamma_i = \frac{P_i^r}{\sum_{j=1, j\neq i}^{K} P_j^r + \sigma_i^2} \tag{4.1}$$

If the terms G_{ii} and G_{ji} represent the link gain between the i-th user and the BS and the link gain between the j-th ($j \neq i$) interfering user and the BS, respectively, the i-th user SINR can be expressed in terms of transmit powers of all users $P_1, ...P_K$ as:

$$\gamma_i = \frac{G_{ii}P_i}{\sum_{j=1, j\neq i}^{K} G_{ji}P_j + \sigma_i^2} \tag{4.2}$$

where $P_i^r = G_{ii}P_i$ and $P_j^r = G_{ji}P_j$. The second index i of the term designating a link gain indicates that the antenna pattern is optimised for the i-th user. The link gains can be further expressed in terms of the spatial signature of the desired user $\mathbf{h}_i$ (as given by Eq. 2.22) and that of interfering users $\mathbf{h}_j$ (see Eq. 2.46), assuming that only one Rake finger is active (a flat-fading signal model). The link gains G_{ii} and G_{ji} are, therefore, defined as follows:

$$G_{ii} = N|\mathbf{w}_i^H \mathbf{h}_i|^2 \tag{4.3}$$

$$G_{ji} = |\mathbf{w}_i^H \mathbf{h}_j|^2 \tag{4.4}$$

where $\mathbf{w}_i$ is the antenna weight vector, optimised for the i-th user, and N is the processing gain. The variance of the noise σ_i^2 is given as:

$$\sigma_i^2 = \sigma^2 |\mathbf{w}_i|^2 \tag{4.5}$$

where σ^2 is the variance of the thermal noise at the receiver input, defined in Section 2.5.2. The link quality is regarded acceptable if

$$\gamma_i \geq \gamma_0, i = 1, ...K \tag{4.6}$$

where γ_0 represents the desired target SINR. The link quality condition can be written in a matrix form:

$$[\mathbf{I}_K - \gamma_0 \mathbf{G}]\mathbf{p} \geq \mathbf{u} \tag{4.7}$$

The term $\mathbf{p}$ represents the vector of transmit powers for K users, given as $\mathbf{p} = [P_1, ..., P_K]$, the matrix $\mathbf{I}_K$ is the $K \times K$ unity matrix, $\mathbf{u}$ is the thermal noise vector with elements, defined as:

$$[\mathbf{u}]_i = \frac{\gamma_0 \sigma_i^2}{G_{ii}} \tag{4.8}$$

and the matrix $\mathbf{G}$ is defined as:

$$[\mathbf{G}]_{ij} = \begin{cases} 0, & \text{if } j = i \\ G_{ji}/G_{ii}, & \text{otherwise} \end{cases} \tag{4.9}$$

The fast power control aims to equalise SINR for all users with the given target value γ_0. The minimum transmit power vector that fulfills the link quality condition is given as follows (the solution to the power control optimisation problem):

$$\mathbf{p}_{opt} = [\mathbf{I}_K - \gamma_0 \mathbf{G}]^{-1}\mathbf{u} \tag{4.10}$$

The above given relation represents a perfect power control case, i.e. the target SINR is achieved for all users. The condition for the existence of the optimum solution is as follows [53]:

$$\lambda_{max} < 1/\gamma_0 \tag{4.11}$$

where λ_{max} is the largest eigenvalue, commonly referred to as *spectral radius*, of the non-negative $\mathbf{G}$ matrix.

4.3 Perfect power control

The theoretical analysis of optimum powers in case of a perfect power control is given, first by providing a global insight into the influence of the most dominant parameters in Section 4.3.1 and, then, deriving closed-form expressions for OC and MRC, assuming a simple multi-user scenario, in Section 4.3.2. The simulation results in Section 4.3.3 show the influence of those parameters for a more realistic system and propagation environment.

4.3.1 Identifying dominant parameters

In order to identify the most dominant parameters for the optimum transmit powers result, a closer look is taken into the elements of the $\mathbf{G}$ matrix, which actually represent the ratio between the interfering and the desired signal for each pair of users. The elements of the $\mathbf{G}$ matrix, in case of OC, can be written in the following way:

$$[\mathbf{G}^{oc}]_{ij} = \frac{|(\mathbf{w}_i^{oc})^H \mathbf{h}_j|^2}{N|(\mathbf{w}_i^{oc})^H \mathbf{h}_i|^2} \tag{4.12}$$

or:

$$[\mathbf{G}]_{ij} = \frac{|(\mathbf{R}_{in}^{-1}\mathbf{h}_i)^H \mathbf{h}_j|^2}{N|(\mathbf{R}_{in}^{-1}\mathbf{h}_i)^H \mathbf{h}_i|^2} = \frac{|\mathbf{h}_i^H \mathbf{R}_{in,i}^{-H}\mathbf{h}_j|^2}{N|\mathbf{h}_i^H \mathbf{R}_{in,i}^{-H}\mathbf{h}_i|^2} \tag{4.13}$$

$$[\mathbf{G}]_{ij} = \frac{|\mathbf{h}_j|^2}{N|\mathbf{h}_i|^2} \frac{\cos^2(v_{oc,j})}{\cos^2(v_{oc,i})} \tag{4.14}$$

The last expression shows that the elements of the matrix can be split into three factors: the first one is the processing gain N and represents a multiplication factor common to all elements; the second one represents the ratio between the lengths of spatial signatures for each pair of users $|\mathbf{h}_j|^2/|\mathbf{h}_i|^2$ which include the effect of path-loss and shadowing for the i-th and j-th user; the third element $\cos^2(v_{oc,j})/\cos^2(v_{oc,i})$ represents a factor that is directly dependent on the users' spatial structure. The term $v_{oc,i}$ is defined as the angle between the OC antenna weight vector $\mathbf{w}_i^{oc}$ and the spatial signature of the desired i-th user $\mathbf{h}_i$, given by:

$$\cos(v_{oc,i}) = \frac{|(\mathbf{R}_{in,i}^{-1}\mathbf{h}_i)^H \mathbf{h}_i|}{|\mathbf{R}_{in,i}^{-1}\mathbf{h}_i||\mathbf{h}_i|} \tag{4.15}$$

while the term $v_{oc,j}$, defined analogous to Eq. 4.15, is the angle between $\mathbf{w}_i^{oc}$ and the spatial signature of the j-th interfering user $\mathbf{h}_j$.

In case of MRC, the elements of the matrix $\mathbf{G}$ are defined, as follows:

$$[\mathbf{G}]_{ij} = \frac{|\mathbf{h}_j|^2}{N|\mathbf{h}_i|^2} \cos^2(v_{ij}) \tag{4.16}$$

It is clear that the factor accounting for the influence of the processing gain and the factor that depends on the lengths of the spatial signatures, are the same for OC and MRC. The factor accounting for the spatial structure, given as $\cos^2(v_{ij})$ for MRC, is different from OC case. It represents the angle between spatial signatures of the i-th and j-th user, as defined in Section 3.4.3. The third factor in Eq. 4.14 and Eq. 4.16 that accounts for the spatial structure of users is responsible for the OC versus MRC performance. It has already been indicated that in case the condition given by Eq. 2.70 is valid for MAI, the performance of OC is equal to MRC in a non power-controlled system. With power control included this becomes more complex, since the results represent the composite dependence of the spatial correlation between one user and the rest and it will be different for each user. In [53], it has been reported that the inverse of the maximum eigenvalue of the $\mathbf{G}$ matrix is the maximum achievable SINR and the minimum power vector that satisfies the power control problem equals its corresponding eigenvector. In this analysis, the target SINR values are already pre-defined for different types of services, as given in the table 1.1. The target SINR represents the minimum requirement for a particular service and plays the major role in

defining the sensitivity of transmit powers to system parameters, as well as the antenna processing scheme.

In order to identify the most dominant parameters, some general mathematical analysis will be given first. The power control problem will be written again for clarity:

$$[\mathbf{I}_K - \gamma_0 \mathbf{G}]\mathbf{p}_{opt} = \mathbf{u} \tag{4.17}$$

$$\mathbf{p}_{opt} - \gamma_0 \mathbf{G}\mathbf{p}_{opt} = \mathbf{u} \tag{4.18}$$

The gain matrix $\mathbf{G}$ is a real non-negative matrix. According to the Perron-Frobenius theory [54], the maximum eigenvalue is the only eigenvalue whose corresponding eigenvector is positive, i.e. the elements of the vector are all positive. This particular eigenvalue, also referred to as a *spectral radius*, represents both the right-hand and the left-hand eigenvalue. The left-hand characteristic equation for the matrix $\mathbf{G}$ can be written as:

$$\mathbf{e}^T[\mathbf{G} - \lambda_{max}\mathbf{I}_K] = 0 \tag{4.19}$$

or

$$\mathbf{e}^T\mathbf{G} = \lambda_{max}\mathbf{e}^T \tag{4.20}$$

where $\mathbf{e}$ represents the eigenvector corresponding to the maximum eigenvalue, denoted by λ_{max}. If we apply vector multiplication on both sides of Eq. 4.18, using the eigenvector $\mathbf{e}$, the following is obtained:

$$\mathbf{e}^T\mathbf{p}_{opt} - \gamma_0\mathbf{e}^T\mathbf{G}\mathbf{p}_{opt} = \mathbf{e}^T\mathbf{u} \tag{4.21}$$

Combining Eq. 4.20 with Eq. 4.21, the following can be deduced:

$$\mathbf{e}^T[\mathbf{p}_{opt} - \gamma_0\lambda_{max}\mathbf{p}_{opt}] = \mathbf{e}^T\mathbf{u} \tag{4.22}$$

or,

$$\mathbf{e}^T[(1 - \gamma_0\lambda_{max})\mathbf{p}_{opt} - \mathbf{u}] = 0 \tag{4.23}$$

Since the first multiplicative term in Eq. 4.23 is non-negative, the following is valid, under the condition that the second multiplicative term is also non-negative:

$$\mathbf{p}_{opt} - \gamma_0\lambda_{max}\mathbf{p}_{opt} = \mathbf{u} \tag{4.24}$$

or

$$\mathbf{p}_{opt}[\mathbf{I}_K - \gamma_0\lambda_{max}] = \mathbf{u} \tag{4.25}$$

$$\mathbf{p}_{opt} = \frac{1}{1 - \gamma_0\lambda_{max}}\mathbf{u} \tag{4.26}$$

It can be seen that optimum powers can be expressed in terms of the spectral radius of the $\mathbf{G}$ matrix and the given γ_0. The only restriction to this equality is that the vector $\mathbf{v}$ given by:

$$\mathbf{v} = (1 - \gamma_0 \lambda_{max})\mathbf{p}_{opt} - \mathbf{u} \tag{4.27}$$

is non-negative. The elements of $\mathbf{v}$ are defined as:

$$[\mathbf{v}]_i = \frac{\gamma_0}{G_{ii}}[(1/\gamma_0 - \lambda_{max})[\mathbf{p}_{opt}]_i G_{ii} - \sigma_i^2] \tag{4.28}$$

$$[\mathbf{v}]_i = \frac{\gamma_0}{G_{ii}}[(1/\gamma_0 - \lambda_{max})[\mathbf{p}^r]_i - \sigma_i^2] \tag{4.29}$$

Here, $\mathbf{p}^r$ represents the vector of the received powers, with elements defined as $[\mathbf{p}^r]_i = [\mathbf{p}_{opt}]_i G_{ii}, i = 1, ...K$. In the expression, given by Eq. 4.29, the first multiplicative part, given by γ_0/G_{ii}, is always positive. The term in the second multiplicative part $1/\gamma_0 - \lambda_{max}$ is always positive, representing the condition for the existence of optimum transmit powers for the given target γ_0, as in Eq. 4.11. The expression $(1/\gamma_0 - \lambda_{max})[\mathbf{p}^r]_i, i = 1, ...K$, represents a certain fraction of the received power.

The positivity of the second multiplicative part in Eq. 4.29, therefore, depends on the amount of the received power that is larger than the thermal noise. If γ_0/λ_{max} is small, the fraction of the received power will be very close to the received power itself. The received power is always larger than noise, given the condition that the target SINR is always larger than zero. Whether this fraction of the received power is larger than noise depends on the γ_0/λ_{max} ratio. In the majority of cases simulated this condition is fulfilled.

The analysis above shows that transmit powers are closely linked to the spectral radius of the $\mathbf{G}$ matrix, which gives some basic insight into the sensitivity of the powers to certain system and propagation parameters. For the moment, it is clear that optimum powers do not depend so much on the smart antenna performance for each user individually, but on a more global scale. The processing gain acts as a global-scale parameter that has a significant influence on the eigenvalues of the $\mathbf{G}$ matrix. Let λ_{max} be the eigenvalue in case the processing gain is $N = 1$. Increasing the value of the processing gain by a certain level $N > 1$ is equivalent to dividing the matrix $\mathbf{G}$ with a real constant N. The new maximum eigenvalue is $\lambda'_{max} = \lambda_{max}/N$. If γ_0 is kept constant, more users can be sustained with a larger processing gain, since the condition Eq. 4.11 becomes less critical. This is also the case when the target SINR decreases and the processing gain is kept constant.

Also from Eq. 4.26, it is clear that the ratio between the target SINR value and the processing gain γ_0/N has the most dominant influence on power levels (where $1/N$ is contained in the eigenvalue term).

In the analysis to follow, the gain of OC over MRC in the reduction of the transmit power is derived. The noise vector $\mathbf{u}$ is defined for OC and MRC, respectively, as follows:

$$[\mathbf{u}^{oc}]_i = \gamma_0 \sigma_0^2 \frac{|\mathbf{w}_i^{oc}|^2}{|(\mathbf{w}_i^{oc})^H \mathbf{h}_i|^2} = \gamma_0 \sigma_0^2 \frac{1}{|\mathbf{h}_i|^2 \cos^2(v_{oc,i})} \tag{4.30}$$

$$[\mathbf{u}^{mrc}]_i = \gamma_0 \sigma_0^2 \frac{|\mathbf{w}_i^{mrc}|^2}{|(\mathbf{w}_i^{mrc})^H \mathbf{h}_i|^2} = \gamma_0 \sigma_0^2 \frac{1}{|\mathbf{h}_i|^2 \cos^2(v_{mrc,i})} \tag{4.31}$$

where $v_{oc,i}$ and $v_{mrc,i}$ represent the angle between the spatial signature of the desired user and the antenna weight vector for OC and MRC, respectively. The angle $v_{oc,i}$ is defined as by Eq. 4.15 and the following is always valid for MRC:

$$\cos(v_{mrc,i}) = 1 \tag{4.32}$$

since the antenna vector for MRC is perfectly correlated with the spatial signature of the desired user, regardless of the other users' spatial structure. The gain in the reduction of the transmit power for the two processing schemes is denoted by vector $\mathbf{g}_{oc-mrc}$, with elements defined as:

$$[\mathbf{g}_{oc-mrc}]_i = [\mathbf{P}^{mrc}]_i / [\mathbf{P}^{oc}]_i = \frac{1 - \gamma_0 \lambda^{oc}}{1 - \gamma_0 \lambda^{mrc}} \frac{[\mathbf{u}^{mrc}]_i}{[\mathbf{u}^{oc}]_i}, i = 1, ...K \tag{4.33}$$

This can be rewritten as:

$$[\mathbf{g}_{oc-mrc}]_i = \frac{1 - \gamma_0 \lambda^{oc}}{1 - \gamma_0 \lambda^{mrc}} \cos^2(v_{oc,i}) \tag{4.34}$$

In the last expression the gain $[\mathbf{g}_{oc-mrc}]_i$ is defined for one particular (i-th) user. The average gain for all users in general depends on the factor that contains only eigenvalues λ^{oc} for OC and eigenvalues λ^{mrc} for MRC, given by $(1 - \gamma_0 \lambda^{oc})/(1 - \gamma_0 \lambda^{mrc})$.

It can be observed that the gain between OC and MRC is dominated by the ratio γ_0/N. The factor $1/N$ is contained in eigenvalue terms λ^{mrc} and λ^{oc}, as already explained. If the ratio is low, Eq. 4.34 is close to unity. This basically makes the gain of OC over MRC less sensitive to a concrete spatial structure of users.

The antenna array size has an influence on the users' spatial structure, i.e. the third factor in Eq. 4.14 and Eq. 4.16. The spatial structure is a

complex notion, depending on both the users' spatial distribution and the antenna array size. Antenna array size is another system parameter that has a global influence on power levels. As the antenna array size increases, all elements of the matrix tend to be smaller, because the interference is, then, suppressed better and a larger number of users can be sustained. The fact that the antenna array size has global influence on power levels is, naturally, understandable without the formal eigenvalue analysis. The question is to what degree the antenna array size is influential to the results, especially to the OC versus MRC comparison. It is difficult to find the direct relation between the spectral radius of the **G** matrix and users' spatial structure. The following inequality can give some indication about possible results regarding the influence of the spatial structure [54]:

$$\min_i \sum_{j=1}^{K} [\mathbf{G}_{ij}] \leq \lambda_{max} \leq \max_i \sum_{j=1}^{K} [\mathbf{G}_{ij}] \tag{4.35}$$

This means that the spectral radius of the matrix is lower-bounded by the minimum column sum and upper-bounded by the maximum column sum. The elements of the matrix generally represent interference-to-desired signal ratio for each pair of users. Each row of the matrix has a factor originating from the desired user in common (see Eq. 4.3), whereas each column has one of the interferers as a common factor (see Eq. 4.4). The minimum sum of columns indicates which of the users has the least interfering influence on others. The maximum sum of columns indicates the user which acts as the strongest interferer. The performance of the optimisation process involving combined power control and antenna array processing is limited by the influence of the user that acts as the strongest interferer to other users. Even though the inequality does not provide the exact relationship, it indicates that the eigenvalues can be visibly changed primarily when the status of the critical user can be significantly changed.

This already gives some insight into the sensitivity of the powers to the antenna array size and spatial distribution of users. The antenna array size is quite influential, since users primarily have to minimise the influence of the critical user, this being sufficient with the available degrees of freedom. The number of users also plays an important role. Generally, the OC versus MRC gain can be on average achieved more often with a smaller number of users. As the number of users increases, the strongest interferer gets closer in angular domain to the majority of users in the system. In that case, the gain of OC over MRC tends to decrease since steering nulls towards interference will also reduce the power of the desired user by the same level

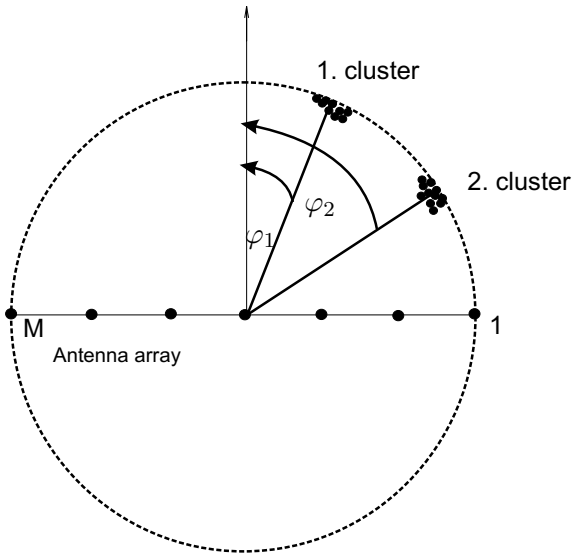

Figure 4.1: Case study multiuser model

but, also, steering the beam towards the desired user will equally favour both the desired user and interference. In the analyses given in Section 4.3.3 and Section 4.4, the influence of these parameters will be shown for the perfect and imperfect power control case, respectively. For the moment it is important to understand that in a realistic scenario, the user that acts as the strongest interferer (which is most often the user that experiences the smallest attenuation of the signal strength) puts the main limitation to the achievement of the desired SINR for all users in the system.

Since it is quite difficult to give any closed-form expression for optimum powers in a realistic scenario, the attempt will be made to provide an expression for a simplified scenario, which will more directly show the dependence of transmit powers to parameters like processing gain, target SINR, antenna array size and number of users.

4.3.2 Case study

In order to clarify some of the notions regarding the impact of the factors mentioned above, a case study is conducted for a simple scenario. The analysis features an arbitrary number of users K, located along a circle around the BS. In the attempt to model a more realistic scattering situation,

the multipath components arrive in clusters. For simplicity, there are only two clusters where the angle between the mean angles of clusters indicates physical separation between them. A single-path propagation is assumed (one multipath component per user) and there is an equal number of users per cluster $K/2$. All multipath components are equal in amplitude and are assumed to arrive at the same time. Basically, the only *ray parameter* included in the analysis is the angle-of-arrival at the BS. This is justified by the aim to analyse the impact of the angular distribution, which is essential for the antenna array analysis. In this simple scenario, there are not users with a dominant interfering effect. All users contribute equally to the result. The optimum powers for MRC are derived first, followed by the result for OC. For the sake of obtaining a relatively simple expression in case of OC, the antenna array is assumed linear. The global conclusions regarding the influence of system parameters on the results, including OC versus MRC gain, are not so sensitive to the antenna array configuration.

MRC results

The main assumption about users grouped in the same cluster is that their antenna steering vectors can be considered equal, since their separation in angular domain is very small. Therefore, the waves belonging to users in one cluster are assumed to arrive at the angle φ_1 with respect to the antenna array and the waves belonging to users in the second cluster at the angle φ_2, as shown in Fig. 4.1. Due to an obvious symmetry, optimum powers for users belonging to one cluster are the same. Since only one multipath component is assigned to each user, the spatial signatures for the desired $\mathbf{h}_i$ and interfering user $\mathbf{h}_j$ become (see Eq. 2.22 and Eq. 2.46):

$$\mathbf{h}_i = \mathbf{a}_i \tag{4.36}$$

$$\mathbf{h}_j = \sqrt{\frac{2}{3}}\mathbf{a}_j \tag{4.37}$$

where $\mathbf{a}_i$ represents the antenna steering vector for the i-th user. The link gains in case of MRC are defined as follows:

$$G_{ii}^{mrc} = N|(\mathbf{w}_i^{mrc})^H\mathbf{a}_i|^2 \tag{4.38}$$

$$G_{ji}^{mrc} = \frac{2}{3}|(\mathbf{w}_i^{mrc})^H\mathbf{a}_j|^2 \tag{4.39}$$

The antenna weight vector for the i-th user is equal to antenna steering vector belonging to that user $\mathbf{w}_i^{mrc} = \mathbf{a}_i$. The gains are, therefore, written

as:

$$G_{ii}^{mrc} = N|\mathbf{a}_i^H \mathbf{a}_i|^2 \tag{4.40}$$

$$G_{ji}^{mrc} = \frac{2}{3}|\mathbf{a}_i^H \mathbf{a}_j|^2 \tag{4.41}$$

The noise vector $\mathbf{u}^{mrc}$ for MRC is given as:

$$[\mathbf{u}^{mrc}]_i = \gamma_0 \sigma_0^2 \frac{|\mathbf{a}_i|^2}{|\mathbf{a}_i^H \mathbf{a}_i|^2} = \frac{\gamma_0 \sigma_0^2}{|\mathbf{a}_i|^2} \tag{4.42}$$

and the following is valid for antenna steering vectors:

$$\mathbf{a}_i^H \mathbf{a}_i = |\mathbf{a}_i|^2 = M \tag{4.43}$$

If the i-th and the j-th user belong to the same cluster, the following result for the gains when the antenna pattern is optimised for the i-th user is obtained:

$$G_{ji}^{mrc}/G_{ii}^{mrc} = \frac{2}{3N} \tag{4.44}$$

since $\mathbf{a}_i = \mathbf{a}_j$. The power control problem can be written as:

$$p_1 - \gamma_0 \sum_{i=1}^{K/2-1} p_1 \frac{2}{3N} - \gamma_0 \sum_{i=1}^{K/2} p_2 \frac{G_{21}}{G_{11}} = \frac{\gamma_0 \sigma^2}{G_{11}} \tag{4.45}$$

$$p_2 - \gamma_0 \sum_{i=1}^{K/2-1} p_2 \frac{2}{3N} - \gamma_0 \sum_{i=1}^{K/2} p_1 \frac{G_{12}}{G_{22}} = \frac{\gamma_0 \sigma^2}{G_{22}} \tag{4.46}$$

$$p_1 - \sum_{i=1}^{K/2-1} p_1 \gamma_0 \frac{2}{3N} - \sum_{i=1}^{K/2} p_2 \gamma_0 \frac{2}{3N} \frac{|\mathbf{a}_1^H \mathbf{a}_2|^2}{|\mathbf{a}_1^H \mathbf{a}_1|^2} = \frac{\gamma_0 \sigma_0^2}{|\mathbf{a}_1|^2} \tag{4.47}$$

$$p_2 - \sum_{i=1}^{K/2-1} p_2 \gamma_0 \frac{2}{3N} - \sum_{i=1}^{K/2} p_1 \gamma_0 \frac{2}{3N} \frac{|\mathbf{a}_2^H \mathbf{a}_1|^2}{|\mathbf{a}_2^H \mathbf{a}_2|^2} = \frac{\gamma_0 \sigma_0^2}{|\mathbf{a}_2|^2} \tag{4.48}$$

$$p_1(1 - (\frac{K}{2} - 1)\gamma_0 \frac{2}{3N}) - \frac{K}{2} p_2 \gamma_0 \frac{2}{3N} \frac{|\mathbf{a}_1^H \mathbf{a}_2|^2}{M^2} = \frac{\gamma_0 \sigma_0^2}{M} \tag{4.49}$$

$$p_2(1 - (\frac{K}{2} - 1)\gamma_0 \frac{2}{3N}) - \frac{K}{2} p_1 \gamma_0 \frac{2}{3N} \frac{|\mathbf{a}_2^H \mathbf{a}_1|^2}{M^2} = \frac{\gamma_0 \sigma_0^2}{M} \tag{4.50}$$

This set of equations is symmetric, taking into account that:

$$|\mathbf{a}_2^H \mathbf{a}_1|^2 = |\mathbf{a}_1^H \mathbf{a}_2|^2 = |\mathbf{a}_1|^2 |\mathbf{a}_2|^2 \cos^2(v_{12}) \tag{4.51}$$

where $\cos(v_{12})$ represents the spatial separation parameter, analogous to Eq. 3.10. In this case, it is defined as the angle between the steering vectors belonging to different clusters and is a measure of spatial separation between them. The following substitutions are made for the equation coefficients:

$$A^{mrc} = 1 - (\frac{K}{2} - 1)\gamma_0 \frac{2}{3N} \tag{4.52}$$

$$B^{mrc} = \frac{K}{2}\gamma_0 \frac{2}{3N} \frac{|\mathbf{a}_2^H \mathbf{a}_1|^2}{M^2} = \frac{K}{2}\gamma_0 \frac{2}{3N} \cos^2(v_{12}) \tag{4.53}$$

$$C^{mrc} = \frac{\gamma_0 \sigma_0^2}{M} \tag{4.54}$$

The power control equations resort to a set of symmetric equations:

$$p_1 A^{mrc} - p_2 B^{mrc} = C^{mrc} \tag{4.55}$$

$$p_2 A^{mrc} - p_1 B^{mrc} = C^{mrc} \tag{4.56}$$

This becomes:

$$(p_1 - p_2)(A^{mrc} - B^{mrc}) = 0 \tag{4.57}$$

which is valid if $p_1 = p_2 = p_{opt}$ or $A^{mrc} = B^{mrc}$. The former condition represents the solution which is generally satisfied for arbitrary coefficients $A^{mrc} \neq 0$, $B^{mrc} \neq 0$, $C^{mrc} \neq 0$ and assuming that the latter condition is not fulfilled. The latter condition is in practice never exactly fulfilled, so the optimum power solution p_{opt}^{mrc} in case of MRC is given as:

$$p_{opt}^{mrc} = p_{opt} = \frac{C^{mrc}}{A^{mrc} - B^{mrc}} \tag{4.58}$$

$$p_{opt}^{mrc} = \frac{\frac{\gamma_0 \sigma_0^2}{M}}{1 - (\frac{K}{2} - 1)\gamma_0 \frac{2}{3N} - \frac{K}{2}\gamma_0 \frac{2}{3N} \cos^2(v_{12})} \tag{4.59}$$

$$p_{opt}^{mrc} = \frac{\frac{\gamma_0 \sigma_0^2}{M}}{1 - \gamma_0 \frac{2}{3N}(\frac{K}{2} - 1 + \frac{K}{2} \cos^2(v_{12}))} \tag{4.60}$$

Positive solutions, $p_{opt}^{mrc} > 0$, are obtained if the following is fulfilled for the number of users K:

$$K < \frac{\frac{3N}{\gamma_0} + 2}{1 + \cos^2(v_{12})} \tag{4.61}$$

It is obvious that as the ratio N/γ_0 increases, the larger number of users can be included and also optimum powers become lower. If the clusters get

closer, which is indicated by the spatial separation parameter approaching unity, the number of users for which the desired target SINR can be achieved is smaller and optimum powers are higher. The number of users is maximum if the two clusters are orthogonal or almost orthogonal in the antenna array space, i.e. when $\cos(v_{12}) << 1$. The optimum power result approaches minimum in that case. It can also be concluded that the ratio N/γ_0 has a much more dominant influence on the result than the spatial separation parameter. In addition to this, it is clear that the antenna array size M has a global effect on the power level reduction and has comparable contribution to the result as the processing gain N.

OC results

In case of OC, the link gains are defined as follows:

$$G_{ii}^{oc} = N|(\mathbf{w}_i^{oc})^H \mathbf{a}_i|^2 \tag{4.62}$$

$$G_{ji}^{oc} = \frac{2}{3}|(\mathbf{w}_i^{oc})^H \mathbf{a}_j|^2 \tag{4.63}$$

The antenna weight vector and the correlation matrix of interference are given as:

$$\mathbf{w}_i^{oc} = \mathbf{R}_{in,i}^{-1} \mathbf{a}_i \tag{4.64}$$

$$\mathbf{R}_{in,i} = \sum_{j=1,j\neq i}^{K} \frac{P_j}{P_i} \mathbf{a}_j \mathbf{a}_j^H + \frac{\sigma^2}{P_i} \mathbf{I}_M \tag{4.65}$$

The antenna weight vector $\mathbf{w}_i^{oc}$ for a linear array can be defined as:

$$\mathbf{w}_i^{oc} = \frac{1}{\sigma^2}\mathbf{a}_i - \frac{\sum_{j=1,j\neq i}^{K} \frac{P_j}{P_i} \mathbf{a}_j \mathbf{a}_j^H \mathbf{a}_i}{\sigma^2(\sigma^2/P_i + \sum_{m=1}^{M} \sum_{j=1,j\neq i}^{K} \frac{P_j}{P_i})} \tag{4.66}$$

The power control equation can be written, taking into account that the optimum powers are the same due to symmetry:

$$p - \gamma_0 \sum_{i=1}^{K/2-1} p - \gamma_0 \sum_{i=1}^{K/2} p \frac{G_{21}^{oc}}{G_{11}^{oc}} = \frac{\gamma_0 \sigma^2 |\mathbf{w}_1^{oc}|^2}{G_{11}^{oc}} \tag{4.67}$$

Also for the OC case, the following result is valid for the link gains when the i-th and the j-th user belong to the same cluster:

$$G_{ji}^{oc}/G_{ii}^{oc} = \frac{2}{3N} \tag{4.68}$$

The gains G_{21}^{oc} and G_{11}^{oc} are derived as follows:

$$(\mathbf{w}_i^{oc})^H = \frac{1}{\sigma^2}\mathbf{a}_i^H - \frac{\sum_{j=1,j\neq i}^{K}\mathbf{a}_i^H\mathbf{a}_j\mathbf{a}_j^H}{\sigma^2(\sigma^2/P_i + M(K-1))} \tag{4.69}$$

$$(\mathbf{w}_i^{oc})^H\mathbf{a}_j = \frac{1}{\sigma^2}\mathbf{a}_i^H\mathbf{a}_j(1 - \frac{KM}{2(\sigma^2/P_i + M(K-1))}) \tag{4.70}$$

$$(\mathbf{w}_i^{oc})^H\mathbf{a}_i = \frac{1}{\sigma^2}M - \frac{1}{\sigma^2(\sigma^2/P_i + M(K-1))}\frac{K}{2}|\mathbf{a}_i^H\mathbf{a}_j|^2 \tag{4.71}$$

$$G_{21}^{oc} = \frac{1}{\sigma^4}|\mathbf{a}_1^H\mathbf{a}_2|^2(1 - \frac{KM}{2(\sigma^2/P_i + M(K-1))})^2 \tag{4.72}$$

$$G_{11}^{oc} = (\frac{1}{\sigma^2}M - \frac{K|\mathbf{a}_1^H\mathbf{a}_2|^2}{2\sigma^2(\sigma^2/P_i + M(K-1))})^2 \tag{4.73}$$

$$|\mathbf{w}_i^{oc}|^2 = \frac{M}{\sigma^4} + \frac{K}{\sigma^4(\sigma^2/P_i + M(K-1))}|\mathbf{a}_j^H\mathbf{a}_i|^2(M\frac{K}{4(\sigma^2/P_i + M(K-1))} - 1) \tag{4.74}$$

The optimum powers solution can be written, analogous to Eq. 4.58:

$$p_{opt}^{oc} = p_{opt} = \frac{C^{oc}}{A^{oc} - B^{oc}} \tag{4.75}$$

where the coefficients are defined as:

$$A^{oc} = 1 - (\frac{K}{2} - 1)\gamma_0\frac{2}{3N} \tag{4.76}$$

$$B^{oc} = \frac{2}{3N}\gamma_0\frac{K}{2}\frac{|\mathbf{a}_1^H\mathbf{a}_2|^2(1 - \frac{KM}{2(\sigma^2/P_i+M(K-1))})^2}{(M - \frac{K}{2(\sigma^2/P_i+M(K-1))}|\mathbf{a}_1^H\mathbf{a}_2|^2)^2} \tag{4.77}$$

$$B^{oc} = \frac{2}{3N}\gamma_0\frac{K}{2}\frac{|\mathbf{a}_1^H\mathbf{a}_2|^2(1 - \frac{KM}{2(\sigma^2/P_i+M(K-1))})^2}{M^2(1 - \frac{KM}{2(\sigma^2/P_i+M(K-1))}\cos^2(v_{12}))^2} \tag{4.78}$$

$$C^{oc} = \gamma_0\sigma^2\frac{M + \frac{K}{(\sigma^2/P_i+M(K-1))}|\mathbf{a}_1^H\mathbf{a}_2|^2(\frac{KM}{4(\sigma^2/P_i+M(K-1))} - 1)}{(M - \frac{K}{2(\sigma^2/P_i+M(K-1))}|\mathbf{a}_1^H\mathbf{a}_2|^2)^2} \tag{4.79}$$

$$C^{oc} = \gamma_0\sigma^2 M\frac{1 + \frac{K}{(\sigma^2/P_i+M(K-1))}M\cos^2(v_{12})(\frac{KM}{4(\sigma^2/P_i+M(K-1))} - 1)}{M^2(1 - \frac{KM}{2(\sigma^2/P_i+M(K-1))}\cos^2(v_{12}))^2} \tag{4.80}$$

The main purpose of this analysis is to illustrate the gain of OC over MRC in the reduction of optimum powers. The coefficients that determine the solution for optimum powers in case of OC can be related to coefficients that determine the optimum powers in case of MRC, as follows:

$$A^{oc} = A^{mrc} \tag{4.81}$$

$$\frac{B^{oc}}{B^{mrc}} = \frac{(1 - \frac{KM}{2(\sigma^2/P_i + M(K-1))})^2}{(1 - \frac{KM}{2(\sigma^2/P_i + M(K-1))}\cos^2(v_{12}))^2} \tag{4.82}$$

$$\frac{B^{oc}}{B^{mrc}} \approx \frac{(1 - \frac{K}{2(K-1)})^2}{(1 - \frac{K}{2(K-1)}\cos^2(v_{12}))^2} \tag{4.83}$$

$$\frac{C^{oc}}{C^{mrc}} = \frac{1 + \frac{KM\cos^2(v_{12})}{(\sigma^2/P_i + M(K-1))}(\frac{KM}{4(\sigma^2/P_i + M(K-1))} - 1)}{(1 - \frac{KM\cos^2(v_{12})}{2(\sigma^2/P_i + M(K-1))})^2} \tag{4.84}$$

$$\frac{C^{oc}}{C^{mrc}} \approx \frac{1 - \frac{K}{(K-1)}\cos^2(v_{12}) + (\frac{K}{2(K-1)})^2\cos^2(v_{12})}{1 - \frac{K}{(K-1)}\cos^2(v_{12}) + (\frac{K}{2(K-1)})^2\cos^4(v_{12})} \tag{4.85}$$

$$\frac{C^{oc}}{C^{mrc}} \approx \frac{1 - \frac{K}{(K-1)}\cos^2(v_{12})(1 - \frac{K}{4(K-1)})}{(1 - \frac{K}{2(K-1)}\cos^2(v_{12}))^2} \tag{4.86}$$

It is obvious that the coefficient B^{oc} always satisfies the following, due to $\cos(v_{12}) \leq 1$:

$$B^{oc} \leq B^{mrc} \tag{4.87}$$

This, basically, tends to decrease the optimum powers of OC with respect to MRC. The behaviour of the coefficient C^{oc} tends to increase transmit powers, since:

$$C^{oc} \leq C^{mrc} \tag{4.88}$$

However, the contribution of the coefficient C^{oc} to the increase of the transmit power is smaller than the contribution of the coefficient B^{oc} to the power reduction. In turn, the optimum powers of OC are decreased with respect to MRC. The separation between the clusters, represented by the factor $\cos(v_{12})$, is the main parameter that determines the difference from MRC. If the clusters get very close to each other, i.e. $\cos(v_{12}) \approx 1$, both B^{oc} and

C^{oc} results approach the MRC coefficients B^{mrc} and C^{mrc}. Again, it is clear that the influence of the spatial separation to the results is small for high N/γ_0 ratio, contained in A^{oc} and B^{oc}. In that case, there is not a significant difference between results for OC and MRC. Also as the antenna array size (contained in C^{oc}) gets larger, the power reduction when using OC with respect to MRC becomes smaller.

This analysis features the scenario when all users contribute equally to the result. The closed-form expressions for optimum powers provide basic insight into the level of influence of system parameters. In a realistic multi-user scenario, a larger number of multipath components belong to one user and there is often one critical user with the smallest attenuation in strength, which, basically, puts the main limitation to the performance by acting as the strongest interferer to other users. The smart antenna performance analysis will be next performed for a more concrete environment and representative system settings.

4.3.3 Simulation results

In the following examples, the influence of the above mentioned parameters will be shown for a concrete micro-cell urban environment. The channel model used for simulations is the ray-tracing tool, developed for urban micro-cells, as previously introduced. The transmit frequency is 1.9 GHz. and the antenna gain in elevation plane is 18 dB_i (antenna assumed omni-directional in azimuth plain). The BS thermal noise level is σ^2=-103 dBm. Part of the TU/e campus, used as a simulation environment, is shown in Fig. 4.2. One of the users is moving along a trajectory, whereas others are assumed fixed, generated like snapshots in the same environment. OC and MRC algorithms are analysed in terms of the reduction in the transmit power for the given target SINR and also compared to the case with a single antenna, which is treated as a reference case. The simulation results are related to transmit power of the moving user. The parameters varied in the simulation are the processing gain, antenna array size, number of users and target SINR. The following iterative procedure, as proposed in [55] and [56], was used to obtain optimum transmit powers for the i-th user:

$$P_i(n+1) = \frac{\gamma_0}{G_{ii}}\left(\sum_{j\neq i} G_{ji}P_j(n) + \sigma_i^2\right) \tag{4.89}$$

In the last expression index n indicates an iteration number. The transmit powers in each iteration are updated on the basis of powers from previous

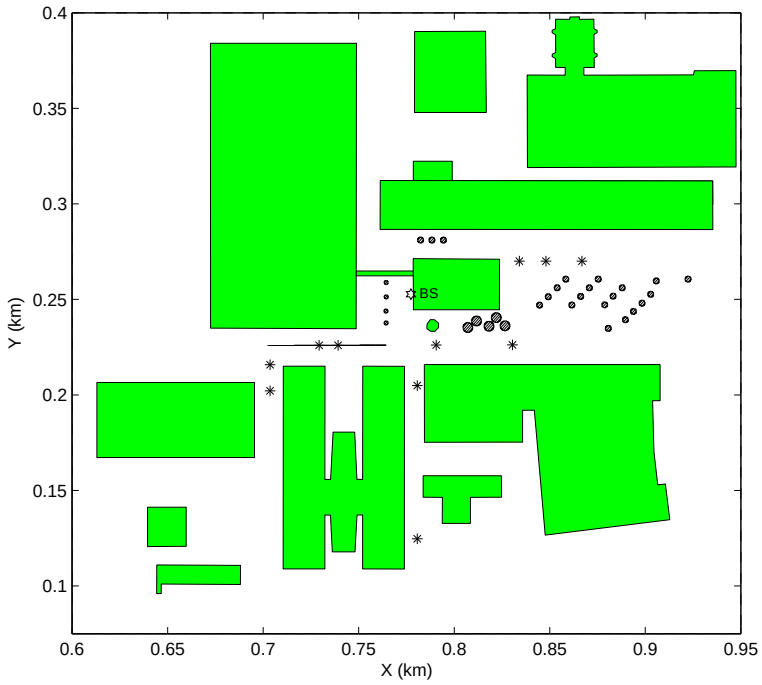

Figure 4.2: Simulation environment: one user moving along the trajectory, $*$ represents a fixed user, BS designates the base station

---

iteration. This iterative procedure converges to the optimal solution (provided that the condition, given by Eq. 4.11 is fulfilled) starting from an arbitrary transmit power vector. The i-th user SINR achieved in the n-th iteration can be expressed as:

$$\gamma_i(n) = \frac{G_{ii}P_i(n)}{\sum_{j\neq i} G_{ji}P_j(n) + \sigma_i^2} \tag{4.90}$$

which converges to the desired γ_0 after a number of iterations (see Appendix B).

Initially, the processing gain was set to $N_{dB} = 10\log N$=25 dB (voice service), the corresponding target SINR being γ_0=5 dB, the number of antenna elements M=3 and the total number of users K=15. The convergence process of the achieved SINR including a single antenna case, MRC and OC for the given set of system parameters is shown in Fig. 4.3. The OC has the best convergence properties, reaching the target SINR after the smallest

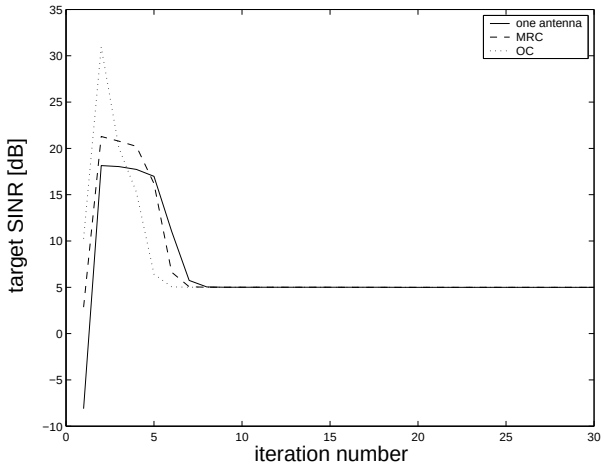

Figure 4.3: The convergence properties of a single antenna case, MRC and OC

number of iterations, as compared to MRC and a single antenna case. MRC has better convergence properties than a single antenna. The convergence of a particular processing scheme towards the desired target value is directly related to the level of interference suppression that can be achieved. The scheme that has better interference suppression properties reaches the target SINR after a smaller number of iterations. In the following examples, the results of optimum transmit powers obtained after the desired target was reached is shown. The main goal is to explain the influence of the system parameters on powers assuming that the power control is instantaneous. The effect of the difference in the convergence properties of OC and MRC in a real-time power control process will be more clear in the imperfect power control analysis in Section 4.4.2 and Section 6.2.2.

The results of optimum transmit powers for K=15, obtained from MRC, OC and a single antenna case, are shown in Fig. 4.4(a). Antenna processing yields considerable gain in the reduction of mobile transmit power over a single antenna case, while the difference between OC and MRC is negligible. In the reference case, the convergence to the desired target SINR value cannot be achieved for K=20, while MRC fails to reach the desired target for K=40. In Fig. 4.4(b), optimum transmit powers for OC are shown for a various number of users K=15, K=20 and K=40. OC succeeds in reaching the target value for all those cases, with only a difference of up to 5 dB in

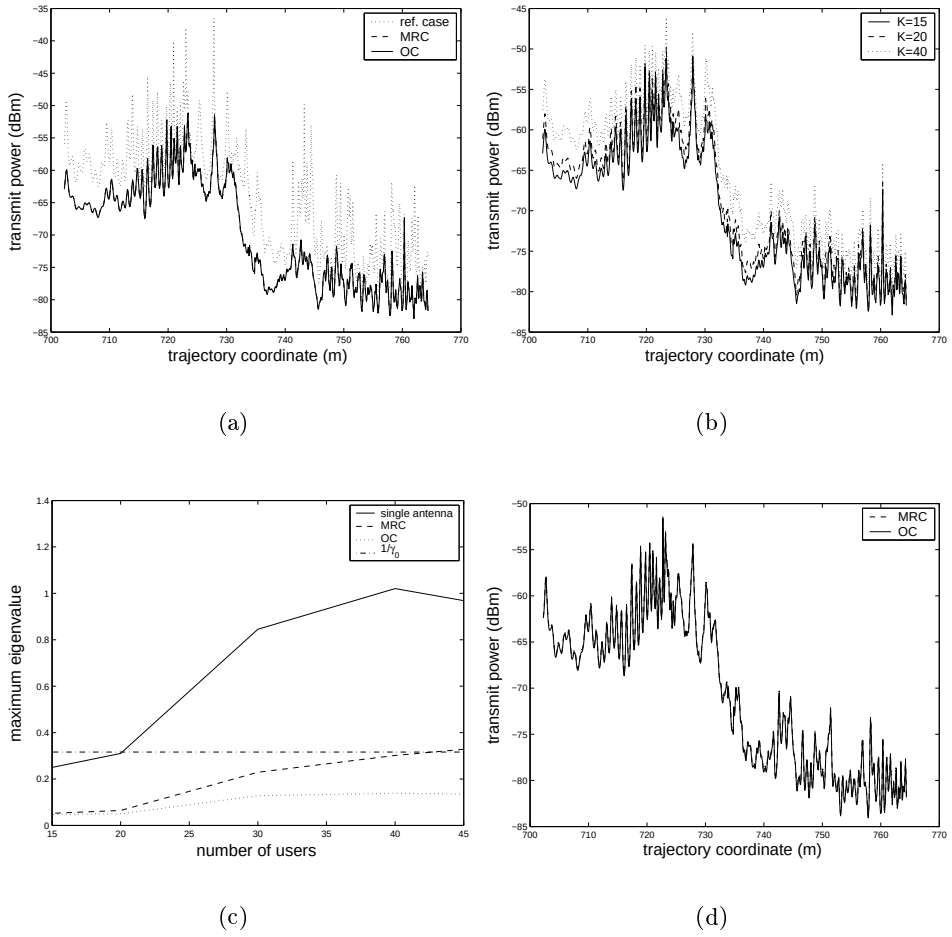

Figure 4.4: (a) Transmit power for OC, MRC and a single antenna case, K=15, N_{dB}=25 dB, M=3, γ_0=5 dB; (b) Transmit power for OC, N_{dB}=25dB, M=3, γ_0 = 5dB, K=15, 20, 40; (c) Eigenvalues for OC, MRC and a single antenna case, N_{dB}=25 dB, M=3, γ_0=5 dB; (d) Transmit power for OC and MRC, K=40, N_{dB}=25 dB, M=5, γ_0=5 dB

transmit power between them.

It can be seen that as the number of users increase for a constant set of other parameters, it becomes more difficult to achieve the desired target SINR for all users in the reference case (already for K=20), involving only

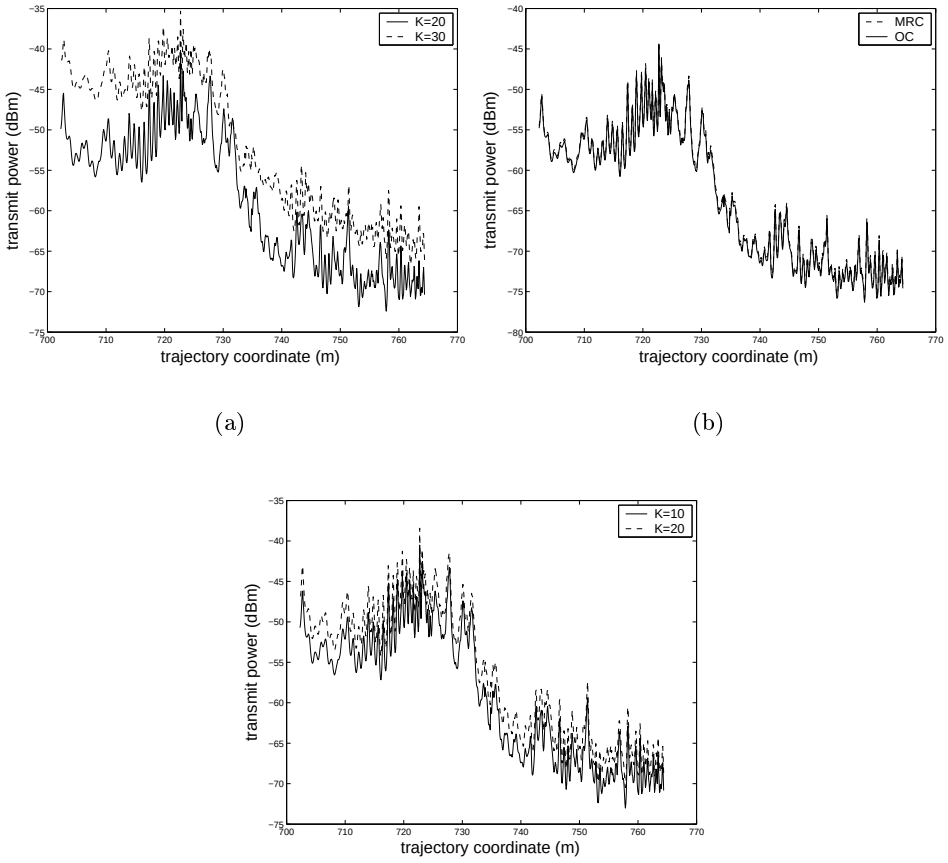

(a) (b)

(c)

Figure 4.5: (a) Transmit power for OC, N_{dB}=15 dB, M=5, γ_0=5 dB; (b) Transmit power for OC and MRC, K=30, N_{dB}=15 dB, M=5, γ_0=1 dB; (c) Transmit power for OC, N_{dB}=10 dB, M=5, γ_0=1 dB

simple correlation with the desired signal, and the antenna processing becomes necessary to sustain that number of users. If the number of users is even further increased (over 40), OC is obviously superior to MRC, which involves plain beamforming towards the desired user. The convergence towards the target SINR is governed by the condition given by Eq. 4.11. As the maximum eigenvalue of the gain matrix $\mathbf{G}$ increases, the given condition

becomes more critical for the constant target γ_0. The dependance of these eigenvalues on the number of users for a single antenna, MRC and OC case are shown in Fig. 4.4(c). The curve for the reference case crosses the critical value of $1/\gamma_0$ for K=20 users, and the curve for MRC case is very close to the critical value for K=40 users, which is in accordance with the achieved results. The curve for a single antenna case is most sensitive to the change in the number of users, whereas OC is most stable for the whole range of number of users simulated. The small difference between eigenvalues corresponding to OC and MRC for a wide range of number of users indicates a negligible difference in optimum powers between the two processing cases. Also, the slow increase of the eigenvalues for OC with the number of users indicates the small increase in the transmit powers, as given by Fig. 4.4(b). In case the antenna array size is increased to M=5, MRC can sustain K=40 users and the performance of MRC and OC, again, becomes almost equal as shown by Fig. 4.4(d). Plain beamforming towards the desired user has much better interference suppression qualities than in the case of M=3 due to a narrower beam. Basically, by choosing the antenna array of a larger size, there is, again, no obvious need to perform OC for the voice service.

The processing gain of N_{dB}=25 dB is relatively large. This is the standard value for the bit-rate of 12.2 kbps, typical for the voice service [4]. Keeping the antenna array size of M=5 and changing the processing gain to N_{dB}=15 dB, the target SINR of γ_0=5 dB can not be achieved in case of MRC already for K=20 users. For this set of parameters, OC is superior in performance to MRC even with the antenna array size of M=5. In Fig. 4.5(a) the results for OC are shown for this new set of parameters. The increase in the transmit power with the increased number of users is more significant (up to 10 dB) with the smaller processing gain and a large target of 5 dB. In case the target value is decreased to γ_0=1 dB, while keeping other parameters equal to those in the previous example, K=30 users can be sustained for both OC and MRC, with equal optimum powers, as shown by Fig. 4.5(b). These examples clearly illustrate the already mentioned theoretical conclusion that the performance of antenna processing largely depends on the ratio between the target SINR value and the processing gain γ_0/N. If the processing gain is further reduced to N_{dB}=10 dB (which corresponds to the bit-rate of 384 kbps for the non-real time data service), while keeping the same target value and antenna array size used in the previous example, K=10 users can be sustained for both OC and MRC, whereas in case of K=20 users, the optimum transmit power solution is obtained only for OC (see Fig. 4.5(c)).

In the examples shown so far, the only obvious advantage of using OC

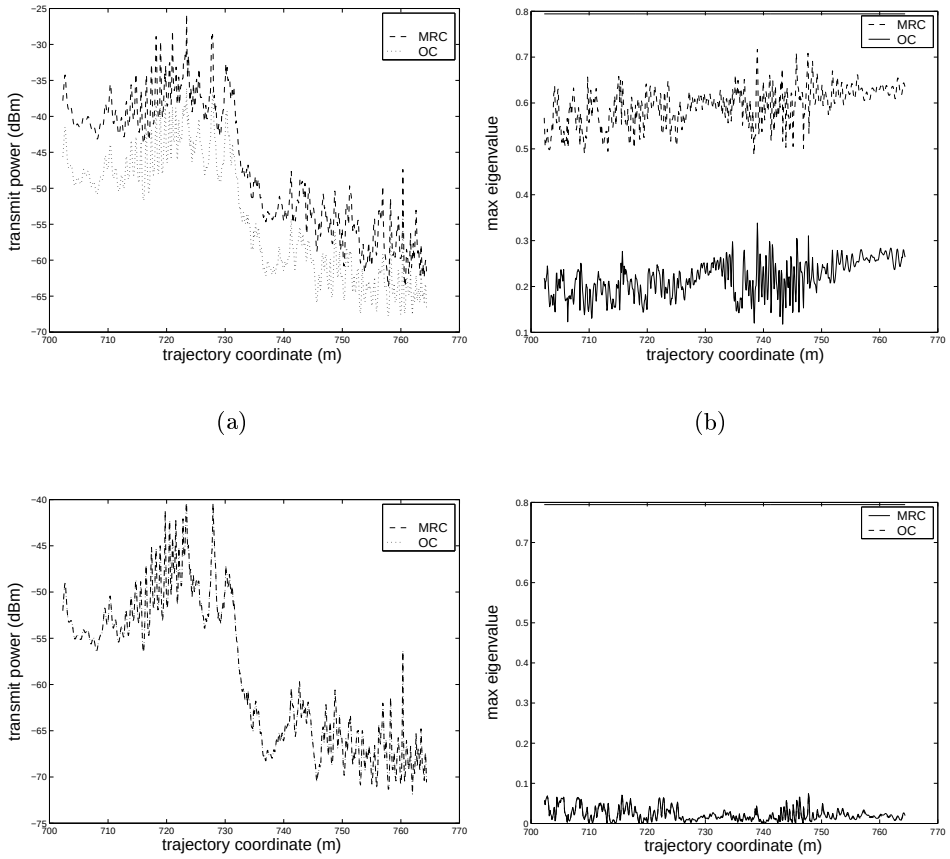

Figure 4.6: K=6, N_{dB}=10 dB, M=3, γ_0=1 dB: (a) Transmit power for OC and MRC in scenario 1; (b) Maximum eigenvalue for OC and MRC in scenario 1; (c) Transmit power for OC and MRC in scenario 2; (d) Maximum eigenvalue for OC and MRC in scenario 2

over MRC is a larger number of users for which the desired target SINR can be achieved. The gain of OC over MRC in the reduction of optimum transmit powers is not so significant for the system settings used. These results are also summarised in [57]. In a non power-controlled environment, the reduction in transmit power of OC over MRC for the desired signal

and constant interference (the power of interfering signals is not changing) can be visible for the given fixed SINR even when the processing gain is high, which only provides additional gain (in terms of separation in code) to antenna processing (due to separation in angular domain). If power control is included, the potential of antenna processing for that user is not fully exploited, because certain requirements in terms of target SINR has to be met for all users. The reduction in transmit power for one user is not so large as compared to a non power-controlled situation because of the need to modify transmit powers of all users. For most services (except for very high data rates of up to 2 Mb/s), the target SINR is considerably lower than the processing gain. When the ratio γ_0/N is high, the interfering users are seen as white noise from the point of view of one user even when the number of users is small, which makes OC performance not significantly advantageous over MRC.

The following example illustrates the case when a significant gain in the power reduction is obtained when comparing MRC with OC. The processing gain is N_{dB}=10 dB and the antenna array size is M=3, i.e. the influence of the most dominant parameters is reduced and the spatial distribution of users becomes more influential. The results for two different spatial distributions of users (referred to as *scenarios* 1 and 2) are shown for K=6 users. In scenario 1, shown by Fig. 4.6(a), the difference of around 10 dB can be observed for OC and MRC, whereas the transmit powers are the same in scenario 2, see Fig. 4.6(c). This is also reflected by the relation of maximum eigenvalues for OC and MRC case, shown by Fig. 4.6(b) and Fig. 4.6(d). In the second scenario, the majority of users are closely spaced in angular domain, resulting in negligible difference between the performance of OC and MRC, as already explained in Section 4.3.2.

In order to provide a better look on the differences between the two scenarios, the antenna patterns for OC and MRC are shown for each user. The antenna pattern optimised for the i-th user is represented as a relative gain $\varsigma_i(\varphi)$ in a given angular direction φ as:

$$\varsigma_i(\varphi) = \frac{|\mathbf{w}_i^H \mathbf{a}(\varphi)|^2}{\mathbf{w}_i^H \mathbf{w}_i} \tag{4.91}$$

where $\mathbf{a}(\varphi)$ is the antenna steering vector and $\mathbf{w}_i$ is antenna weight vector optimised for the i-th user by either OC or MRC scheme. The following figures show antenna patterns simultaneously optimised for all users with respect to the user that acts as the strongest interferer, i.e. the "critical user". The antenna pattern of the "critical user" is not included and multipath components of all users in figures are depicted assuming that their

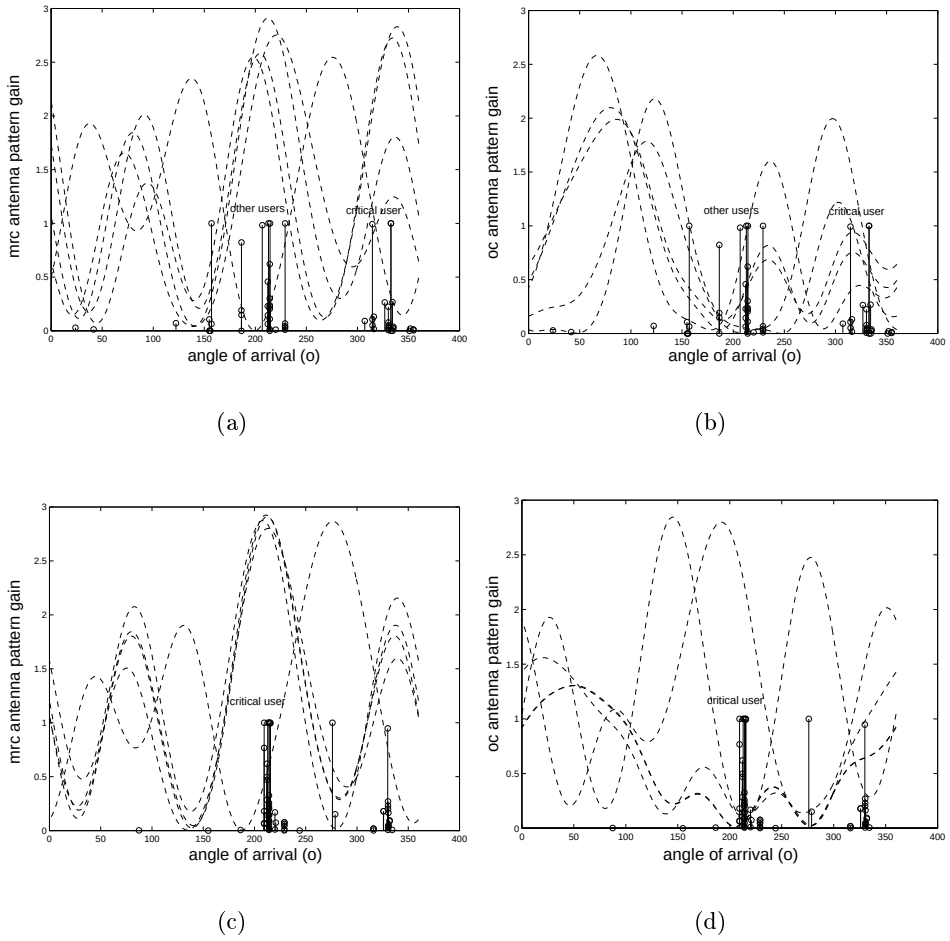

Figure 4.7: the "critical user" clearly separated from other users in angular domain (scenario 1): (a) Antenna pattern for MRC; (b) Antenna pattern for OC; the "critical user" overlaps with other users in angular domain (scenario 2): (c) Antenna pattern for MRC; (d) Antenna pattern for OC

strength is normalised with respect to the maximum value. It can be seen from Fig. 4.7(a) and Fig. 4.7(b) that, in the case of scenario 1, the "critical user" is sufficiently separated in angle from other users and there is a difference between the level of dominant interference suppression between OC and MRC. The antenna patterns optimised for a majority of users provide a

gain in the direction of the "critical user" that is lower in case of OC than for MRC. In scenario 2, the "critical user" is closely spaced in angular domain with the bulk of multipath components belonging to other users, resulting in insignificant difference in OC versus MRC gain; steering a beam towards the desired user when MRC is applied, also favours the "critical user" and steering nulls towards the "critical user", as in case of OC, also suppresses other users, see Fig. 4.7(c) and Fig. 4.7(d).

The results for different system parameters are summarised in the table 4.1. For various system set-up, analysed in previous examples, the ability of a specific processing scheme to converge towards the desired target is shown, followed by the specific influence of system parameters to the result.

N_{dB}	γ_0	M	K	general result	comment
25 dB	5 dB	3	15	OC, MRC, single antenna converg.	up to 10 dB OC, MRC versus single antenna gain
25 dB	5 dB	3	20	OC, MRC converg. negligible OC versus MRC gain	3-element array adequate for the voice service
25 dB	5 dB	3	40	MRC not converg.	MRC critical for a larger num. of users
25 dB	5 dB	5	40	OC, MRC converg. negligible OC versus MRC gain	5-element array better for MRC
15 dB	5 dB	5	20	MRC not converg.	MRC critical for a larger target SINR
15 dB	1 dB	5	30	OC, MRC converg. negligible OC versus MRC gain	5-element array adequate for the data service
10 dB	1 dB	5	20	MRC not converg.	MRC critical for the data service
10 dB	1 dB	5	10	OC, MRC converg. negligible OC versus MRC gain	
10 dB	1 dB	3	6	OC, MRC converg.	up to 10 dB OC versus MRC gain

Tabel 4.1: Perfect power control results for different system set-up

In the perfect power control case, there were not many scenarios when a significant power reduction was obtained for OC with respect to MRC. The spatial structure of users was not so influential for the majority of system settings and the only advantage of OC over MRC was a better ability to accommodate a larger number of users. The analysis with the imperfect power control case will yield more examples for which a significant reduction of power is obtained.

4.4 Imperfect power control

Having shown the influence of the most dominant parameters for the antenna array processing under perfect power control, the next step is to analyse the same trends including a more realistic power control process. The imperfections in the power control modelled in this analysis stem from two aspects of the fast power control implemented in UMTS:

- Finite time allocated for the update of the transmit power. Optimum powers can not be reached at the same moment when the channel conditions change. This makes the system performance dependent on the MS speed and the power control frequency.
- Constant step-size of 1 dB in the transmit power update process. Since the power update is based on increments/decrements of 1 dB, irrespective of the level of change in the channel between two successive update time instants, the achieved SINR fluctuates around the desired target SINR, never settling at the exact value.

The modelling of the realistic power control is explained in Section 4.4.1. The simulation results will be presented in Section 4.4.2, for the same set of system parameters as used in Section 4.3.3.

4.4.1 Modelling imperfect power control

Fast power control in UMTS is performed at the frequency of $f_{pc} = 1500$ Hz, i.e. every $t_{pc} = 6.66 \cdot 10^{-4}$ s. In order to model the effect of the finite update time with satisfactory accuracy for the given MS speed v using the spatial channel model concept, described in Chapter 2, the channel composition should be calculated for the positions on the trajectory with a sufficiently small spacing. The power update process itself is performed for the spacing d_{pc} defined by the MS speed and the duration of the time slot allocated for the power update, as $d_{pc} = vt_{pc}$. For the pedestrian speed of v=3 km/h,

the corresponding spacing will be $d_{pc} = 5.5 \cdot 10^{-4}$ m, which for the carrier frequency f_c =1.9 GHz translates into $d_{pc} = 0.0036 \cdot \lambda_c$. This is much smaller than half wavelength spacing, already indicated in Section 3.4 as sufficient for modelling small-scale channel characteristics. Regarding the power update procedure, the spacing corresponding to the MS speed of v=3 km/h is taken as a reference spacing d_{ref}. For MS speeds v larger than the reference speed v_{ref}=3 km/h ($v > v_{ref}$) the power update takes place every $d_{pc} = vt_{pc} > d_{ref}$. For the positions "contained inside" one time slot t_{pc} (or over the d_{pc} length), the same power levels obtained in the previous step are applied on the users' spatial signatures.

The difference between the transmit power in the imperfect power control case from the transmit power when the exact target is reached for all users is shown in Fig. 4.8(a). Only one user is included with the aim to illustrate the channel tracking properties of the realistic power control process and the dependence of the results on different mobile velocities. In Fig. 4.8(a), the speed was varied from v=3 km/h to v=50 km/h (low to moderate speed, typical for urban environments) and the results obtained for a trajectory of 3 m length. At the beginning of the trajectory, the transmit power is equal to a maximum mobile power of 24 dBm. After a short transient period optimum power levels are reached. As the speed increases, the transient period is longer. Power control tracks fast fading successfully at low speeds. The envelope of the signal obtained after antenna array processing for M=3 is shown in Fig. 4.8(b) for a trajectory length of 1 m. A close-up of the change in the transmit power for the same 1 m trajectory is shown in Fig. 4.8(c). This shows that the fast fading of the optimum transmit power is inverse to the fast fading of the signal envelope, as expected. The changes in the achieved SINR for mobile speeds of v=3 km/h to v=50 km/h are shown in figures Fig. 4.9(a), Fig. 4.9(b) and Fig. 4.9(c). The achieved SINR fluctuates around the desired target value of γ_0=5 dB with the error of around 1 dB for the speed of v=3 km/h. As the speed increases, the transient period becomes longer, the same as with the transmit powers. The deviations from the desired target value once the optimum level is reached, go up to 3 dB for v=20 km/h and 5 dB for v=50 km/h.

In case there are more users in the system, the situation becomes more complex, because the desired target SINR need to be reached for all users. The first observation is that the condition for the SINR requirement is not so strict. It is no longer possible to achieve the exact target for all users due to errors inherent in the realistic power control. In consequence, the comparison between OC and MRC will be looked at from a slightly different point of view. In the analysis to follow, the power control requirement is

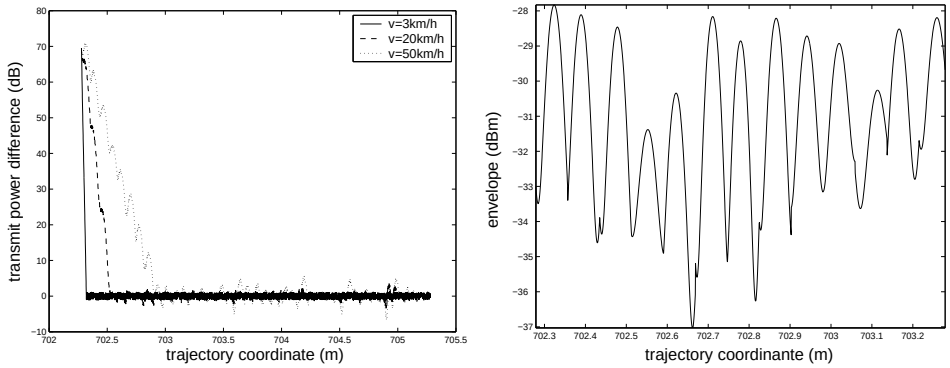

(a)

(b)

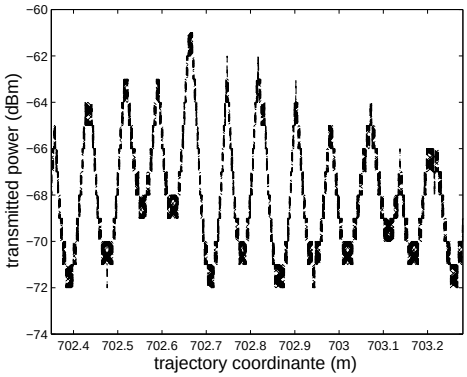

(c)

Figure 4.8: (a) The difference in the transmit power from the perfect power control case, M=3, v=3 km/h-50 km/h; (b) Signal envelope, M=3; (c) Transmit power, M=3, v=3 km/h

---

said to be fulfilled if the achieved SINR fluctuates around the desired target value for all users. When a certain number of users can not be sustained for a particular system set-up, SINR will fluctuate around a mean value that is different from the desired target γ_0, for at least one user. In this way, a larger number of users can be considered than in the perfect power control case for the same system parameters, since the deviations in the achieved

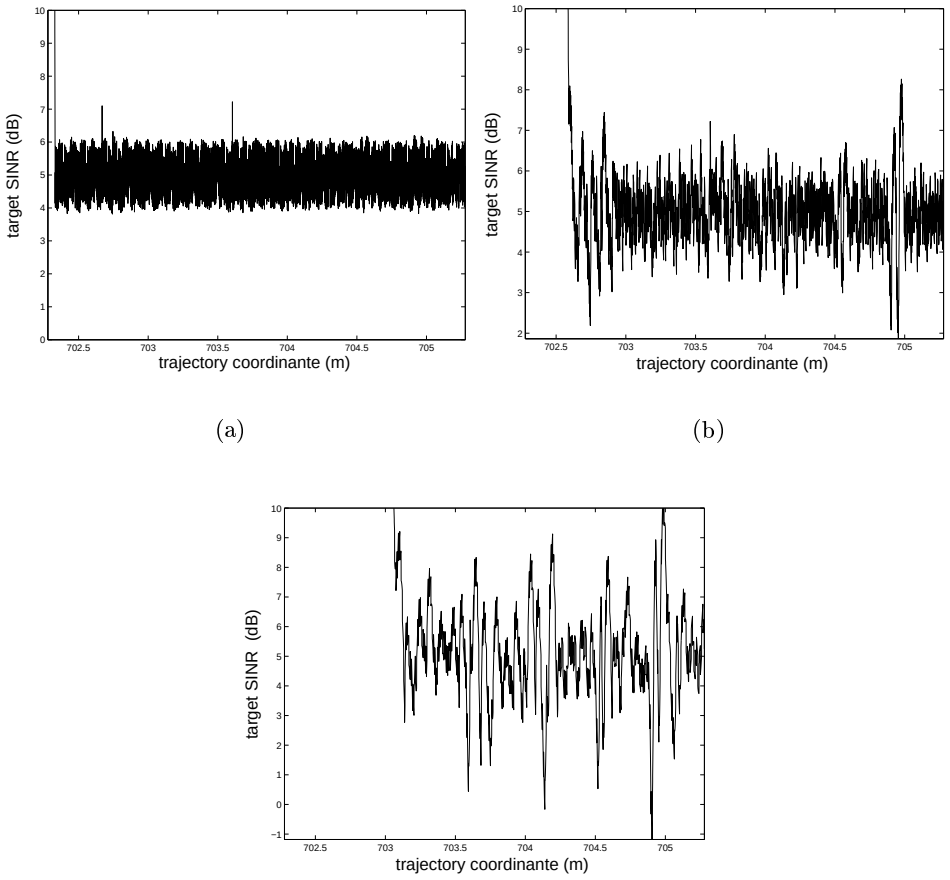

Figure 4.9: The changes in the achieved SINR, M=3: (a) v=3 km/h; (b) v=20 km/h; (c) v=50 km/h

---

SINR from the target γ_0 are now "allowed".

4.4.2 Simulations and results

The simulations featuring imperfect power control have been performed for the same system parameters and users' locations, as in Section 4.3.3. The trajectory length is 3 m and the starting powers of all users are equal to the

maximum mobile power of 24 dBm. The difference in the transmit power from the perfect power control case for K=15 users, the processing gain N_{dB}=25 dB (voice service) and the antenna array size M=3 for three MS speeds is shown in Fig. 4.10(a). It can be seen that the results are no longer centred around zero, as was the case with one user, shown by Fig. 4.8(a). With more users involved in the power control process, their power levels also deviate from the perfect optimum values. For larger speeds, the transient periods also become larger and power levels deviate more from the perfect power control case, just like in the example with one user, shown in Section 4.4.1. The results from Fig. 4.10(a) are represented in terms of probability density function (pdf) in Fig. 4.10(b). For the trajectory length of 3 m, there are more than 5000 samples, which is sufficient to obtain statistically reliable results. This can be regarded as a more compact representation of the transmit power results, where the shape of pdfs is determined by the spatial behaviour of power both in the transient and the stable period.

The pdfs, each obtained for a different MS speed, are also convenient for the analysis of the influence of the speed on the power levels. It is clear that for low to moderate speeds there is not a significant difference in the distribution of optimum powers. The curves follow a similar pattern in shape and are characterised by a slightly larger spread round the mean value as the MS speed increases. The fast fading effects are not so pronounced for this environment and the deviation from the perfect case is not significantly different as MS speed changes. The gain of OC over MRC in the reduction of transmit power for different MS speeds is also represented in terms of a pdf obtained on the basis of the difference in transmit powers between these two processing schemes, as in Fig. 4.10(c). The gain is centred around zero for this example, which is in accordance with the results in the perfect power control case for the same set of system parameters. The representation of the simulation results to follow will be given in terms of pdfs only, both for the optimum transmit power difference and OC versus MRC gain.

The solution for optimum powers in case of the perfect power control, however, does not exist for all system parameters, as already shown in Section 4.3.3. Therefore, it is not always possible to provide pdfs on the basis of difference from the perfect power control for both OC and MRC. For that reason, the pdfs for the results to follow were computed on the basis of transmit power difference from the case when the MS speed is v=3 km/h, treated as a reference case. The results for the current system settings is shown in Fig. 4.10(d). The influence of different speeds on the results can also be analysed on the basis of this type of representation for both OC and MRC. The curves are centred around zero and the increased spread of the

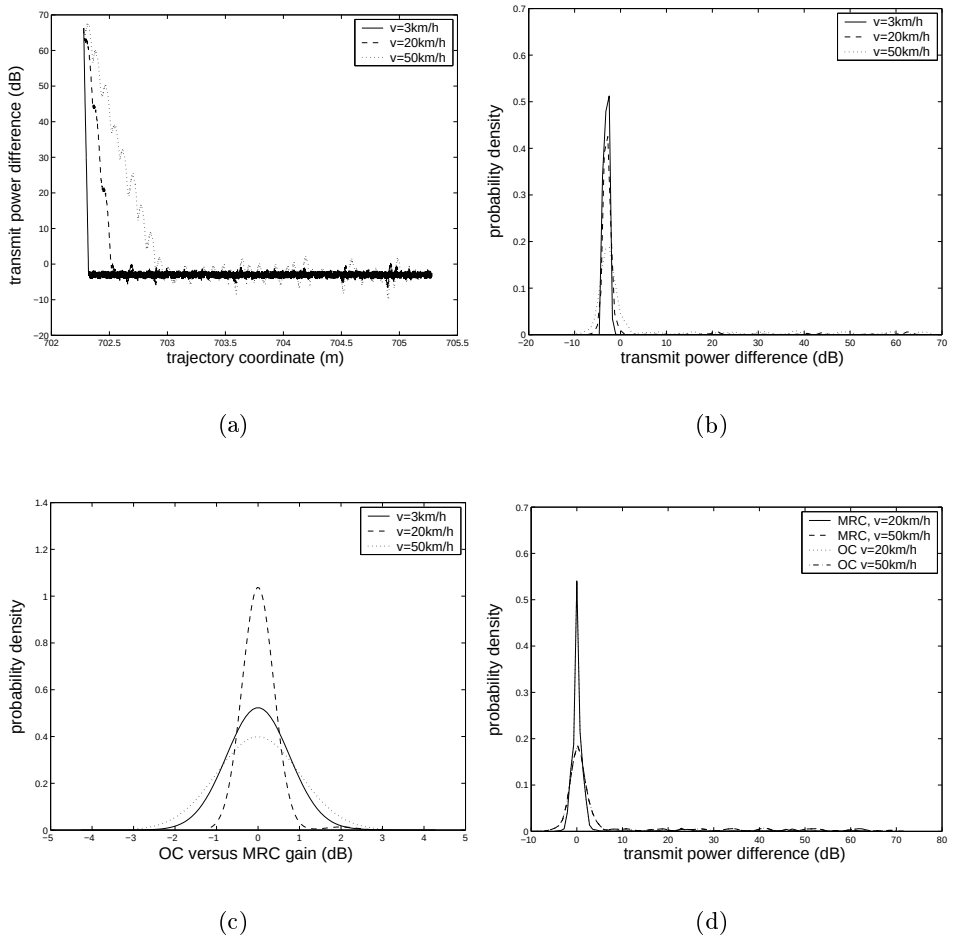

Figure 4.10: K=15, N_{dB}=25 dB, M=3, γ_0=5 dB: (a) The difference in the transmit power from the perfect power control for OC; (b) The probability density of the difference in transmit power from the perfect power control for OC; (c) The probability density of OC versus MRC power reduction; (d) The probability density of the difference in the transmit power from the case when v=3 km/h for OC and MRC;

---

pdf curve as the MS speed increases is also visible here.

It has been shown in Section 4.3.3 that if the number of users is increased to K=40 for the same system parameters, OC can achieve the exact desired

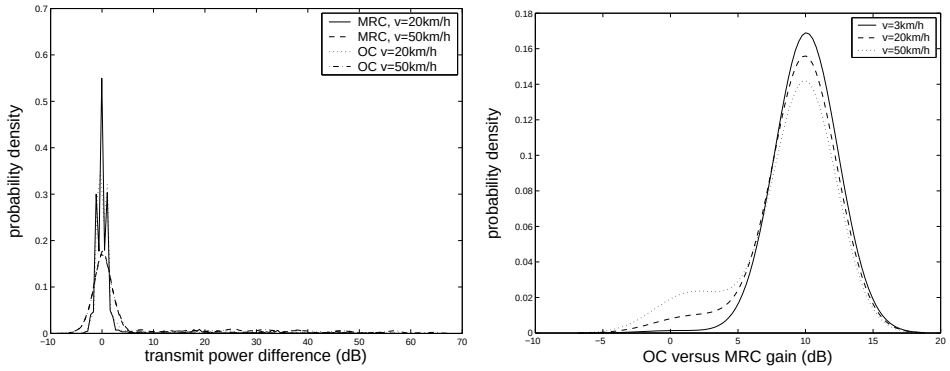

(a) (b)

Figure 4.11: K=40, N_{dB}=25 dB, M=3, γ_0=5 dB: (a) The probability density of the difference in transmit power from the case when v=3 km/h for OC and MRC; (b) The probability density of OC versus MRC power reduction

target for all users, contrary to MRC. Allowing deviations from the desired target value, MRC also achieves SINR that fluctuates around the desired target γ_0=5 dB for all three MS speeds. The results for this case are shown in Fig. 4.11(a) and Fig. 4.11(b). The power reduction of 10 dB obtained by OC over MRC is visible here. In the perfect power control analysis, it has been stated that for the voice service (high processing gain) the transmit power levels are the same for both OC and MRC (in case the target SINR can be reached for both antenna processing schemes). This is valid for a large range of number of users. As the number of users is increased, there is a point when MRC can no longer fulfill the condition given by Eq. 4.11 and then the main conclusion was that the only obvious advantage of OC is the ability to sustain a larger number of users. When MRC can not perform as good as OC, it means that the spatial structure of users become influential for the results. This is reflected in the transmit power reduction gain of OC over MRC, when the power control condition is not so strict, i.e. allowing deviations from the desired target SINR.

The examples to follow show results for the data service, with processing gains of N_{dB}=15 dB and N_{dB}=10 dB. In Section 4.3.3, it has been shown that the antenna array size should be increased to M=5 to accommodate relatively large number of users for a lower processing gain. The results

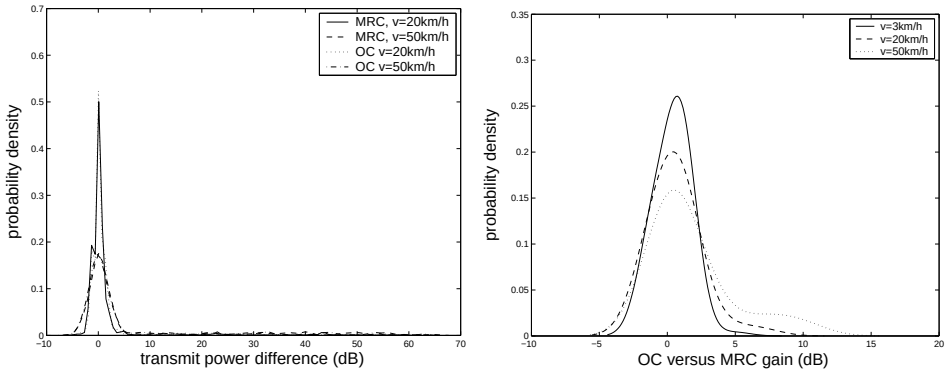

(a) (b)

Figure 4.12: K=30, N_{dB}=15 dB, M=5, γ_0=1 dB: (a) The probability density of the difference in the transmit power from the case when v=3 km/h for OC and MRC; (b) The probability density of OC versus MRC power reduction

---

for the data service, when the processing gain is N_{dB}=15 dB and antenna array size of M=5, are shown in figures Fig. 4.12(a) and Fig. 4.12(b). The results for the processing gain of N_{dB}=10 dB are given by Fig. 4.13(a) and Fig. 4.13(b), featuring K=20 users, and by Fig. 4.13(c) and Fig. 4.13(d), featuring K=10 users. A negligible gain in power reduction of OC over MRC, which is also in accordance with the results given in Section 4.3.3, was obtained for the following system settings: N_{dB}=15 dB, K=30 (see Fig. 4.12(b)) and N_{dB}=10 dB, K=10 (see Fig. 4.13(d)). Different results from the perfect power control were obtained for K=20 and N_{dB}=10 dB. For the perfect power control case, the same target for K=20 users could be achieved using OC for this system settings, while MRC failed. Again, when the power control condition is relaxed by allowing deviations from the desired target, MRC also achieves a satisfactory performance. If OC is used, a significant reduction in transmit power of around 8 dB has been obtained, as shown in Fig. 4.13(b).

When the number of users is small, below K=10, the antenna array size of M=3 is sufficient, as already shown in Section 4.3.3. A significant gain of OC over MRC has been observed for the perfect power control case, which is also reflected when imperfections are included, as shown by Fig. 4.14(b). From Fig. 4.14(a) it is clear that the effect of the MS speed is more pro-

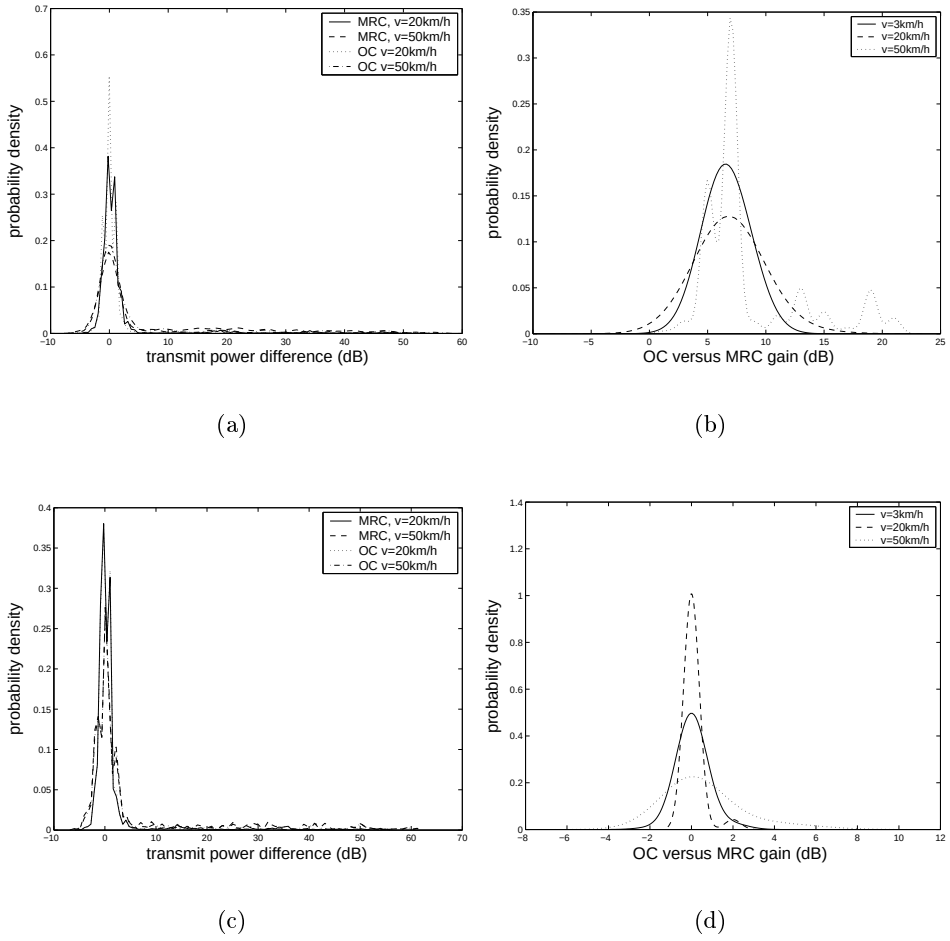

Figure 4.13: (a) The probability density of the difference in the transmit power from the case when v=3km/h for OC and MRC, K=20, N_{dB}=10 dB, M=5, γ_0=1 dB; (b) The probability density of OC versus MRC power reduction, K=20, N_{dB}=10 dB, M=5, γ_0=1 dB; (c) The probability density of the difference in the transmit power from the case when v=3 km/h for OC and MRC, K=10, N_{dB}=10 dB, M=5, γ_0=1 dB; (d) The probability density of OC versus MRC power reduction, K=10, N_{dB}=10 dB, M=5, γ_0=1 dB

nounced for this example as compared to other system settings. The transmit power reduction gain of OC over MRC varies from 8 dB-12 dB for the three

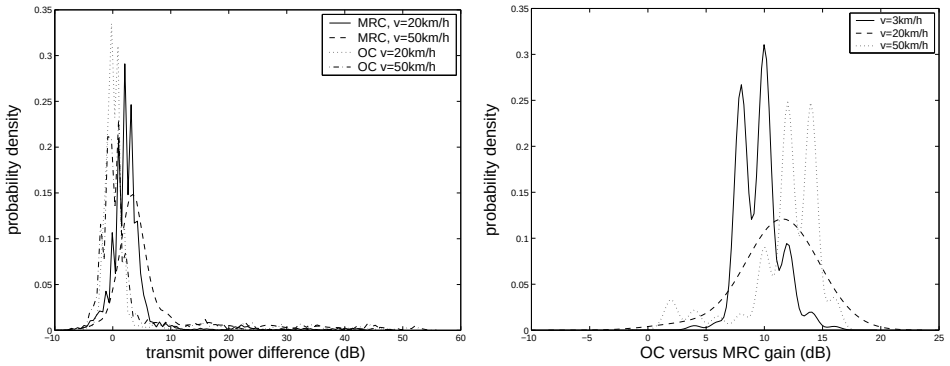

(a) (b)

Figure 4.14: K=6, N_{dB}=10 dB, M=3, $\gamma_0 = 1$ dB: (a) The probability density of the difference in the transmit power from the case when v=3 km/h for OC and MRC; (b) The probability density of OC versus MRC power reduction

---

MS speeds. The influence of different speeds is more visible for MRC in comparison to OC. In case of OC the effect is not that significant, as was the case with the previous examples. The effect is manifested as a visible shift of pdfs towards higher power levels, as the MS speed increases. The main cause is related to weaker interference suppression properties of MRC, which become pronounced when the spatial structure is influential for the result. This example is representative of cases when the spatial structure of users becomes particularly influential, because of the lower processing gain and the small antenna array size, as shown in Section 4.3.3. As the MS speed increases, the channel changes faster with respect to the update time and power levels for all users deviate more from the optimum ones. The increase in transmit power with speed indicate greater influence of interference for MRC, given the fact that it does not directly control interference, as is the case with OC. MRC is, generally, more sensitive to speed than OC and it takes longer to converge to the desired target SINR, as already explained.

The results for different system parameters are summarised in the table 4.2. The influence of MS speed in addition to the convergence of a specific processing scheme towards the desired target is shown. The analysis with imperfect power control showed similar results with the perfect power control case regarding the main trends of the dependance of the transmit powers

N_{dB}	γ_0	M	K	general result	comment
25 dB	5 dB	3	15	OC, MRC converg. negligible influence of MS speed	negligible OC versus MRC gain
25 dB	5 dB	3	40	OC, MRC converg. negligible influence of MS speed	up to 10 dB OC versus MRC gain
15 dB	1 dB	5	30	OC, MRC converg. negligible influence of MS speed	negligible OC versus MRC gain
10 dB	1 dB	5	20	OC, MRC converg. negligible influence of MS speed	up to 5 dB OC versus MRC gain
10 dB	1 dB	5	10	OC, MRC converg. negligible influence of MS speed	negligible OC versus MRC gain
10 dB	1 dB	3	6	OC, MRC converg. visible influence of MS speed	up to 12 dB OC versus MRC gain

Tabel 4.2: Imperfect power control results for different system set-up

on different system parameters for two antenna processing schemes. The only difference is that the reduction in transmit powers of OC over MRC is achieved for a larger number of scenarios. The cases where MRC failed to achieve the exact target for all users in the perfect power control case, yield a significant gain of OC over MRC because the requirement for the achieved SINR is not so strict. On the whole, the influence of speed on optimum powers is relatively negligible for both OC and MRC. The angular spread at the side of MS is quite low, $\Lambda = 10^o$, which makes fast fading not that critical for this environment at the frequency of 1.9 GHz.

4.5 Conclusions

The analysis of antenna array processing for UMTS was done for an urban micro-cell environment using a deterministic model and the results are given in terms of optimum transmit powers for a given target SINR. The perfect

power control was dealt with first in order to establish the basic influence of parameters such as the processing gain, antenna array size and number of users, on optimum transmit powers. The ability of different processing schemes to converge towards the desired target SINR corresponds to the sensitivity of the maximum eigenvalue of the gain matrix $\mathbf{G}$ to the increase in the number of users.

The most dominant parameter which puts the limitation on the number of users is the processing gain. For a moderate number of users in a micro-cell, up to 15, it is possible to achieve the desired target value for a single antenna case when the processing gain is 25 dB. The antenna array size is the second dominant parameter. Increasing the size of the array to M=5 improves the convergence properties of MRC, which performs almost equally to OC even for a relatively high number of users in a micro-cell, up to 40. OC is clearly superior to MRC regarding the number of users that can be sustained for the data service, i.e. lower processing gains.

The analysis including imperfections in the power control due to finite time available for the power update, shows that the gain of OC over MRC in the reduction of transmit power is achieved for a larger number of scenarios. In the imperfect power control, it is no longer feasible to assume equal SINR for all users. The fluctuations of the achieved SINR around the desired target is inherent to the realistic power control process, which is further aggravated by the increase in the mobile speed. The advantage of using OC over MRC is reflected by the reduction in transmit power, that can go up to 10 dB. The satisfactory performance for both OC and MRC can be achieved using an antenna array size of M=5 in a variety of scenarios. Only in case of a small number of users per cell, below 10, and for scenarios dominated by a high processing gain, the antenna array size of M=3 can be expected to be sufficient. The influence of MS speed on power levels was not significant for neither OC nor MRC for the majority of system settings due to a very low angular spread of $\Lambda = 10^o$ at the mobile terminal.

5

Pixel size analysis

5.1 Introduction

The ray-tracing model has capabilities to compute the composition of waves for a given set of coordinates in a certain environment. The main question dealt with in this chapter is defining an area, called *pixel*, where certain channel and signal properties do not change significantly. This is in relation with the problem described in [58], where the concept of a *pixel* was initially introduced to calculate the local signal power received at the side of the MS for a certain trajectory/area. The idea was to compute the composition of waves, i.e. *ray parameters* (assumed constant within one pixel), directly from the ray-tracing model at the central point of the pixel area and, in turn, extrapolate signals for any other point within that pixel on the basis of that information. Local power was determined as an average value over one pixel. According to this procedure, the local signal power can be determined for a larger trajectory/area of possible MS locations without having to compute the channel information for all points on that trajectory/area. The trajectory/area can be divided into pixels resulting in computation of the wave composition for only one point per pixel. This can reduce the computational time needed for the ray-tracing simulations.

In this study, different signal properties are analysed with a view of defining a pixel area. The procedure from [58] for the extrapolation of the signal within the pixel using *ray parameters*, obtained at the pixel center, will be used and described in Section 5.2. Contrary to the approach in [58], the received signal power at the MS is not the parameter of interest, but the achieved SINR in the power control process. The motivation for choosing this parameter, is to define the concept of the pixel from system point of

view. The power control process tends to compensate fast fading effects in the channel and it is not sensible to choose parameters that describe more general channel characteristics.

In Section 5.3, the criterion to define the pixel size on the basis of errors between the achieved SINR and a desired target value as a result of extrapolation is described. The simulation results are given in Section 5.4 on the basis of the same urban micro-cell environment, as in Chapter 4 (TU/e campus). The analysis is based on a flat-fading signal model, since only one Rake finger collects significant power for this environment, as indicated in Chapter 3.

5.2 Signal model

The procedure for extrapolating the received signal at the BS, as the MS moves within a pixel area, using the wave composition at the pixel center, will be described in this section. The notion of a *pixel* commonly implies a two-dimensional (2D) area (propagation surface is divided into smaller areas that are, naturally, 2D). In this study the *pixel* is one-dimensional (1D), i.e. the size of the pixel is defined as the length of a part of the trajectory. The 1D approach can easily be extended to 2D.

The spatial signature at the central point of the pixel is defined, as given by Eq. 2.22:

$$\mathbf{h} = \sum_{q=1}^{Q} \alpha_q \exp(\jmath\phi_q)\mathbf{a}(\varphi_q)R_s(\tau_q - \tau_0) \tag{5.1}$$

The index designating a specific user is omitted for the simplicity of the extrapolation method desription. The spatial signature for the point at the distance d from the pixel center is defined as follows:

$$\mathbf{h}'(d) = \sum_{q=1}^{Q} \alpha_q \exp(\jmath\phi_q + \jmath\frac{2\pi}{\lambda_c} d\cos(\varphi_q^{MS}))\mathbf{a}(\varphi_q)R_s(\tau_q - (d/c)\cos(\varphi_q^{MS}) - \tau_0) \tag{5.2}$$

where $\varphi_q^{MS}, q = 1, ...Q$ represents the angle-of-arrival of the q-th multipath at the side of the MS, determined with respect to the angle of the trajectory. This result represents the approximation of the spatial signature which can be obtained directly from the ray-tracing model. As d gets smaller, the approximate spatial signature is closer to the accurate value. The last equation implies that each multipath component changes only in phase, as MS moves within a pixel, which is directly related to the angle-of-arrival

$\varphi_q^{MS}, q = 1, ...Q$. It is based on the fact that, within a small length, the time delay of each multipath component changes only due to the change in the covered distance, which is by the value of $d\cos(\varphi_q^{MS})$ larger than the delay of the ray arriving at the pixel center, see Fig.5.1. This resembles the standard procedure of modelling fast fading effects in a multipath channel. Within a short trajectory length, amplitude and angle-of-arrival of multipath components do not change significantly. The only change is in the phase, as shown by the term $\exp(j\frac{2\pi}{\lambda_c}d\cos(\varphi_q^{MS}))$.

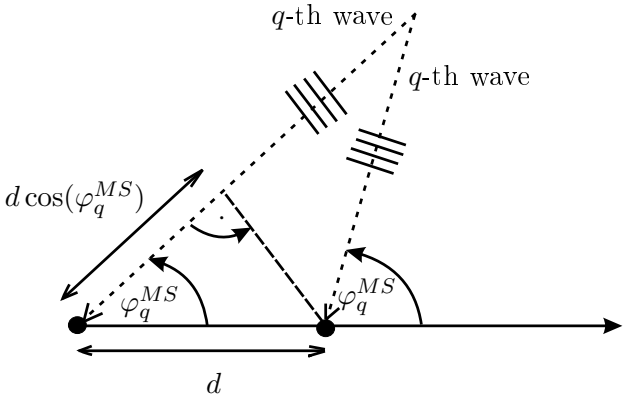

Figure 5.1: The wave composition remains the same at the small distance d from the reference point; the only change is in the phase due to the difference in the covered distance $d\cos(\varphi_q^{MS})$, which is a function of the angle-of-arrival φ_q^{MS}

The classical statistical channel modelling approach that was derived by [59], assumed that a mobile channel is characterised by *Wide-Sense Stationary-Uncorrelated Scattering* (WSSUS) property. *Wide-Sense Stationary* basically means that the channel statistics is time-invariant, while *Uncorrelated Scattering* property implies that multipaths with different path delays are mutually uncorrelated. WSSUS channel can be completely characterised by functions describing the distribution of power in delay and angular domain, which implies that the channel composition is basically assumed unchanging in an area within which the WSSUS property is valid.

In a micro-cellular environment, channel composition is changing very dynamically, as already stated. In [60], the changes in the channel along a trajectory can be modelled through spatial intervals, where the WSSUS

property is valid, each characterised by a different wave composition that is essentially constant. Within each interval the channel can be deterministically described as a sum of waves interacting with a fixed environment, while transitions between deterministic intervals are characterised by random models, describing the change in the wave composition before a new one begins. There is some similarity in this approach to dividing a trajectory into pixels within which the wave composition is assumed unchanging. The difference lies in the criterion for the size of the spatial interval, since the approach in this thesis includes the influence of the system, while the modelling approach used in [60] is more generally applicable, focusing on pure propagation.

In [58], the parameter of interest was the local average power which was calculated on the basis of a narrowband impulse response h_{MS} at the MS, defined in terms of *ray parameters* as:

$$h_{MS} = \sum_{q=1}^{Q} \alpha_q \exp(\jmath\phi_q + \jmath\frac{2\pi}{\lambda_c} d\cos(\varphi_q^{MS})) \tag{5.3}$$

It can be seen that the impulse response h_{MS} has only amplitude and phase as parameters that can cause deviations from the original result, which is not the case with the spatial signature $\mathbf{h}$ where a larger number of parameters is included. Antenna processing at the BS is included in the current analysis and the change in the angle-of-arrival $\varphi_q, q = 1, ...Q$ at the side of the BS can also influence the results by causing the change in the antenna steering vector $\mathbf{a}(\varphi_q)$. There is an additional factor, namely the autocorrelation properties of CDMA codes, in the thesis idealised in the form of a triangular function $R_s(\cdot)$. This function performs appropriate scaling of the amplitude of multipath components on the basis of the time delay $\tau_q, q = 1, ...Q$, as shown by Eq. 2.23. The extrapolation of delays might, thus, have an influence to the final result, as well. The effect of all these parameters will be analysed further.

5.3 Pixel size definition

In this section, the attempt is made to define the criterion for the pixel size on the basis of the difference between the SINR obtained with approximate spatial signatures (as a result of extrapolation) and a desired target value. The concept of the target SINR in the power control process was introduced and explained in Chapter 4. Only OC is treated in this analysis, because similar trends in the SINR spatial characterisation have been observed with MRC. Similarly to the experimental set-up, described in Chapter 4, there

is a total of K users, one among which is moving along a pixel trajectory and the rest are fixed. If the moving user is designated with an index 1, the target SINR for that user γ_0 is defined as:

$$\gamma_0 = \frac{G_{11}P_1}{\sum_{j=2}^{K} G_{j1}P_j + \sigma_1^2} \tag{5.4}$$

where $[P_1, ...P_K]$ represents the vector of optimum transmit powers. Given that the antenna weight vector for the user 1 is $\mathbf{w}_1$, the expression above can be rewritten as:

$$\gamma_0 = N\frac{|\mathbf{w}_1^H\mathbf{h}_1|^2P_1}{\sum_{j=2}^{K} |\mathbf{w}_1^H\mathbf{h}_j|^2P_j + \sigma^2|\mathbf{w}_1|^2} \tag{5.5}$$

It has already been indicated by Eq. 2.12 that, in case of OC this reduces to a compact form:

$$\gamma_0 = N\mathbf{h}_1^H\mathbf{R}_{in,1}^{-1}\mathbf{h}_1 \tag{5.6}$$

where the spatial correlation matrix of the total interference $\mathbf{R}_{in,1}$ is defined as:

$$\mathbf{R}_{in} = \sum_{j=2}^{K} \frac{P_j}{P_1}\mathbf{h}_j\mathbf{h}_j^H + \frac{\sigma^2}{P_1}\mathbf{I}_M \tag{5.7}$$

In general, the optimum transmit power vector $[P_1, ...P_K]$ for a given target SINR γ_0 is the function of spatial signatures of the desired user $\mathbf{h}_1$ and spatial signatures of interfering users: $\mathbf{h}_2, \mathbf{h}_3, ...\mathbf{h}_{K-1}$, as shown in the equations above. This dependence can be symbolically represented, for each position on the trajectory, as:

$$[P_1, ...P_K] = f(\gamma_0, \mathbf{h}_1, \mathbf{h}_2, \mathbf{h}_3, ...\mathbf{h}_K) \tag{5.8}$$

The optimum power vector, determined on the basis of approximate spatial signatures within a certain pixel of length $D, -D/2 < d < D/2$, can be represented as:

$$[P_1^{'}, ...P_K^{'}] = f(\gamma_0, \mathbf{h}_1^{'}(d), \mathbf{h}_2, \mathbf{h}_3, ...\mathbf{h}_K) \tag{5.9}$$

It should be noted that spatial signatures of the fixed users do not change, since they remain at the same place during the movement of user 1 along the trajectory. If the approximate power vector $[P_1^{'}, ...P_K^{'}]$ is applied to real, non-approximate spatial signatures $\mathbf{h}_1$, the obtained SINR $\gamma_0^{'}$ will deviate from the target value γ_0. The change will become larger as the distance between the center of the pixel and the current position d increases. The approximate SINR for OC is further obtained as follows:

$$\gamma_0^{'} = N\mathbf{h}_1^H(\mathbf{R}_{in,1}^{'})^{-1}\mathbf{h}_1 \tag{5.10}$$

where:

$$\mathbf{R}_{in,1}^{'} = \sum_{j=2}^{K} \frac{P_j^{'}}{P_1^{'}} \mathbf{h}_j \mathbf{h}_j^H + \frac{\sigma^2}{P_1^{'}} \mathbf{I}_M \tag{5.11}$$

The approximate optimum powers are computed assuming perfect power control. The SINR calculated by applying approximate optimum powers on the non-approximate spatial signatures, will oscillate around the fixed desired target value within the pixel. The difference between the approximate SINR $\gamma_0^{'}$ and the desired target SINR γ_0 tends to be larger for larger distances from the pixel center. The distance at which the deviation of $\gamma_0^{'}$ from γ_0 gets unacceptable will indicate how big the pixel size D can be for the purpose of the analysis. Before the criterion for the acceptable difference is established, the spatial behaviour of the approximate SINR will be shown next, relating to propagation factors that have the most dominant influence on the result.

5.4 Simulation results

The simulation environment used for this analysis is the same as given in Chapter 4. In this case, there is a total of K=6 users in the system, one user moving along a pixel trajectory and the rest are fixed and located in the surrounding trajectories. The length of the initial pixel chosen is $40\lambda_c$ (6.24 m), because large-scale propagation characteristics do not change considerably over the length in question [61]. Four propagation cases are defined in the simulation. A propagation case is determined by the location of the pixel trajectory along which the user 1 moves. The simulation environment including the users' locations and four propagation cases, designated with numbers 1-4, are shown in Fig. 5.2. The accurate spatial signatures $\mathbf{h}_1$ are calculated using *ray parameters*, taken directly from the ray-tracing at $\lambda_c/2$ spacing. The extrapolated spatial signatures $\mathbf{h}_1^{'}$ for positions on each side of the center of the pixel are also calculated at $\lambda_c/2$ spacing within the length of $40\lambda_c$. The simulation results show the deviation of the approximate target SINR $\gamma_0^{'}$ from the real value γ_0 for all users. Before looking into different propagation conditions, some basic impacts of the small-scale propagation effects on the spatial behaviour of the approximate SINR $\gamma_0^{'}$ are shown for propagation case 1, which represents a typical non line-of-sight (NLOS) scenario.

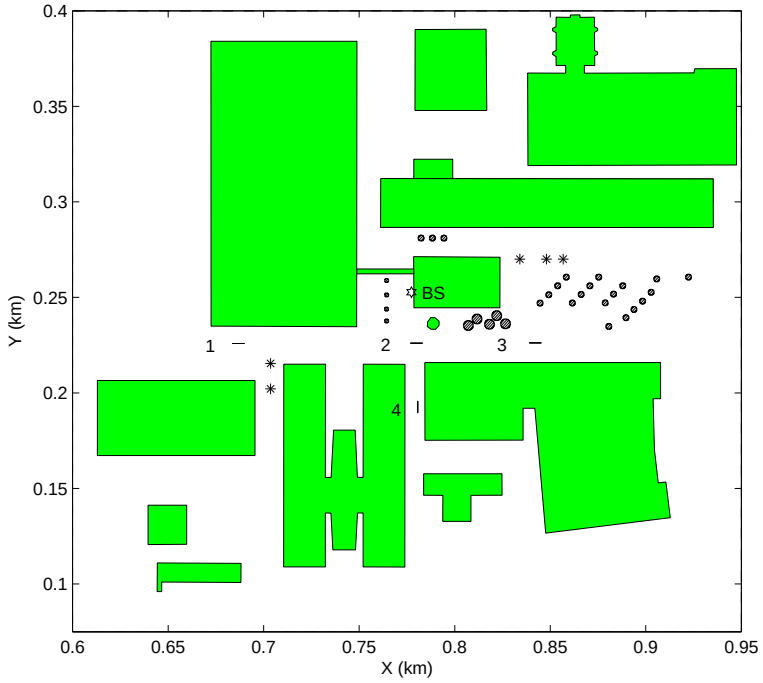

Figure 5.2: Simulation environment: $*$ represents a fixed user, numbers 1-4 denote propagation cases, BS designates the base station

5.4.1 Influence of the system and propagation factors

Since the propagation channel in an urban micro-cell environment is subject to frequent and abrupt changes in the wave composition, a small number of dominant multipath components is initially taken into account Q_i=Q=5, $i = 1, ...K$. This has been done as a first step, which provides a closer look at the small-scale effects and facilitates further explanations of the results.

The simulation results are obtained for the following system settings: the processing gain N_{dB}=10 dB, target SINR γ_0=1 dB and the antenna array size M=3. The results for the propagation case 1 from Fig. 5.2 are shown in Fig. 5.3(a), which represents the spatial characterisation of the achieved SINR within the pixel for the six users. The SINR is equal to the desired target γ_0 in the pixel center. The curve with the biggest deviation from the target SINR corresponds to the moving user, whereas the other five curves represent the deviation in the achieved SINR of the fixed users. The achieved SINR of the moving user experiences small deviation of up to 0.5 dB

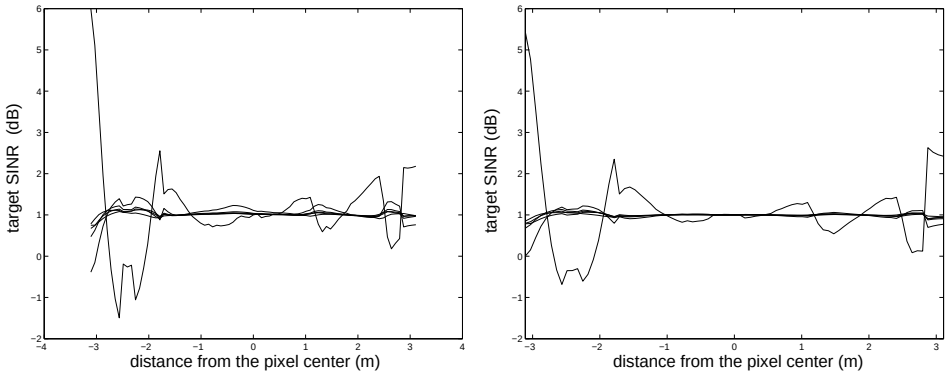

(a) (b)

Figure 5.3: N_{dB}=10 dB, γ_0=1 dB, M=3, Q=5: (a) The change in $\gamma_0^{'}$ within the pixel for propagation case 1; (b) The change in $\gamma_0^{'}$ within the pixel, when only phase effects are taken into consideration

---

from the accurate value, within the length of 3.5 m around the pixel center. Outside that range the deviations become more drastic, caused by a more significant change in the composition of waves. It can also be observed that the deviations of $\gamma_0^{'}$ for fixed users is much smaller in comparison to that of the moving user. This means that optimum transmit power for the moving user $P_1^{'}$ experiences larger deviations due to extrapolation of waves than optimum powers for fixed users $P_2^{'}, ...P_K^{'}$. That result is expected looking at Eq. 5.5 and applying it in an analogous way to any of the five fixed users. In the process of approaching the desired γ_0 for a fixed user, the only changing component is one of five other interfering components and that component is even further suppressed by the antenna processing gain that favours the fixed user. In the case of the moving user, the component that changes is the desired signal component, which is favoured most by the antenna processing, and, therefore, the transmit power for the moving user changes most significantly.

The next step will be analysing the main cause of small deviations in the SINR, which occur already at very small distances from the pixel center. In Section 5.2, it has been indicated that the potential parameters that cause deviations of the extrapolated spatial signatures from the original one (and in turn the deviations of $\gamma_0^{'}$ from γ_0) are the amplitude, autocorrelation function

based on delays, angles-of arrival at the BS and the extrapolated phase based on the angles-of-arrival at the MS. The result for the target SINR in case amplitudes $\alpha_q, q = 1, ...Q$ and angles-of-arrival at the BS $\varphi_q^{MS}, q = 1, ...Q$ are assumed unchanging in the original spatial signature $\mathbf{h}$, within the $40\lambda_c$ pixel, is depicted in Fig. 5.3(b). Also, the autocorrelation function has not been included in the definition of the original spatial signature. It can be seen that the influence of the phase error has the most dominant effect, because when all other parameters are originally taken as constant, the resulting SINR follows very similar pattern to the one from Fig. 5.3(a).

In the analysis from [58], featuring the local received power at MS, as a parameter of interest, the pixel size used was D=5 m and the deviations of the approximate from the accurate result within the pixel were quite small. In the calculation of the received power at the MS, the averaging over the whole pixel was preformed and thus the effect of fast fading due to phase error was efficiently averaged out. Antenna processing also performs certain averaging of the fast fading effects by means of diversity. The sensitivity of the results to the phase error is larger in this approach than in [58]. The effect of averaging over an area, which is significantly larger than the antenna array size with element spaced at half the wavelength distance, is much more efficient.

The difference in accurate phases obtained directly from μFipre and extrapolated phases on the basis of angles-of-arrival are shown in Fig. 5.4(b) for each multipath component, whereas the angles-of-arrival are shown in Fig. 5.4(c). The phase error of all multipath components increase slightly farther from the pixel center, which brings small deviations in the SINR within the range of 3.5 m, as shown by Fig. 5.3(a). More drastic errors in phase coincide with those in the SINR and also with the change in the composition of waves, as can be seen from Fig. 5.4(a) and Fig. 5.4(c).

The influence of the antenna array size and the processing gain will be next analysed. The result obtained for a larger antenna array size M=5 is shown in Fig. 5.5(a). The deviations due to phase error seem to be decreased in comparison to a three-element antenna array. The deviations lower than 0.5 dB occur within the length of 4.5 m, which is larger than in the case when M=3. Antenna combining using more elements has better properties in averaging out fast fading due to the increased number of diversity branches.

The influence of a different processing gain is shown in Fig. 5.5(b) for the antenna array size M=3. The processing gain has been increased to N_{dB}=25 dB, with the corresponding target SINR γ_0=5 dB. The deviation pattern of $\gamma_0^{'}$ for the moving user is the same, as when the processing gain is

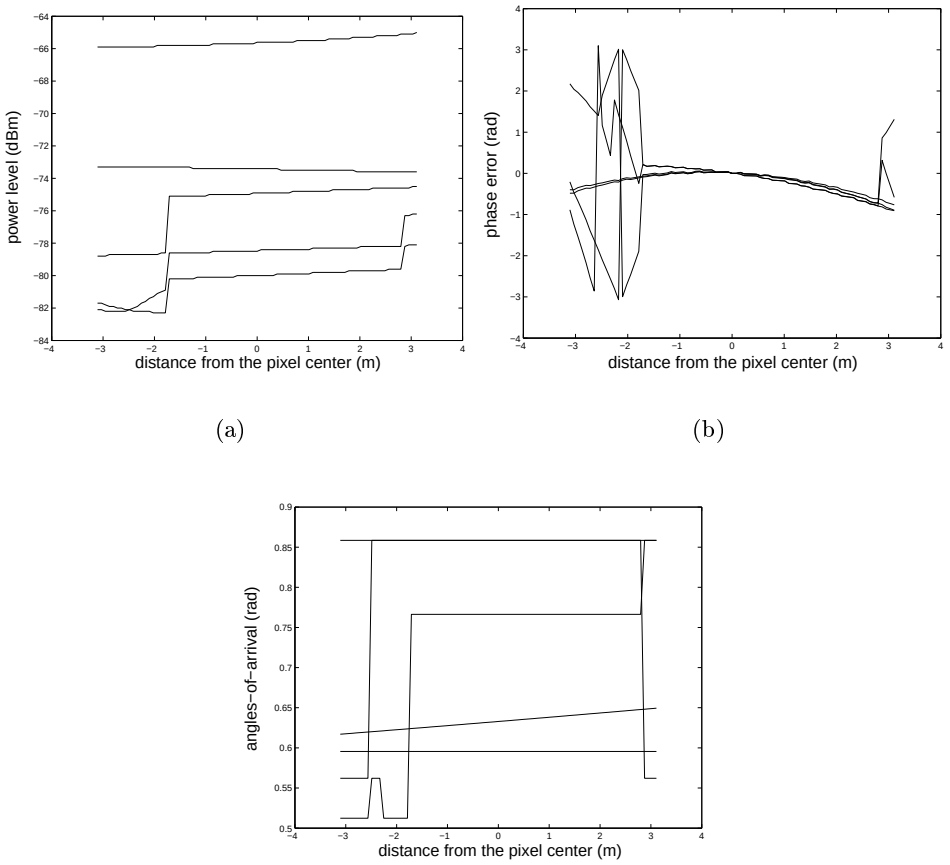

(a) (b)

(c)

Figure 5.4: The change in the channel composition for Q=5: (a) Power level; (b) Phase error; (c) Angle-of-arrival

---

N_{dB}=10 dB. What is obviously different in this example is the deviation of $\gamma_0^{'}$ for other fixed users, which is almost negligible. From a point of view of a fixed user, the only interfering component (user 1) is even more suppressed due to a higher processing gain, see Eq. 5.5.

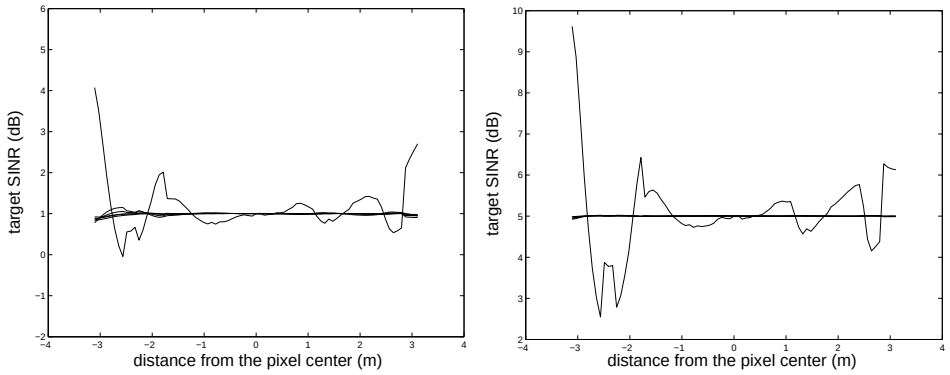

(a) (b)

Figure 5.5: The change in $\gamma_0^{'}$ within the pixel: (a) N_{dB}=10 dB, γ_0=1 dB, M=5; (b) N_{dB}=25 dB, γ_0=5 dB, M=3

5.4.2 Analysing different propagation cases

The influence of propagation and system parameters has been shown including only five dominant multipath components. If more contributing components are included, the deviations in the SINR values get larger. This is because drastic changes in the wave composition tend to occur at smaller distances from the pixel center for less dominant components. Figures Fig. 5.6(a), Fig. 5.6(b) and Fig. 5.6(c) depict power levels, phase error and angles-of-arrival for propagation case 1, respectively, when seven dominant components are included. The seven components fall into a power range of around 20 dB, as shown by Fig. 5.6(a). They all contribute significantly to the result, since a spatial signature is obtained as a result of summation of complex signals on amplitude level (the squared power). Drastic changes in the channel composition occur closer to the pixel center in comparison to the case when five components are included, resulting in larger deviations in the achieved SINR, see Fig. 5.6(d). This also coincides with the change in wave composition, which is shown by Fig. 5.6(a) and Fig. 5.6(c).

The following results show the deviation in SINR for various propagation conditions, represented by the four propagation cases depicted in Fig. 5.2. Here, all contributing multipath components are taken into account. The results corresponding to propagation case 1 for three-element and five-element antenna array are shown in Fig. 5.7(a) and Fig. 5.7(b), respectively. The

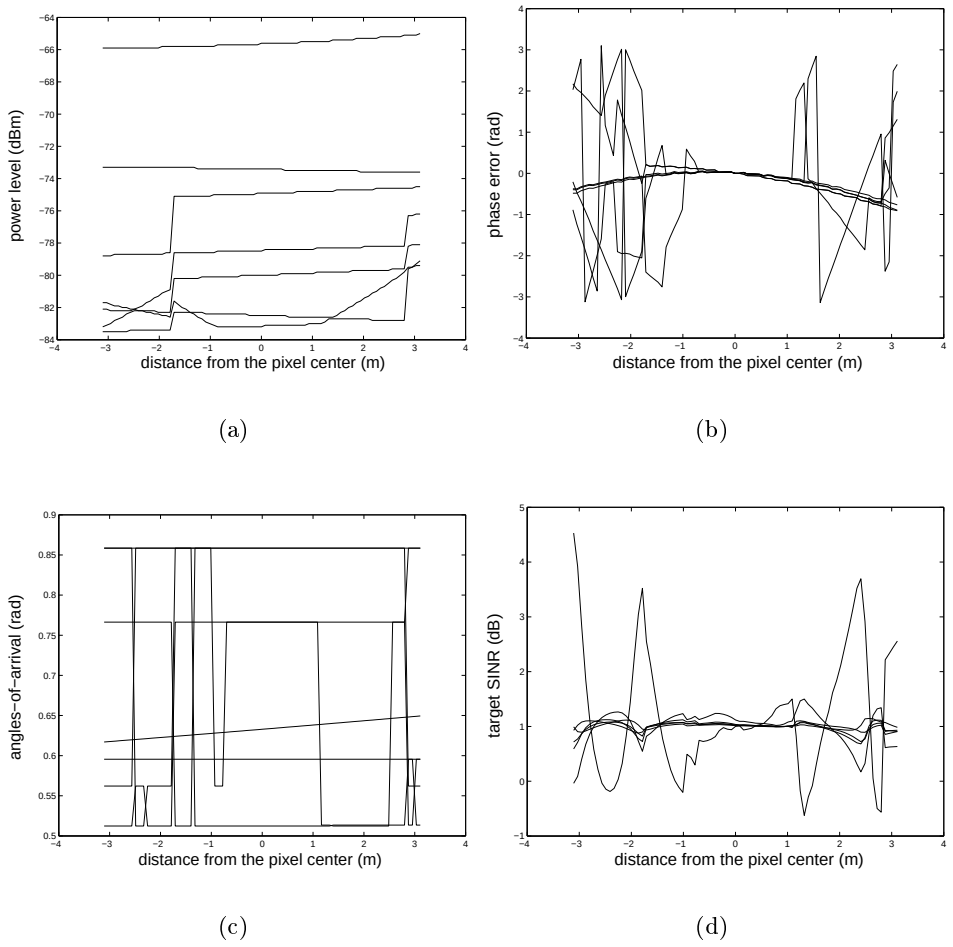

Figure 5.6: The change in the channel composition within the pixel for Q=7: (a) Power level; (b) Phase error; (c) Angle-of-arrival; (d) approximate target SINR $\gamma_0^{'}$

deviations from the desired target occur already at less than 0.5 m distance for both M=3 and M=5. The deviations on a larger scale are smaller for a larger antenna array size, as already explained in Section 5.4.1. The results for propagation case 2, shown by Fig. 5.8(a), yield smaller deviations close to the pixel center, as compared to scenario 1. This can be attributed to the fact that propagation case 1 is characterised predominantly by shado-

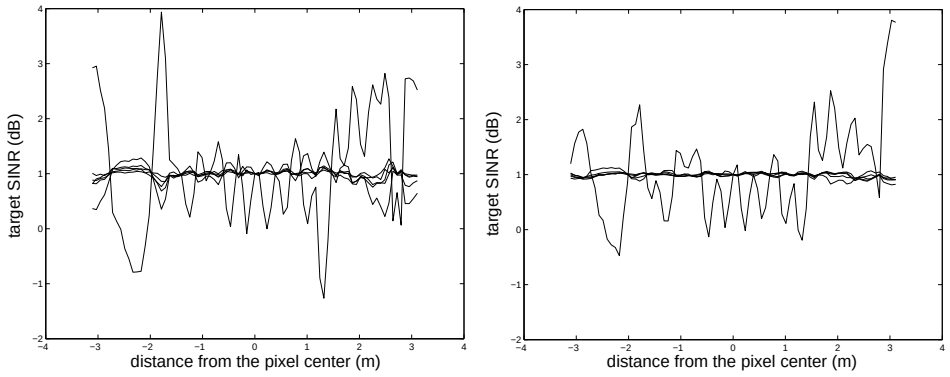

(a) (b)

Figure 5.7: The change in γ_0' within the pixel for propagation case 1, N_{dB}=10 dB, γ_0=1 dB: (a) M=3; (b) M=5

wing effects behind the big building, whereas the pixel trajectory for the case 2 is partially in LOS, partially in NLOS situation and, also, closer to the BS (see Fig. 5.2). The power range of the most dominant multipath components for the propagation case 2 is larger when compared to propagation case 1, because the former is dominated by a few components that are not seriously obstructed on the BS-MS path, whereas there are more multipath components with comparable levels in the latter. For the propagation case 3, deviations of up to 3 dB occur for less than 1 m distance from the pixel center. This case is characterised by diverse propagation mechanisms including both interaction with buildings and scattering from nearby trees. The number of multipaths with comparable power levels is the largest for this situation. NLOS micro-cell propagation conditions can lead to diverse results strongly depending on the local features of the environment. The case 4, on the other hand, represents a typical LOS situation, where the deviations of up to 1 dB occur at a distance larger than 2 m. In this scenario the direct component is the most dominant and the deviations of SINR are much smaller compared to all NLOS situations analysed.

The next task is to define the maximum tolerable deviation of SINR from the desired target value in order to determine the pixel size. Obviously, a NLOS situation with M=3 is most critical for the result. The drastic changes in SINR deviations for all three NLOS cases occur at distances from

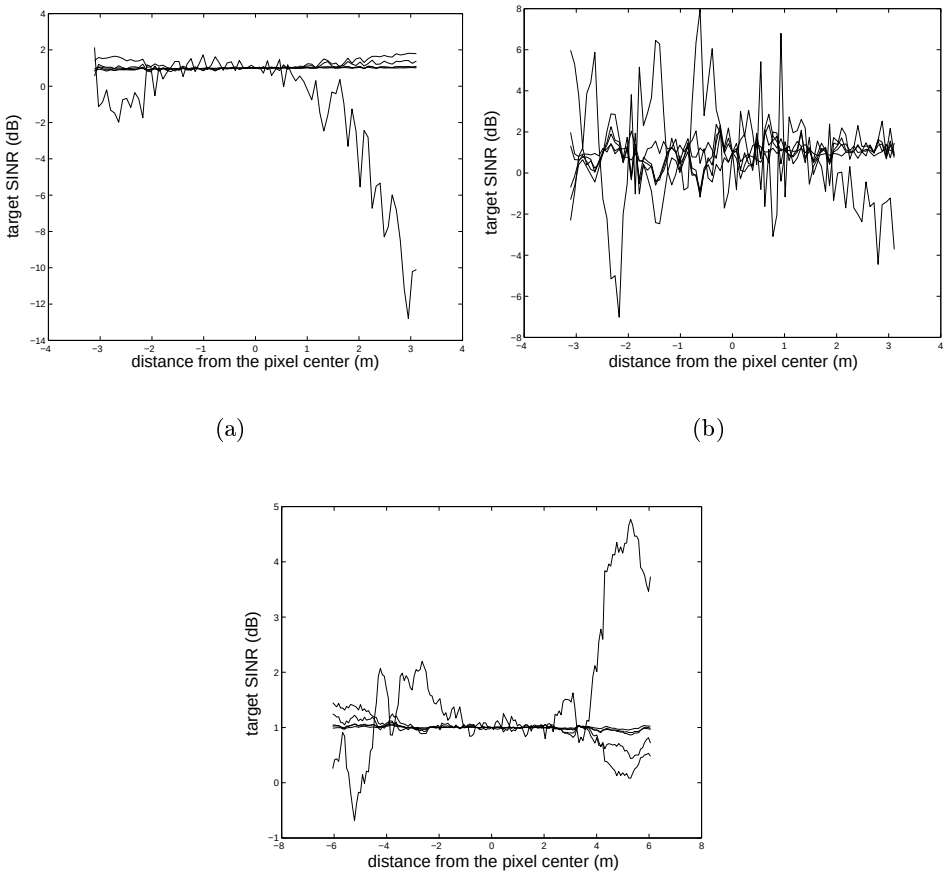

Figure 5.8: The change in γ_0' within the pixel, N_{dB}=10 dB, γ_0=1 dB, M=3: (a) Propagation case 2; (b) Propagation case 3; (c) Propagation case 4

---

the pixel center when 1.5 dB deviation has been reached. This result can be regarded acceptable also judging by the achieved SINR spatial behaviour in the realistic power control process. In Section 4.4, it has been shown that SINR deviates from the desired target value by 1 dB, 3 dB and 5 dB for low to moderate MS speed of v=3 km/h, v=20 km/h and v=50 km/h, respectively. This means that 1.5 dB deviation is lower than what happens in reality on average. The total length of the pixel trajectory, within which

SINR deviations do not exceed 1.5 dB, is D=2.8 m, D=3.3 m and D=0.2 m for NLOS propagation cases 1, 2 and 3 respectively. The average result is, therefore, $\bar{D}$=2 m.

5.5 Conclusions

The concept of the *pixel* is introduced in order to decrease the computational time of the ray-tracing simulations. The main idea is to compute the exact composition of waves for the pixel center and extrapolate the signal vector on the basis of that information for any other point within the pixel. The deviation in the approximate target SINR from the accurate one in the power control process is used as a criterion to determine the size of the pixel. Four representative propagation cases in an urban micro-cell environment were considered and the influence of system parameters was also analysed. Small deviations in the achieved SINR within the pixel are shown to be predominantly influenced by errors in the phase, which is calculated on the basis of angles-of-arrival at the side of the MS. For a five-element array, the pixel size tends to be larger, since phase errors are better averaged out due to the larger diversity order. The processing gain does not influence the deviation of the target SINR for the moving user, whereas that of the fixed users is considerably decreased with a larger processing gain.

The deviation of 1.5 dB has been identified as an acceptable criterion to determine the size of the pixel, taking into account the following: the deviations larger than 1.5 dB fall into the region where drastic changes in the channel occur; the average level of deviations in the achieved SINR from the desired target value is even higher in a realistic power control process. Since NLOS cases are more critical than LOS, the result for the pixel size was based on the several NLOS situations, resulting in an average length of $\bar{D}$=2 m. This result is related to the environment represented by the university campus. In Chapter 6, pixel size analysis will be done for a different type of an urban environment, namely a city center.

6

Urban city environment

6.1 Introduction

The investigation of the smart antenna performance under power control and pixel size analysis have been done for one type of an urban environment, represented by the TU/e campus. Similar analysis will be done for a different type of environment, represented by the Hague city center. This environment is characterised by a densely packed array of buildings and a more clearly defined street pattern, as compared to the university campus. This dictates specific channel characteristics around the BS and MS, which has significant influence on the results for an urban city center.

Regarding the smart antenna performance, there is only a limited number of different directions from which dominant rays, coming from users distributed in the environment, arrive to the BS. The main reason is that the majority of rays arrive via streets by means of multiple reflections from buildings on both sides of the street. The wave guiding effect is dominant, since the strength of rays transmitted through buildings is much lower than those that are guided via multiple reflections towards the BS. This means that users are less separable in angular domain (arriving almost from the same direction) than in the previous environment where the incoming rays are more randomly scattered around the BS.

Another difference is a larger delay spread. The most dominant components undergo a large number of successive reflections which increases the total length covered by waves on the way between MS and BS, and in turn the delay in arrival, with respect to the first incoming ray. In this new type of environment two Rake fingers will be active, instead of one, which was the case with the university campus. The channel in the new environment is, thus, frequency selective.

The spatial evolution of multipath components at the MS is also different from the previous scenario. The waves arriving at the MS are also the result of reflections from the array of building faces. The most dominant multipath components are expected to have slow and smooth changes in angles-of-arrival over a larger trajectory length with respect to the university campus where those changes are very frequent and abrupt.

These aspects represent major differences between the environment that is analysed here and the one studied in previous chapters. The environment represented by the university campus will be referred to as the *university campus environment* and the environment currently introduced as the *city center environment* further in the text. The analysis regarding smart antenna performance for imperfect power control and pixel size will be done for the *city center environment* and comparisons will be made with the results obtained from the *university campus environment*

6.2 Power control analysis

The aim of power control analysis for the *city center environment* is to study the trends regarding the smart antenna performance versus system parameters for a different type of environment. The mathematical formulation of the power control process is given in Section 6.2.1, followed by simulation results in Section 6.2.2.

6.2.1 Mathematical formulation

The mathematical formulation of the power control is given in general terms by simply extending the main concept presented in Section 4.2 to a frequency selective channel. The power control equation will be repeated for clarity:

$$[\mathbf{I}_K - \gamma_0 \mathbf{G}]\mathbf{p}_{opt} = \mathbf{u} \tag{6.1}$$

where the gain matrix $\mathbf{G}$, optimum power vector $\mathbf{p}_{opt}$, noise vector $\mathbf{u}$ and target SINR γ_0 are defined as in Section 4.2. The gain matrix $\mathbf{G}$ contains elements that are defined on the basis of gains between the BS and MS for each pair of users, as already given by Eq. 4.9:

$$[\mathbf{G}]_{ij} = \begin{cases} 0, & \text{if } j = i \\ \frac{G_{ji}}{G_{ii}}, & \text{otherwise} \end{cases} \tag{6.2}$$

For a frequency selective channel, which characterises the new environment, the total gain between the BS and MS is the result of Rake combining in

addition to antenna array processing. In Section 2.3, the basic principle of the combined Rake-antenna processing was given, where the antenna processing is performed for each Rake finger, prior to final Rake combining. Therefore, the terms G_{ji} and G_{ii} can be expressed in case of OC, as:

$$G_{ji}^{oc} = |\sum_{l=1}^{L}(\zeta_{l,i})^* I_{l,i,j}^{oc}|^2 \tag{6.3}$$

$$G_{ii}^{oc} = N|\sum_{l=1}^{L}(\zeta_{l,i})^* S_{l,i}^{oc}|^2 \tag{6.4}$$

The terms $S_{l,i}^{oc}$ and $I_{l,i,j}^{oc}$, introduced in Section 2.5.3 as the i-th user desired signal for the l-th Rake finger obtained after OC and the corresponding interfering signal coming from the j-th user, respectively, are defined as:

$$S_{l,i}^{oc} = (\mathbf{w}_{l,i}^{oc})^H \mathbf{h}_{l,i} \tag{6.5}$$

$$I_{l,i,j}^{oc} = (\mathbf{w}_{l,i}^{oc})^H \mathbf{h}_j \tag{6.6}$$

Here $\mathbf{w}_{l,i}^{oc}$ represents the i-th user optimum antenna weight vector applied on the l-th Rake finger. The coefficient $\zeta_{l,i}$ represents the Rake finger weight applied subsequent to OC, which is equal to the desired signal $\zeta_{l,i} = S_{l,i}^{oc}$ (see Section 2.5.3) and N is the processing gain. In case of MRC, the terms G_{ji} and G_{ii} are defined as follows:

$$G_{ji}^{mrc} = |\sum_{l=1}^{L}(\mathbf{w}_{l,i}^{mrc})^H \mathbf{h}_j|^2 \tag{6.7}$$

$$G_{ii}^{mrc} = N|\sum_{l=1}^{L}(\mathbf{w}_{l,i}^{mrc})^H \mathbf{h}_{l,i}|^2 \tag{6.8}$$

where $\mathbf{w}_{l,i}^{mrc}$ represents the i-th user optimum antenna weight vector for MRC that corresponds to the l-th Rake finger.

The main difference from the analysis featuring only one Rake finger is a more complex dependence of the gains on interfering signals which are, in this case, present on both Rake fingers. The following simulation results regarding smart antenna performance will show that the main difference from the *university campus environment* lies rather in a different angular distribution of multipath components arriving at the BS than in the frequency selectivity of the channel.

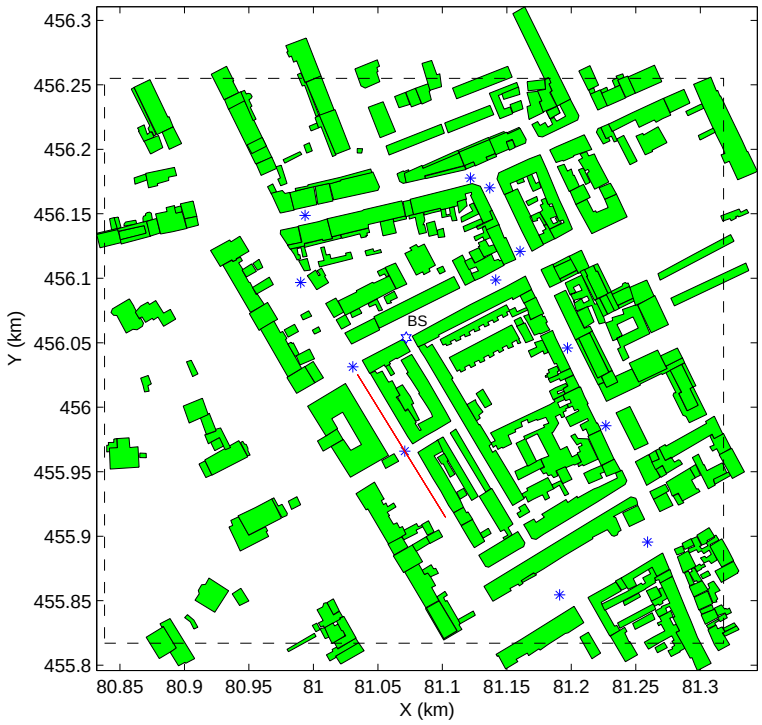

Figure 6.1: Simulation environment: one user moving along the trajectory, $*$ stands for a fixed user, BS designates the base station

6.2.2 Simulation results

The simulation environment is represented by Fig. 6.1. Analogous to the *university campus environment*, there is one user moving along a trajectory, whereas other users are fixed and located in the streets around the BS. The simulation results to follow are given in terms of pdfs for transmit powers, using the same set of system parameters as for the *university campus environment*. The results also include three different values for MS speed: v=3 km/h, v=20 km/h and v=50 km/h. Similarly to the analysis presented in Section 4.4.2, the results are given in terms of pdfs obtained on the basis of the difference between the transmit powers from the reference case when v=3 km/h and pdfs obtained on the basis of the power reduction gain of OC over MRC (the trajectory length is again 3 m).

The results shown in Fig. 6.2(a), Fig.6.2(b), Fig. 6.2(c) and Fig. 6.2(d) correspond to a system set-up with processing gain N_{dB}=25 dB (voice ser-

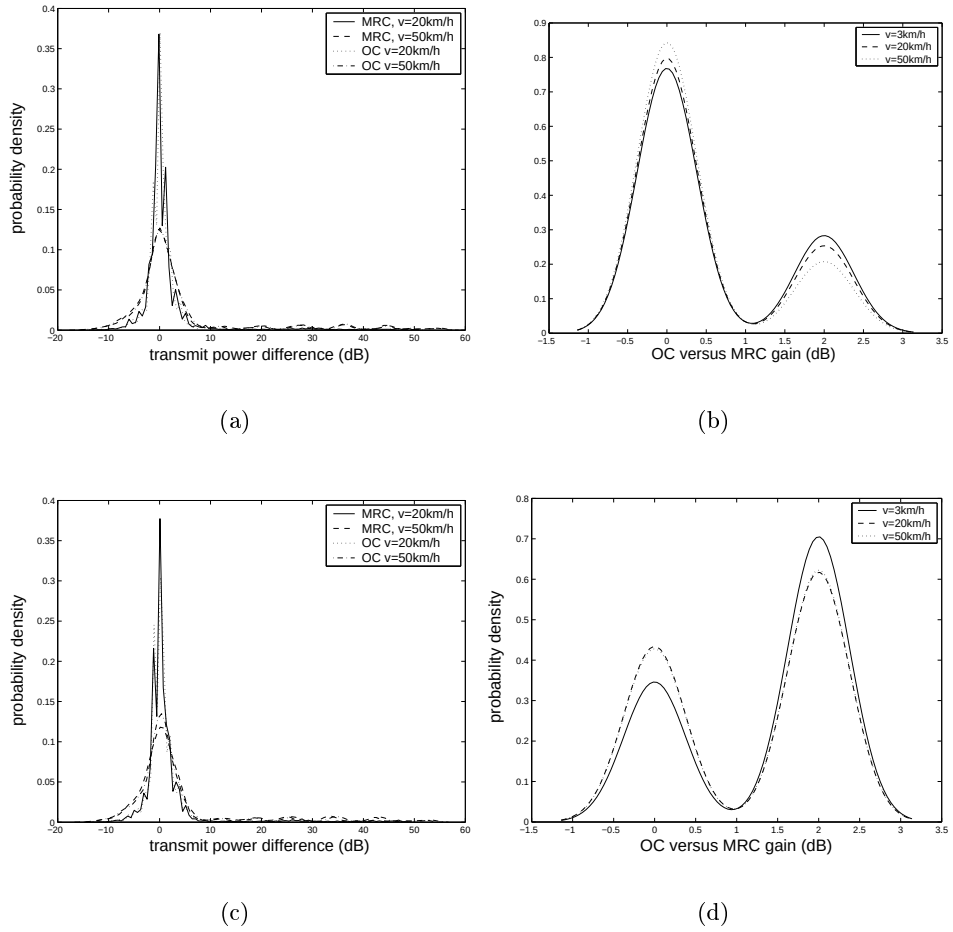

Figure 6.2: N_{dB}=25 dB, M=3, γ_0=5 dB: (a) The probability density of the difference in transmit power from the case when v=3 km/h for OC and MRC, K=15; (b) The probability density of the power reduction of OC over MRC, K=15; (c) The probability density of the difference in transmit power from the case when v=3 km/h for OC and MRC, K=40; (d) The probability density of the power reduction of OC over MRC, K=40

vice) and antenna array size M=3, featuring K=15 and K=40 users. In the *city center environment*, it is also possible to sustain up to K=40 users for the voice service (high processing gain) and a small antenna array. The

main difference from the *university campus environment* is a small gain in OC over MRC. The most dominant multipath components coming from different users are very closely spaced in angular domain, which results in similar performance of OC versus MRC, according to the theory presented in Section 4.3.1.

The results for the data service are shown in Fig. 6.3(a), Fig. 6.3(b), Fig. 6.3(c) and Fig. 6.3(d), featuring the processing gain N_{dB}=15 dB (non-real time data service) and N_{dB}=10 dB (real time data service) using a five-element antenna array M=5. In case N_{dB}=15 dB, up to K=30 users can be sustained for both OC and MRC, just like in the previous environment. However, only up to K=10 users can be achieved for N_{dB}=10 dB, contrary to the *university campus environment*, where that number goes to K=20 if OC is used. The *city center environment* is more critical concerning the number of users that can be maintained for a lower processing gain, due to the fact that the maximum distance from the BS is twice as large than in the *university campus environment*. The ratio between distances of different users is larger and the powers for users farther from the BS tend to increase above the permitted maximum level of 24 dBm, since the impact of strong interferers closer to the BS is larger with a lower processing gain.

Finally, the results featuring system parameters when the spatial structure of users is most influential for OC versus MRC comparison, is shown in figures Fig. 6.4(a), Fig. 6.4(b) and Fig. 6.4(c). The processing gain is N_{dB}=10 dB, the antenna array size M=3 and the number of users K=6, as given in Section 4.3.3. The results are obtained for two different spatial distributions of users (two scenarios). In the first scenario, shown by Fig. 6.4(a) and Fig. 6.4(b), both OC and MRC yield similar optimum power levels, unlike the result for the *university campus environment*, where the difference in transmit powers was significant. Again, the main reason is a higher spatial correlation of users in the *city center environment*, due to close angles-of-arrival of waves belonging to different users. In the second scenario, the average distance of users is farther from the BS than in the first case. As already explained, the interference becomes more critical for users far from the BS. In consequence, MRC fails to achieve the desired target value for all users (unlike OC) due to weaker interference suppression properties. Only the results for OC are shown for this case, see Fig. 6.4(c).

From the examples given above, the main difference in the results from the previous environment originates from a different type of scattering around the BS. The angles-of-arrival are closely spaced in the *city center environment* due to a wave guiding effect and more randomly distributed in the *university campus environment*. Local scattering at the BS, which direct-

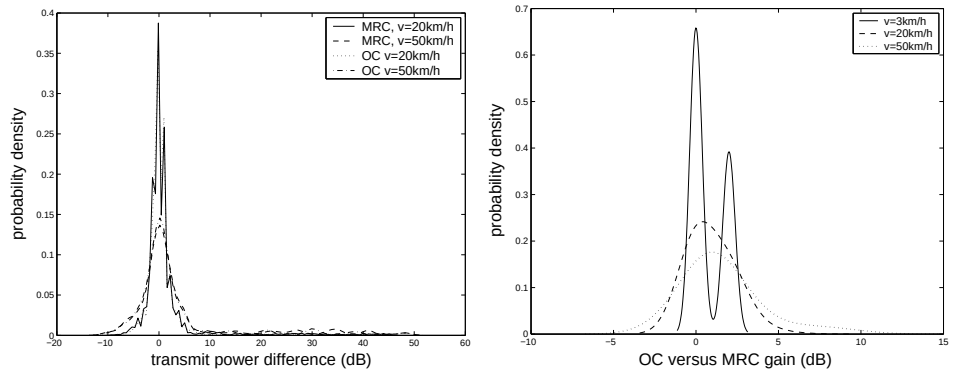

(a) (b)

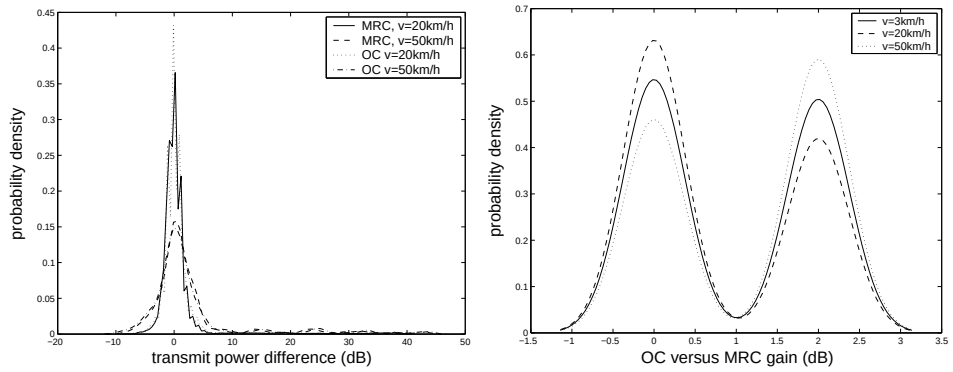

(c) (d)

Figure 6.3: (a) The probability density of the difference in transmit power from the case when v=3 km/h for OC and MRC, K=30, N_{dB}=15 dB, M=5, γ_0=1 dB; (b) The probability density of OC versus MRC power reduction, K=30, N_{dB}=15 dB, M=5, γ_0=1 dB; (c) The probability density of the difference in transmit power from the case when v=3 km/h for OC and MRC, K=10, N_{dB}=10 dB, M=5, γ_0=1 dB; (d) The probability density of OC versus MRC power reduction, K=10, N_{dB}=10 dB, M=5, γ_0=1 dB

ly influences the angular distribution of multipath components, is the most dominant propagation factor.

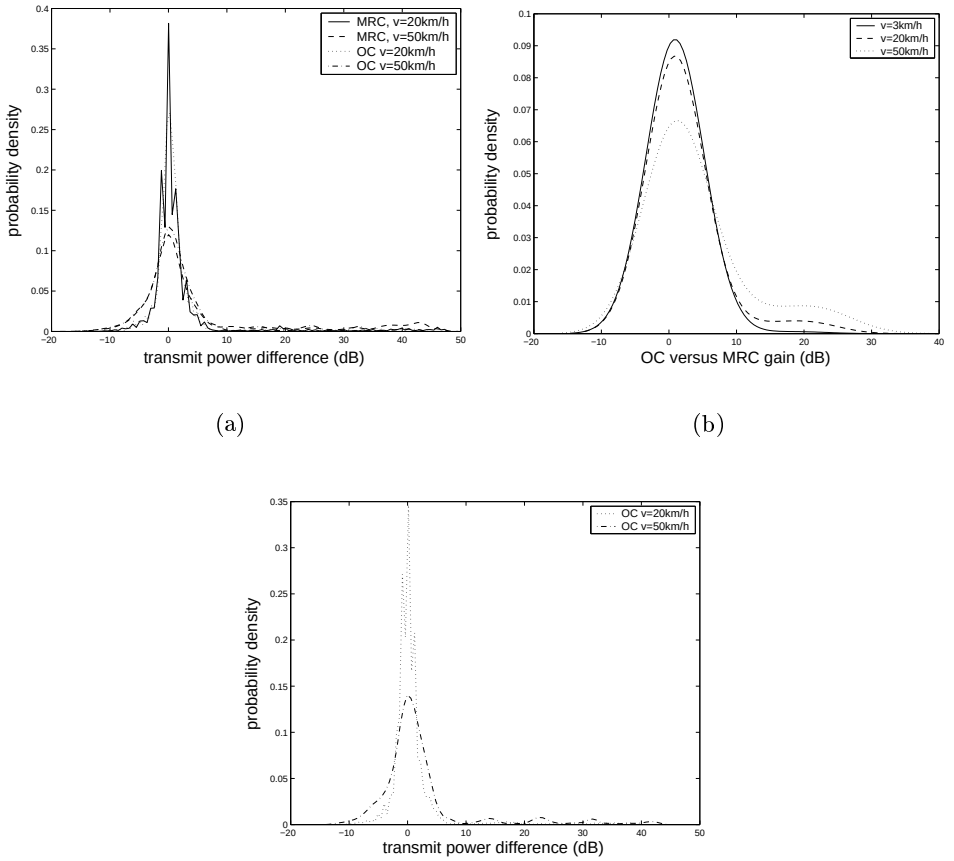

(a) (b)

(c)

Figure 6.4: K=6, N_{dB}=10 dB, M=3, γ_0=1 dB: (a) The probability density of the difference in transmit power from the case when v=3 km/h for OC and MRC, scenario 1; (b) The probability density of OC versus MRC power reduction, scenario 1; (c) The probability density of the difference in transmit power from the case when v=3 km/h for OC, scenario 2

Another difference from the *university campus environment* is reflected in the influence of the MS speed on the transmit power. All pdfs, regardless of the system set-up, are characterised by a larger spread around the mean value, indicating the transmit power difference of around 5 dB for both OC

and MRC. The fast fading effects are more pronounced for the *city center environment* and the main reason lies in a larger spread in the angles-of-arrival at the MS, as a result of reflections from the array of building faces at both sides of the street where the MS is moving. The average angular spread in the *university campus environment* was $\Lambda = 10^o$, while in the *city center environment* it is five times as large, $\Lambda = 50^o$.

The more pronounced influence of the MS speed in the *city center environment* is also manifested by a small persistent gain of up to 2 dB of OC over MRC in the power reduction. The gain actually alternates between zero and 2 dB, indicated by mean values of the peaks in pdfs shown in Fig. 6.2(b), Fig. 6.2(d), Fig. 6.3(b) and Fig. 6.3(d). This effect reflects different convergence properties between OC and MRC. In Fig. 4.3 (Section 4.3.3), it can be seen that MRC converges to the target SINR more slowly than OC. In the *university campus environment*, this was not so critical in the imperfect power control case due to a much lower angular spread. In this situation, when the channel exits from a fading dip, the power of the signal when OC is applied is, at one moment, increased by 1 dB, whereas in the case of MRC it still stays at the level which is 1dB lower, resulting in a total OC versus MRC gain of 2 dB. At another moment, the signal in case of MRC reaches a power level that is the same as with OC, resulting in a gain of zero. The fact that MRC is slower in reaching optimum values is aggravated by the fact that there is interference on both Rake fingers.

One can, in general, expect a larger OC versus MRC gain for highly delay dispersive environments for more Rake fingers are needed to capture the main energy of signals arriving at the receiver. The multipath components captured by one Rake finger represent just a "portion" of the total signal that arrives from one user. The components belonging to each finger have different levels of angular separation from interfering multipath components. As a result, a small gain of OC over MRC obtained for one Rake finger can yield even larger gain after combining all Rake fingers. In this scenario, only two Rake fingers are used and, in addition to that, the waves arrive from directions which are very close in angle. The small gain of 2 dB stems primarily from the power updates of ± 1 dB in the environment where fast fading is critical, which occur later for MRC with respect to OC due to their different convergence properties.

The fact the maximum distance of users from the BS is twice as large as in the previous scenario results in higher power levels needed for the satisfactory performance. This also makes the *city center environment* more critical for the maximum number of users for a lower processing gain. This has no influence, however, on the main trends regarding the dependence of

the results on the system parameters.

The results for different system parameters are summarised in the table 6.1. The influence of MS speed in addition to the convergence of a specific processing scheme towards the desired target is shown.

N_{dB}	γ_0	M	K	result	comment
25 dB	5 dB	3	15	OC, MRC converg. MRC more sensitive to MS speed	up to 2 dB OC versus MRC gain;
25 dB	5 dB	3	40	OC, MRC converg. MRC more sensitive to MS speed	up to 2 dB OC versus MRC gain;
15 dB	1 dB	5	30	OC, MRC converg. MRC more sensitive to MS speed	up to 2 dB OC versus MRC gain;
10 dB	1 dB	5	20	OC, MRC not converg.	data service critical for a larger coverage
10 dB	1 dB	5	10	OC, MRC converg. MRC more sensitive to MS speed	up to 2 dB OC versus MRC gain;
10 dB	1 dB	3	6	OC converg. MRC not converg.	MRC critical for a larger coverage with small antenna array

Tabel 6.1: Imperfect power control results for different system set-up

6.3 Pixel size analysis

As already explained in Section 5.4, the result for a pixel size depends largely on the evolution of the angles-of-arrival for the most dominant multipath components. A signal model for a frequency selective channel is first given in Section 6.3.1, followed by simulation results in Section 6.3.2. The experimental set-up in simulations is similar to the one given in Section 5.4, with

one user moving within a pixel of $40\lambda_c$ (6.24 m) length, while other users are fixed. The results are also given in terms of deviations of the achieved SINR from the desired target value for the moving user, as was the case with the *university campus environment*.

6.3.1 Signal model

The extrapolation of spatial signatures on the basis of *ray parameters*, obtained at the pixel center, and using the assumption that the only changing parameter within a pixel is the phase of multipath components, was given in Section 5.2. The achieved SINR, which deviates from the desired target value as a result of extrapolation, gives an indication about the maximum size of the trajectory/area within which *ray parameters* can be taken as unchanging. The definition of the pixel and the criterion for the maximum tolerable deviation is presented in Section 5.3. In the current analysis, the only difference from the *university campus environment* in the signal model is due to an additional Rake finger. The achieved SINR for the moving user, designated with index 1, is given as:

$$\gamma_0 = \frac{G_{11}P_1}{\sum_{j=2}^{K} G_{j1}P_j + \sigma_1^2} \tag{6.9}$$

$$\gamma_0 = N\frac{|\sum_{l=1}^{L} \zeta_{l,1}^* S_{l,1}^{oc}|^2 P_1}{\sum_{j=2}^{K}\sum_{l=1}^{L} |\zeta_{l,1}^* I_{l,1,j}|^2 P_j + \sigma_1^2} \tag{6.10}$$

$$\gamma_0 = N\frac{|\sum_{l=1}^{L} \zeta_{l,i}^* (\mathbf{w}_{l,1}^H \mathbf{h}_{l,1})|^2 P_1}{\sum_{j=2}^{K}\sum_{l=1}^{L} |\zeta_{l,i}^* (\mathbf{w}_{l,1}^H \mathbf{h}_j)|^2 P_j + \sigma_1^2} \tag{6.11}$$

The expression for the achieved SINR is a bit more complex than that for a flat fading channel, given by Eq. 2.68. In a frequency selective channel, the maximisation of SINR is performed for one Rake finger, whereby this compact form for the resulting SINR can only be related to a single finger. In general, SINR obtained as a result of Rake-antenna combining can not be given by a simple, closed-form expression, as shown by Eq. 2.80. The principle about finding the approximate SINR $\gamma_0^{'}$ is, nevertheless, the same as for the *university campus environment*. In Section 5.3, the approximate SINR is given as the function of the original spatial signatures and approximate optimum transmit powers. The latter were found on the basis of extrapolated spatial signatures, as in Eq. 5.10. Approximate optimum powers were contained in the spatial correlation matrix of interference, see Eq. 5.11. The

same is valid for the approximate SINR $\gamma_0^{'}$ in the current analysis, which is given as:

$$\gamma_0^{'} = N \frac{|\sum_{l=1}^{L} (\zeta_{l,i}^{'})^* ((\mathbf{w}_{l,1}^{'})^H \mathbf{h}_{l,1})|^2 P_1^{'}}{\sum_{j \neq 1}^{K} \sum_{l=1}^{L} |(\zeta_{l,i}^{'})^* ((\mathbf{w}_{l,1}^{'})^H \mathbf{h}_j)|^2 P_j^{'} + \sigma_1^2} \tag{6.12}$$

where $\mathbf{w}_{l,1}^{'}$ and $\zeta_{l,1}^{'}$ represent the approximate antenna weight vector and the weight coefficient for the l-th Rake finger, obtained as:

$$\mathbf{R}_{in,1}^{'} = \sum_{j=2}^{K} \frac{P_j^{'}}{P_1^{'}} \mathbf{h}_j \mathbf{h}_j^H + \frac{\sigma_1^2}{P_1^{'}} \mathbf{I}_M \tag{6.13}$$

$$\mathbf{w}_{l,1}^{'} = (\mathbf{R}_{in,1}^{'})^{-1} \mathbf{h}_{l,1} \tag{6.14}$$

$$\zeta_{l,1}^{'} = (\mathbf{w}_{l,1}^{'})^H \mathbf{h}_{l,1} \tag{6.15}$$

The following simulations will show, like in the analysis from Section 6.2.2, that the ultimate result largely depends on the channel angular characteristics.

6.3.2 Simulation results

The system set-up in the simulations is the same as in the *university campus environment*. The processing gain is N_{dB}=10 dB, target SINR γ_0=1 dB, antenna array size M=3 and the total number of users K=6. Two representative propagation cases are analysed for this type of environment. In the first case, the MS is relatively closer to the BS, as compared to the second case. Pixel trajectories for the two propagation cases are depicted in Fig. 6.5 and denoted by numbers 1-2. The spatial evolution of angles-of-arrival at the side of MS is distinctly different for these two cases. The basic differences between the cases can be seen in Fig. 6.6(a) and Fig. 6.6(b), depicting the spatial behaviour of angles-of-arrival for the first five dominant components. The propagation case 1 (see Fig. 6.6(a)) resembles a typical NLOS situation from the *university campus environment*. The spatial evolution of angles-of-arrival is characterised by a smooth and slow linear change only within the length of 1 m around the pixel center, with very abrupt changes beyond the 1 m window. The fact that these abrupt changes occur close to the pixel center is also found for NLOS propagation scenarios in the previous environment.

The propagation case 2 is characterised by smooth changes in angles-of-arrival for the whole length of $40\lambda_c$ (see Fig. 6.6(b)). This angular behaviour is governed by the specific building and street pattern structure, as already explained. From Fig. 6.5, it can be seen that for the propagation case 2, the

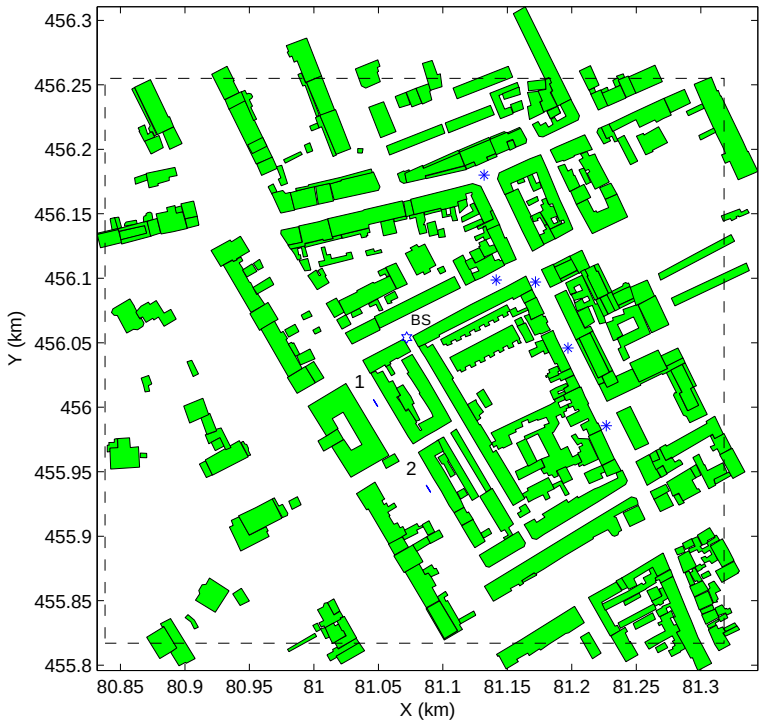

Figure 6.5: Simulation environment: $*$ stands for a fixed user, numbers 1-2 denote propagation cases, BS designates the base station

scattering at the side of the MS is dominated by reflections from building faces at both sides of the street. For the case 1, where the MS is located closer to the BS, more diverse propagation mechanisms take place, especially since the MS gets closer to the street crossing. The angles-of-arrival of the dominant components that arrive far from the BS via reflections from an array of building faces change very slowly, contrary to the case 1, where the scattering involves reflection and diffraction from buildings that are more randomly distributed. The pixel size result is, therefore, expected to be larger for situations represented by the case 2.

The simulation results of the spatial changes in the approximate target SINR, $\gamma_0^{'}$ are given in Fig. 6.7(a) and Fig. 6.7(c) for the propagation case 1 and 2, respectively. On the whole, the deviations from the desired target γ_0=1dB are substantially smaller for the case 2, as expected. The influence of the number of Rake fingers is shown for the propagation case 1 by comparison

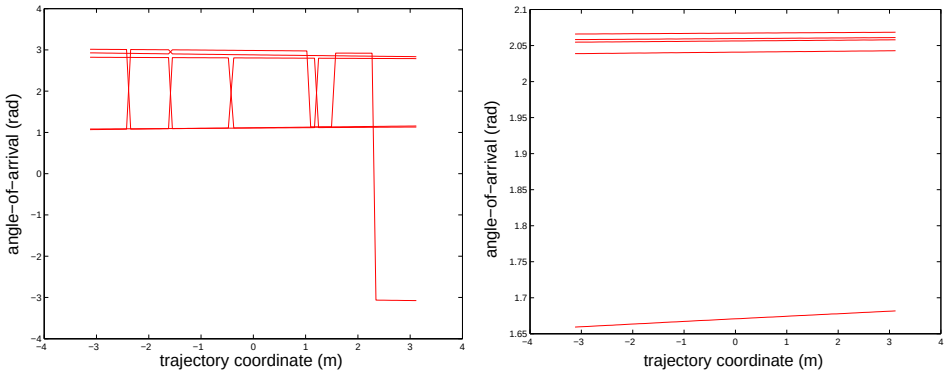

(a) (b)

Figure 6.6: Angles-of-arrival for five dominant multipath components: (a) Propagation case 1; (b) Propagation case 2

---

between the result in Fig. 6.7(a), with two Rake fingers active and the result in Fig. 6.7(b), with only one Rake finger. The deviations are smaller for two Rake fingers, which is analogous to the result found in Section 5.4.1 about the influence of the number of antenna array elements. The main reason for the SINR deviation is the phase error due to extrapolation applied to every multipath component. The increase in the number of Rake fingers has a similar effect as the increase in the antenna array elements: Rake combining involving a larger number of fingers works more efficiently in averaging out phase errors. This concept is similar to obtaining the reduction in the fast fading using a larger number of diversity branches, represented by either antenna array elements or Rake fingers (or the combination of both). In the following analysis only the results with two Rake fingers are considered, since both are necessary to capture the main energy of the received signals.

The result for the pixel size will be discussed for these two propagation cases by applying the criterion for the maximum tolerable deviation of 1.5 dB, established in Section 5.4. If the criterion is strictly applied, i.e. deviations are bounded by the exact value of 1.5 dB, the pixel size result is inconsistent for propagation case 2. Using 1.5 dB deviation tolerance, the critical SINR is -0.5 dB, as a lower-bound, and 2.5 dB is an upper-bound. The pixel size for propagation cases 1 and 2 were found to be 0.7 m and 1 m, respectively. While the result for the propagation case 1 is in accordance

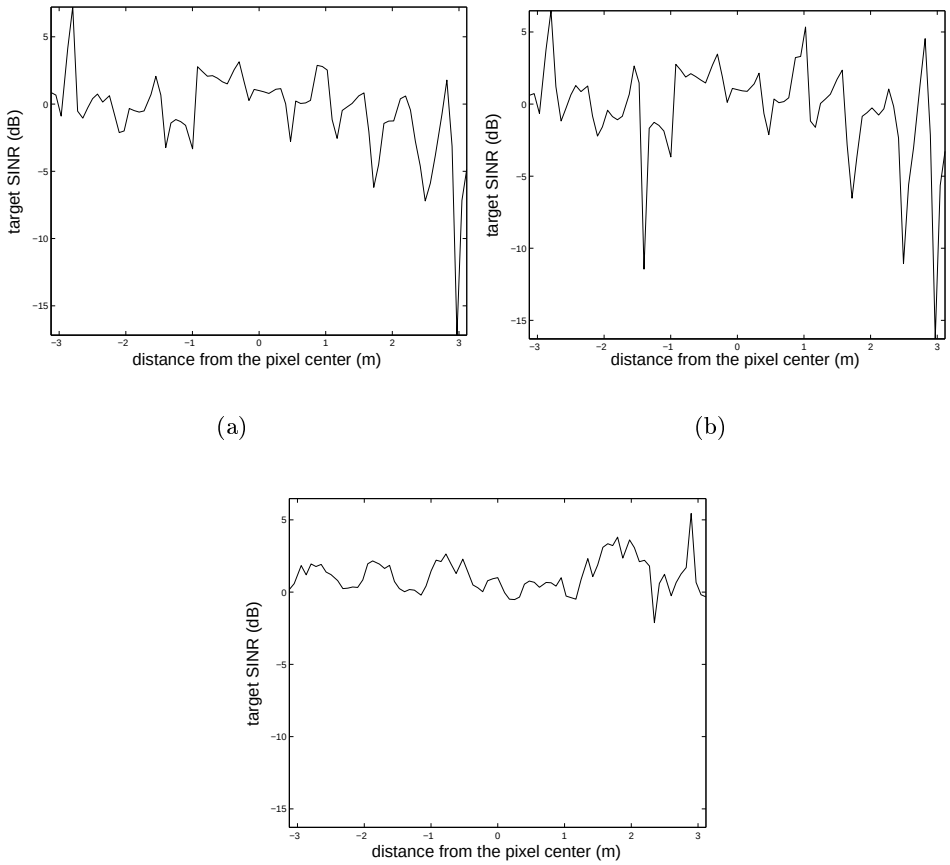

Figure 6.7: The change in $\gamma_0^{'}$ within the pixel, N_{dB}=10 dB, γ_0=1 dB, M=3: (a) two Rake fingers, propagation case 1; (b) one Rake finger, propagation case 1; (c) two Rake fingers, propagation case 2

---

with the NLOS situations shown in Section 5.4.2, where the pixel size varied in the [0.2 m-3.3 m] range, the result for the case 2 does not correspond to a more stable angular behaviour, shown by Fig. 6.6(b).

If the bounds are a little bit relaxed so that the lower-bound goes down to -0.52 dB and the upper-bound goes up to 2.65 dB, the pixel size for the case 2 is increased to 4.5 m, whereas the result for the case 1 remains the

same. If the bounds are only slightly changed, a new result is obtained which is also more consistent with the expectations. In Section 5.4.1, it is indicated that the pixel size result is very sensitive to phase errors as a result of extrapolation. The phase error is always present even for the part of a pixel where angles-of-arrival do not change significantly. This is because the extrapolation of phases is very sensitive to high frequencies (small wavelenghts). The point where the established boundary is exceeded depends not only on the abrupt changes in angles-of-arrival, but also on the way the phases of individual components "add up". For the case 2, the phases of multipath components "add up" so that the boundary is exceeded by a small value of 0.02 dB for a lower boundary and 0.15 dB for an upper boundary.

In order to relate more closely the changes in the spatial evolution of angles-of-arrival to a corresponding change in the target SINR, as was done for the *university campus environment*, the behaviour of a larger number of multipath components will be analysed. Angles-of-arrival of ten dominant multipath components for the propagation case 1 are depicted in Fig. 6.8(a) and the close-up of the achieved SINR in Fig. 6.8(b). The SINR curve for the propagation case 1 crosses the boundaries at the point where angles-of-arrival experience abrupt changes, as was the case with all NLOS scenarios from the *university campus environment*. The abrupt change in angles-of-arrival results in an abrupt change in phases of individual multipath components which, in turn, causes radical deviations in approximate SINR from the desired target. The influence of all multipath components within a power range of 20 dB is still significant. The pixel size analysis for the *university campus scenario* shows that weaker multipath components, with abrupt changes very close to a pixel center, still contribute to the result. For this reason, the pixel size tends to be smaller with a larger number of contributing multipath components.

Angles-of-arrival for the case 2 exhibit a behaviour quite different from the case 1. In Fig. 6.9(a), depicting ten dominant multipath components for the propagation case 2, eight strongest components are characterised by slow, linear changes, like in Fig. 6.6(b), while the two weakest components experience very abrupt changes close to the pixel center. The two components, however, show a very correlated behaviour. Namely, angles-of-arrival for each of the components alternate between two fixed values, 1.9 rad and 2.35 rad, within the 3 m window around the pixel center. The explanation for this phenomenon becomes more clear from Fig. 6.9(c), depicting power levels for those components. The ten components are located in a small power range of 6 dB. The two weakest components have almost the same value, with only a small difference in power levels that also alternate between

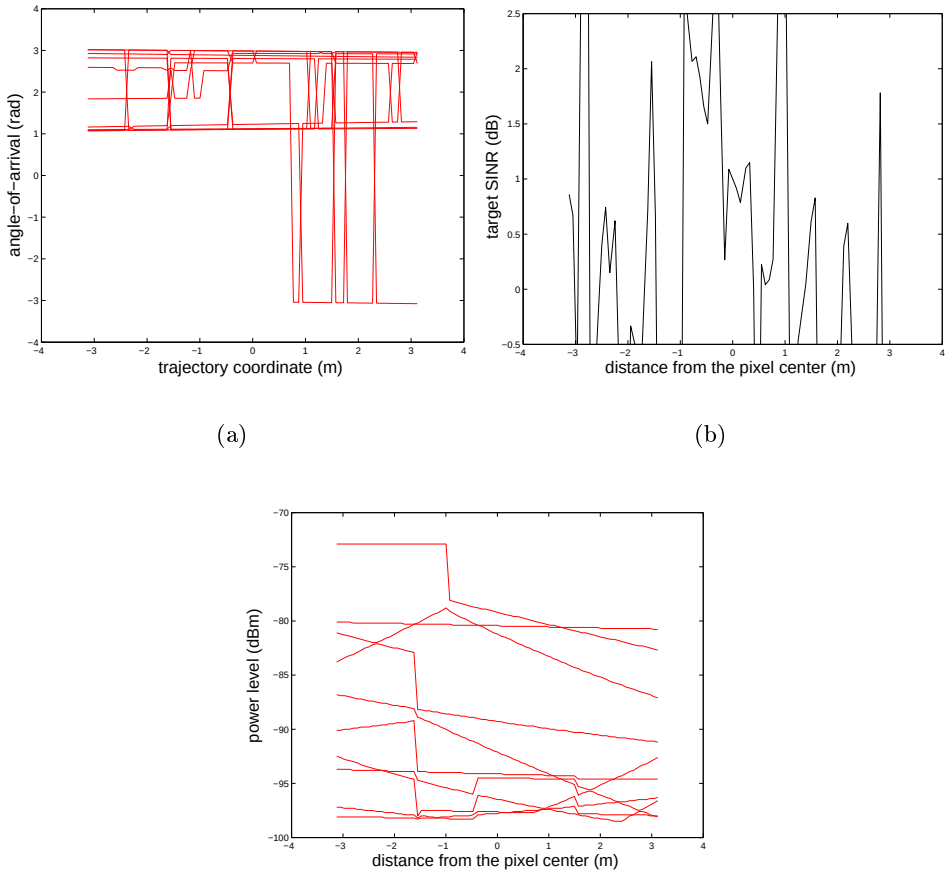

(a) (b)

(c)

Figure 6.8: Propagation case 1: (a) Angles-of-arrival for ten dominant multipath components; (b) The close-up of the change in γ_0' within the pixel, N_{dB}=10 dB, γ_0=1 dB, M=3; (c) Power levels for ten dominant multipath components

---

two very close values. This means that the angle-of-arrival of 1.9 rad and the angle-of-arrival of 2.35 rad actually belong to the same two components whose power levels do not change significantly, so that within certain parts of the pixel one of the components has a slightly higher power level than the other and vice versa.

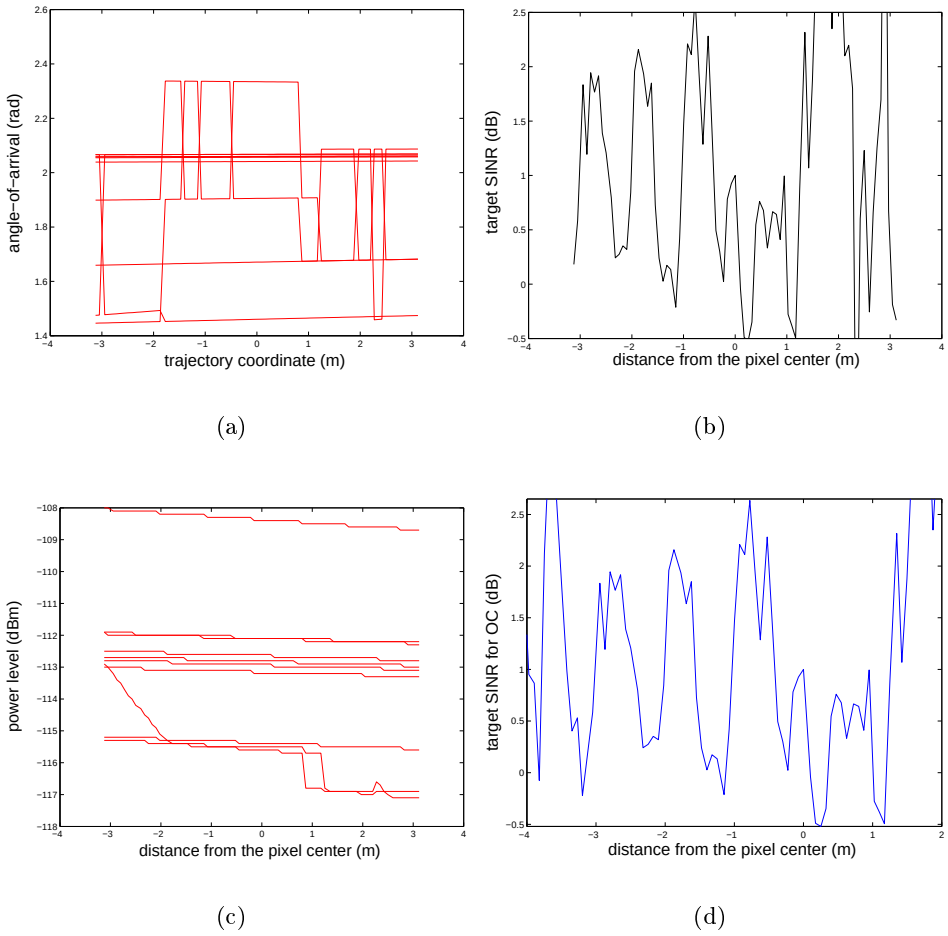

(a) (b)

(c) (d)

Figure 6.9: Propagation case 2: (a) Angles-of-arrival for ten dominant multipath components; (b) The close-up of the change in $\gamma_0^{'}$ within $40\lambda_c$ pixel, N_{dB}=10 dB, γ_0=1 dB, M=3; (c) Power levels for ten dominant multipath components; (d) The change in $\gamma_0^{'}$ within $80\lambda_c$ pixel, N_{dB}=10 dB, γ_0=1 dB, M=3

On the whole, there are ten multipath components with almost equal amplitudes and unchanging angles-of-arrival within a 3 m window. The summation of those components does not cause a significant change in the target SINR for a large part of the pixel. The result for the extended part of

a pixel trajectory, given by Fig. 6.9(d), shows at what points the SINR curve crosses newly established boundaries at both sides of the pixel center. The result gives a pixel size of 5 m for this case. The shift in boundaries, however, does not influence the result for case 1. The propagation case 1 is a clear-cut situation when abrupt changes in the channel composition occur within a 1 m-2 m window around the pixel center, which is clear both from the angles-of-arrival and power level spatial behaviour, as shown by Fig. 6.8(a) and Fig. 6.8(c), respectively.

It can be concluded that if the boundaries are strictly applied, the pixel size can be very small even if angles-of-arrival do not change significantly for a larger part of the pixel. Small phase errors that inevitably occur for each multipath component, as the result of the extrapolation method proposed in Section 5.2, can cause an 'overshoot' beyond the established boundaries, which depends on whether phases "add up" constructively or not. It is,

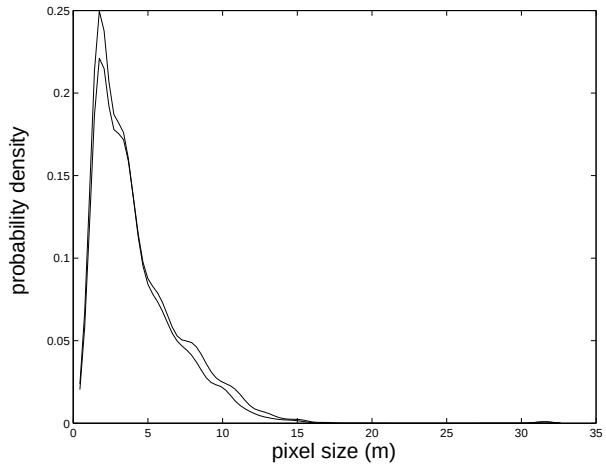

Figure 6.10: The probability density of a pixel size result for two close criterion boundaries

therefore, necessary to find a stable method that is not so sensitive to small shifts in the given boundaries. One of the ways is to "move" the center of a pixel over a larger trajectory, establish the size of the pixel at each point according to specified boundaries and make an average of the obtained results.

The probability density of the pixel size results, obtained according to the newly proposed procedure, is shown in Fig 6.10 for two different criterion boundaries. The center points of pixels are taken at $\lambda_c/2$ spacing and the

trajectory over which the results were taken is shown in Fig. 6.1. This comprises situations represented by the propagation case 1 and propagation case 2. One of the pdf curves corresponds to the boundary with 1.5 dB deviation in the achieved SINR and the other when the boundary is slightly relaxed, resulting in 1.65 dB deviation. The two pdfs show that the pixel size result becomes more stable and less sensitive to small shifts in a criterion boundary. The average value for the pixel size when the initially specified deviation of 1.5 dB represents the maximum tolerable error, is $\bar{D}$=4 m. This result represents an average over the cases when abrupt changes in the channel occur close to a pixel center and the cases where changes are more slow and stable.

6.4 Conclusions

The performance of smart antenna under power control and pixel size analysis was done for another type of a micro-cell urban environment, represented by a typical city center. The aim was to compare the results with the previously analysed environment, represented by the university campus. The main differences in the results can be related to global differences in propagation conditions characterising the two environments.

The propagation condition that has the largest impact on results for smart antenna performance is a local scattering at the BS. There is no significant advantage of OC over MRC in reducing transmit power for an urban city center, due to the fact that the bulk of multipath components, belonging to different users, arrives from directions that are closely spaced in angle. The propagation in a city center is primarily governed by multiple reflections from a densely packed array of buildings, which results in a wave-guiding effect via streets. This is a major difference from the *university campus scenario*, where the scattering of rays around the BS occurs from diverse directions and OC versus MRC gain of up to 10 dB can be obtained.

Another dominant propagation factor is angular spread at the side of the MS. It can have significant influence on the dependence of power levels, even for low to moderate speeds. The influence of MS speed was not that significant in the *university center environment*, due to a very low angular spread of 10^o. The angular spread is five times larger in the *city center environment*, resulting in a power level difference of 5 dB. The more pronounced influence of the speed is also manifested in a small persistent OC versus MRC transmit power gain of 2 dB. This is directly related to the difference in convergence properties between OC and MRC scheme, that becomes visi-

ble in environments with more pronounced fast fading effects. The 2 dB gain is the result of a step size of 1 dB in the realistic power update process. The fact that the channel is frequency selective, i.e. more than one Rake finger is active, aggravates the convergence of MRC scheme, due to an increased level of interference that is present on Rake fingers.

The *city center environment* is more critical for the maximum number of users that can be sustained for when the processing gain is lower, since the maximum distance between users and the BS is almost twice as large than in the *university campus environment*. This, however, does not change basic trends regarding the impact of system parameters on the results. In case of a voice service, up to 40 users can be sustained using a small antenna array size M=3 for both OC and MRC. For a data service, up to 20-30 users can be supported using a larger antenna array M=5 for both OC and MRC. MRC is more critical than OC for larger distances from the BS.

In the pixel size analysis, two main propagation cases were investigated. Like in the *university campus environment*, the spatial behaviour of angles-of-arrival at the side of the MS has the largest impact on the result. The case where the MS was located close to the BS was comparable to a typical NLOS situation in the *university campus environment*. This case is characterised by abrupt changes in angles-of-arrival of the most dominant multipath components, that occur within a 1 m-2 m window around the pixel center. The second case, where the MS was located farther from the BS, was characterised by smooth, linear changes in the angles-of-arrival for the whole pixel length of 6 m. The results are found to be quite sensitive to phase errors, that occur as a result of the extrapolation method analysed, even over the part of a trajectory where angles-of-arrival do not change significantly.

A small phase error was, however, not critical for the result regarding the propagation case 1, since the size of the pixel corresponds to points at which abrupt changes in angles-of-arrival take place. This was also the case for all NLOS scenarios analysed in the previous environment. The phase error was critical for the propagation case 2, when the result obtained applying the pixel size criterion strictly, was not consistent with a stable behaviour of angles-of-arrival. The result is very sensitive to small shifts in the criterion boundary. In order to obtain a result that is more stable for the initially specified deviation of 1.5 dB in the achieved SINR, an averaged value for the pixel size was computed for a trajectory of 100 m length. The resulting pixel size found is $\bar{D}$=4 m and this includes both the cases with abrupt changes in the channel composition within 1 m-2 m from a pixel center and the cases when the change in angles-of-arrival is insignificant for a larger part of the trajectory. In Section 5.4, it is indicated that accurate spatial signatures

were calculated using *ray parameters* obtained at $\lambda_c/2$ spacing directly from μFipre. This represents a reference resolution for the computation of the channel composition from the ray-tracing model. The pixel size result of $\bar{D}$=4 m shows that it is possible to obtain the efficiency in the reduction of the computational burden of $2\bar{D}/\lambda_c \approx 50$.

7

Summary, conclusions and recommendations

7.1 Summary and conclusions

The main subject of this thesis is analysing the effects of realistic propagation in an urban micro-cell environment on UMTS performance using smart antenna. In relation to this, some fundamental issues about channel modelling for UMTS are addressed.

In the first part of the thesis, a novel method that incorporates UMTS aspects using a deterministic channel model is proposed. A signal and receiver model for Rake-antenna array processing is described. Spatial channel model is derived, on the basis of which the delay and angular spread can be calculated for an arbitrary position in the environment, as well as average powers of the desired and interfering signals for any spatial distribution of users. The antenna processing schemes included are: optimum combining and maximum ratio combining. The main motivation is to make use of the exact channel information for every user, thus avoiding assumptions about average power profiles and also reflecting the mutual spatial correlation between users correctly. This enables proper analysis of the use of smart antenna in an urban micro-cell environment, where spatial changes are very diverse being subject to local characteristics.

In order to illustrate the importance of providing more accurate information about angular profiles for the users, but also to find what is essentially lacking in the current stochastic models with respect to deterministic ones, a novel comparison between a stochastic and a deterministic model is performed in Chapter 3. It is shown that stochastic models do not reflect spatial correlation between users (or spatial structure of interference with respect to the desired user) properly.

The antenna array processing results obtained, using the stochastic WDCM and the deterministic ray-tracing μFipre model, were compared on the basis of a simple interference scenario. Two different approaches were applied to tune the input of the stochastic model which enables a fair comparison with the ray-tracing model. According to the first approach, the WDCM was tuned to global channel characteristics: the delay and angular spread. This gave a significant difference in the predicted SINR, due to a differently predicted level of separation between spatial signatures of the desired and interfering user. This separation level is expressed in terms of a *spatial separation parameter*.

In the second approach, the WDCM was tuned on the basis of this parameter, being very influential for the final SINR result. It was established that the street width is the only input parameter for WDCM, which has a significant influence on the value of the *spatial separation parameter*. The values for the street width that provide the best match between the results of the two models for three LOS streets of different widths, showed that the model does not incorporate real physical conditions in a consistent way.

The prediction of smart antenna performance requires more details about the spatial structure of interference, especially if it can not be considered as spatially-white. Therefore, the deterministic model μFipre was used for further analysis featuring power control combined with the antenna array processing in an environment represented by a part of the TU/e campus. This is presented in Chapter 4.

The perfect power control case was dealt with first in order to establish the influence of parameters such as the processing gain, antenna array size and spatial distribution of users on optimum transmit powers. Two antenna array processing algorithms, optimum combining and maximum ratio combining, are considered with the aim to find out the benefits of using algorithms that utilise information about the spatial structure of interference over algorithms that only steer the beam towards the desired user. The most dominant parameter which puts the main limitation on the number of users is the processing gain. Antenna array size is the second dominant parameter. It improves the convergence properties of MRC. OC is clearly superior to MRC regarding the number of users for which the convergence to a desired target can be achieved.

The analysis including imperfections of the power control process due to a finite time available for power updates and due to a fixed power increment/decrement of 1 dB, shows that the reduction in transmit power when OC is used with respect to MRC can go up to 10 dB for a large number of scenarios. Five-element antenna array can provide satisfactory performance

for both OC and MRC in a variety of scenarios. In case of a small number of users per cell, below 10, and for scenarios dominated by a high processing gain the antenna array size of M=3 can be expected to be sufficient.

It is obvious that accurate prediction of channel information for users is important for urban micro-cells and the use of deterministic models can not be avoided. However, it would be very cumbersome to compute the channel composition using the ray-tracing model for each location on a trajectory. Therefore, it is important to find the way to decrease the computational burden of the ray-tracing tool. This issue was addressed in Chapter 5, by considering the concept of a *pixel*. The basic idea is to compute the channel composition for the center of the pixel and extrapolate spatial signatures for any point within the pixel on the basis of the information. The pixel size was defined as the maximum length around the pixel center, where the achieved SINR deviates from the desired target, as a result of extrapolation, within tolerable limits. It was observed that small deviations occur very close to a pixel center which is predominantly influenced by errors in extrapolated phases, related to angles-of-arrival at the side of the MS. More drastic changes occur farther from the pixel center and this coincides with a significant change in the composition of waves.

The deviation in the achieved SINR of 1.5 dB has been identified as a tolerable deviation, since errors larger than 1.5 dB fall into the region where more drastic changes start to occur in the channel. This is also acceptable judging by the spatial behaviour of SINR in the imperfect power control process, where average fluctuations are even larger. The average result for the pixel size of $\bar{D}$=2 m was found on the basis of several NLOS propagation cases, being far more critical for the result than LOS situations. This result was obtained using a three-element antenna array. In case of a five-element array, the pixel size tends to be larger, since phase errors are better averaged-out using a larger antenna array. This makes a three-element array more critical for the result.

The smart antenna performance and pixel size were also analysed for another type of urban environment, represented by the Hague city center. The comparison of the obtained results with those corresponding to the environment used in previous chapters provided better understanding about the influence of propagation factors. The aspects of propagation that were identified to pose main restrictions on the system performance are the local scattering at the base station, which is directly responsible for the power reduction gain when using OC over MRC, and angular spread at the side of a mobile terminal, which is related to the influence of a mobile speed on optimum transmit powers.

The scattering of multipath components belonging to different users at the side of the BS was more diverse in angle in the university campus environment, contrary to a city center, where the majority of multipath components comes from the same direction. This gave insignificant power reduction of OC over MRC, as compared to the university campus. The propagation in the city center is primarily governed by a wave-guiding via multiple reflections from densely packed buildings, whereas the university campus is characterised by a larger number of diverse propagation mechanisms with comparable influence, including diffractions and scattering from vegetation. The influence of a mobile speed was analysed for low to moderate speeds, v=3 km/h-50 km/h, typical for a micro-cell scenario. The MS speed did not have a significant influence on power levels in the university campus due to a very low angular spread $\Lambda = 10^o$ at the side of the MS. The angular spread in the city center is five times larger, $\Lambda = 50^o$, resulting in around 5 dB difference in optimum transmit power. The fast fading effects are, thus, very critical at the frequency of around 2 GHz, since the power level difference is quite significant for moderate angular spreads. The influence of the MS speed in the city center is also reflected in the difference between OC and MRC scheme regarding tracking of the fast fading, which results in a small persistent 2 dB gain of OC for the power update step-size of 1 dB.

The pixel size analysis for the city center yields some additional aspects of the extrapolation method proposed. One of the propagation cases in the city center was characterised by slow and smooth changes in angles-of-arrival within the length of 6 m, which was different from cases in the university campus, where abrupt changes occur within a length of 1 m-2 m. If the pixel size criterion of 1.5 dB maximum tolerance for SINR deviation from the desired target is strictly applied, the result can be much smaller than the length when abrupt changes in the channel composition occur, which appears to be contrary to previous conclusions. This is directly the consequence of the fast fading effects, that are more pronounced at high frequencies, and related phase errors. A small shift in the criterion boundary yields results that are more consistent with the expectations. For this reason, the pixel size result was eventually established as an average value over a large number of scenarios for a trajectory of 100 m. This significantly reduces the sensitivity to small shifts in the criterion boundary and yields the pixel size result of $\bar{D}$=4 m for the initially specified 1.5 dB deviation. This result "covers" scenarios where abrupt changes occur closer to a pixel center, like NLOS scenarios from the university campus environment, and scenarios with slow changes in the composition of waves for the larger part of a trajectory. Assuming that half wavelength ($\lambda_c/2$) spatial spacing between two points

on a trajectory is sufficient for proper characterisation of the channel, the result of $2\bar{D}/\lambda_c \approx 50$ shows that it is possible to decrease the computational burden of a deterministic model by a factor of 50.

7.2 Recommendations

In this thesis a method to model system aspects by utilising deterministic channel information is proposed. The propagation aspects were analysed on the basis of urban environments where the dispersion in delay domain was not so large. This reduced the analysis of the smart antenna performance to primarily angular characteristics of the channel. The proposed theory can be extended to environments with more pronounced dispersion in delay domain, resulting in a larger number of Rake fingers necessary to collect the energy of the signal. Larger OC versus MRC gains in transmit power reduction are expected, because of a more complex dependence on interference, which is present on all Rake fingers.

The method to minimise the amount of deterministic data from a concrete environment, by using the concept of a *pixel*, is characterised by a considerably high sensitivity to phase errors. The pixel size result was eventually found as an average over a large number of pixel trajectories using the proposed extrapolation method. The extrapolation method itself can be improved by linearly interpolating the values of angles-of-arrival within a pixel using the angle-of-arrival information at the center of the current pixel and that at the center of the neighboring pixels. More precisely, the values for angles-of-arrival on the left-hand side of the pixel center (within half the pixel length) should be interpolated using the angle-of-arrival information in the center of the current pixel and the pixel center on the left-hand side, the same being done for angles-of-arrival on the right-hand side. The modified procedure does not require more information about *ray parameters* per pixel than the method used in the thesis and also has the potential to yield a larger pixel size result. In this way, the efficiency of the method can be significantly improved.

A

Derivation of the Optimum Combining Antenna Weights

In section 2.3, SINR achieved for a desired user as a result of OC for the l-th Rake finger is given as:

$$\gamma_l = \frac{P|\mathbf{w}_l^H \mathbf{h}_l|^2}{\sum_{j=1}^{K-1} P_j |\mathbf{w}_l^H \mathbf{h}_j|^2 + \sigma^2 |\mathbf{w}_l|^2} \tag{A.1}$$

assuming $K-1$ interfering users with corresponding transmit powers P_j and spatial signatures $\mathbf{h}_j$, $(j = 1, ...K-1)$, while P and $\mathbf{h}_l$ represent the transmit power and the l-th Rake finger spatial signature of the desired user, respectively. For simplicity of the derivation to follow, the index l, denoting a Rake finger, will be omitted and Eq. A.1 can be rewritten as:

$$\gamma = \frac{P|\mathbf{w}^H \mathbf{h}|^2}{\sum_{j=1}^{K-1} P_j |\mathbf{w}^H \mathbf{h}_j|^2 + \sigma^2 |\mathbf{w}|^2} = \frac{\mathbf{w}^H \mathbf{R}_d \mathbf{w}}{\mathbf{w}^H \mathbf{R}_{in} \mathbf{w}} \tag{A.2}$$

where $\mathbf{R}_d$ and $\mathbf{R}_{in}$ represent the desired signal and interference+noise correlation matrices, respectively and are given by:

$$\mathbf{R}_d = \mathbf{h}\mathbf{h}^H \tag{A.3}$$

$$\mathbf{R}_{in} = \sum_{j=1}^{K-1} \frac{P_j}{P} \mathbf{h}_j \mathbf{h}_j^H + \frac{\sigma^2}{P} \mathbf{I}_M \tag{A.4}$$

The problem is to find antenna weights $\mathbf{w} = \mathbf{w}_{opt}$ that maximise Eq. A.2. The solution can be found starting from a symmetric factorisation of the interference+noise correlation matrix $\mathbf{R}_{in}$:

$$\mathbf{R}_{in} = \mathbf{A}\mathbf{A} \tag{A.5}$$

Since $\mathbf{R}_{in}$ is a Hermitian matrix, the following is valid: $\mathbf{A} = \mathbf{A}^H$. Applying the transformation:

$$\mathbf{v} = \mathbf{A}\mathbf{w} \tag{A.6}$$

and defining: $\mathbf{B} = \mathbf{A}^{-H}\mathbf{R}_d\mathbf{A}^{-1}$, the following can be written:

$$\mathbf{w}^H = \mathbf{v}^H\mathbf{A}^{-H} \tag{A.7}$$

and

$$\gamma = \frac{\mathbf{v}^H\mathbf{A}^{-H}\mathbf{R}\mathbf{A}^{-1}\mathbf{v}}{\mathbf{v}^H\mathbf{A}^{-H}(\mathbf{A}\mathbf{A})\mathbf{A}^{-1}\mathbf{v}} = \frac{\mathbf{v}^H\mathbf{B}\mathbf{v}}{\mathbf{v}^H\mathbf{v}} \tag{A.8}$$

The form given by Eq. A.8 is maximised by choosing for $\mathbf{v}$ the eigenvector belonging to the largest eigenvalue of $\mathbf{B}$. Using the definition $\mathbf{x} = \mathbf{A}^{-1}\mathbf{h}$, matrix $\mathbf{B}$ can be written in the form:

$$\mathbf{B} = \mathbf{x}\mathbf{x}^H \tag{A.9}$$

Since $\mathbf{B}$ is a rank-one matrix, it has only one non-zero eigenvalue λ with a corresponding eigenvector $\mathbf{e}$. The following is valid for $\mathbf{e}$:

$$\mathbf{e} = \mathbf{A}^{-1}\mathbf{h} \tag{A.10}$$

This can be confirmed by: $\mathbf{B}\mathbf{e} = \lambda\mathbf{e}$. Using $\mathbf{e}$ for $\mathbf{v}$ and substituting for $\mathbf{w}$ yields the following optimum antenna weight vector:

$$\mathbf{w}_{opt} = \kappa\mathbf{R}_{in}^{-1}\mathbf{h} \tag{A.11}$$

where κ is an arbitrary constant. If the optimum weight vector is applied in Eq. A.2, the following is obtained for SINR:

$$\gamma = \mathbf{h}^H\mathbf{R}_{in}^{-1}\mathbf{h} \tag{A.12}$$

B

The Convergence of the Power Control Algorithm

In Section 4.3.3, an iterative power control algorithm has been introduced which assures that all users achieve the same desired target SINR γ_0. The update of the i-th user transmit power in the n-th iteration is performed on the basis of interference coming from other users $I_i(n) = \sum_{j \neq i} G_{ji} P_j(n)$ and is given by:

$$P_i(n+1) = \frac{\gamma_0}{G_{ii}}(I_i(n) + \sigma_i^2) \tag{B.1}$$

$$P_i(n+1) = \frac{\gamma_0}{G_{ii}}(\sum_{j \neq i} G_{ji} P_j(n) + \sigma_i^2) \tag{B.2}$$

This iterative procedure always converges to the optimal solution (provided that it exists), starting from an arbitrary transmit power vector $[P_1^0, ...P_K^0]$, with K users assumed in the system. The problem is to prove the convergence of the given procedure. The notation used in the following derivation is given in Chapter 4. If the i-th user SINR obtained in the n-th iteration $\gamma_i(n)$ is defined as:

$$\gamma_i(n) = \frac{P_i(n) G_{ii}}{I_i(n) + \sigma^2} \tag{B.3}$$

the power control procedure for the i-th user can be written as:

$$P_i(n+1) - P_i(n) = -\frac{I_i(n)}{G_{ii}}(\gamma_i(n) - \gamma_0) \tag{B.4}$$

If there exists a power vector $\mathbf{p}_{opt} = [P_1^{opt}, P_2^{opt}, ...P_K^{opt}]$ for which the desired SINR value γ_0 is attained for each user, so that $\lim_{n \to \infty} \gamma_i(n) = \gamma_0$, each $P_i(n)$ will converge to P_i^{opt}, according to Eq. B.4, for an arbitrary initial power vector $\mathbf{p}(0) = [P_1(0), ...P_K(0)]$.

Proof: The iterative procedure can be rewritten as:

$$P_i(n+1) - P_i(n) = -[P_i(n) - \frac{\gamma_0}{G_{ii}}[\sigma^2 + \sum_{j \neq i} G_{ji} P_j(n)]] \tag{B.5}$$

or in a vector form:

$$\mathbf{p}(n+1) - \mathbf{p}(n) = (\gamma_0 \mathbf{G} - \mathbf{I}_K)\mathbf{p}(n) + \mathbf{u} \tag{B.6}$$

At the desired $\mathbf{p}_{opt}$, the following is valid:

$$(\mathbf{I}_K - \gamma_0 \mathbf{G})\mathbf{p}_{opt} = \mathbf{u} \tag{B.7}$$

Substituting for $\mathbf{C} = \gamma_0 \mathbf{G}$, the solution of the iteration starting from an initial power vector $\mathbf{p}(0)$ is:

$$\mathbf{p}(n) = \mathbf{C}^n \mathbf{p}(0) + (\mathbf{I}_K + \mathbf{C} + \mathbf{C}^2 + ...\mathbf{C}^n)\mathbf{u} \tag{B.8}$$

Using a geometric series property, the following is obtained:

$$\mathbf{p}(n) = \mathbf{C}^n \mathbf{p}(0) + \frac{\mathbf{I}_K - \mathbf{C}^{n+1}}{\mathbf{I}_K - \mathbf{C}}\mathbf{u} \tag{B.9}$$

The matrix $\mathbf{C}$ is assumed to be sufficiently random and have K distinct eigenvalues (a diagonalizable matrix). It can be factored as:

$$\mathbf{C} = \mathbf{P}\mathbf{D}\mathbf{P}^{-1} \tag{B.10}$$

where $\mathbf{P}$ is the matrix containing eigenvectors of $\mathbf{C}$ and $\mathbf{D}$ is the matrix with corresponding eigenvalues, as its diagonal entries. Using a well-known property of functions of diagonalizable matrices $f(\mathbf{C}) = \mathbf{P}f(\mathbf{D})\mathbf{P}^{-1}$, the following is valid:

$$\mathbf{C}^n = \mathbf{P}\mathbf{D}^n\mathbf{P}^{-1} \tag{B.11}$$

Provided that all moduli of the eigenvalues of $\mathbf{C}$ are strictly less then unity, the limit of the form given by Eq. B.9 becomes:

$$\lim_{n\to\infty} \mathbf{p}(n) = (\mathbf{I}_K - \mathbf{C})^{-1}\mathbf{u} = \mathbf{p}_{opt} \tag{B.12}$$

The eigenvalues of the matrix $\mathbf{C} = \gamma_0 \mathbf{G}$ are equal to the eigenvalues of the gain matrix $\mathbf{G}$ multiplied with a constant γ_0. The moduli of eigenvalues of $\mathbf{C}$ are less than unity if the spectral radius of $\mathbf{C}$ (the module of the largest eigenvalue, which is positive for non-negative matrices) is less than unity. This condition equals the convergence condition $\gamma_0 \lambda_{max} < 1$, given in Section 4.2, where λ_{max} represents the maximum eigenvalue of the gain matrix $\mathbf{G}$.

References

[1] S. Haykin and M. Moher, *Modern Wireless Communications*, Pearson Prentice Hall, 2005.

[2] S. Blust, "Wireless Standards Development-A New Paradigm," *plenary talk at IEEE Vechicular Technology Conference*, 2000.

[3] S. Glišić, *Spread Srectrum CDMA Systems for Wireless Communications*, Artech House Publishers, 1997.

[4] H. Holma and A. Toskala, *WCDMA for UMTS: radio access for third generation mobile communications*, Wiley, 2001.

[5] D. Mottier, L. Brunel, P. Pinho, A. Silva, L. Goncalves, A. Morgado, P. Marques, M. Pesce, D. Dahlhaus, J. Gil, J. Mendez, L.M. Correia, P. Hertach, L. Herault, and F. Bucci, "Final Report of the Different Algorithms in terms of Link Performance," *IST Asilum Public Deliverable D4.4*, 2002.

[6] M.J. Heikkila and et al., "Review and Selection of Relevant Algorithms," *Metra Public Deliverable*, 2000.

[7] Y.L.C. Jong, *Measurement and Modelling of Radiowave Propagation in Urban Microcells*, Ph.D. thesis, Eindhoven University of Technology, May 2001.

[8] J. Ylitalo and et al., "Definition of Power Control, Channel Estimation and SIR Estimation Procedures," *Metra Public Deliverable D3.2*, 2000.

[9] M.P.J. Baker and T.J. Moulsley, "Power Control in UMTS Release '99," *IEE 3G Mobile Communication Technologies*, , no. 471, pp. 36 –40, 2000.

[10] J.G. Proakis, *Digital Communications*, McGraw-Hill, 1989.

[11] A. Algans, K.I. Pedersen, and P.E. Mogensen, "Experimental Analysis of the Joint Statistical Properties of Azimuth Spread, Delay Spread and Shadow Fading," *IEEE Trans. on Communications*, vol. 20, no. 3, pp. 523–531, 2002.

[12] L. Schumacher, L.T. Berger, and J. Ramiro Moreno, "Recent Advances in Propagation Characterization and Multiple Antenna Processing in the 3GPP Framework," *XXVIth URSI General Assembly proceed.*, 2002.

[13] M. Steinbauer, A.F. Molisch, and E. Bonek, "The Double Directional Channel Model," *IEEE Antennas and Propagation Magazine*, vol. 43, pp. 51–63, 2001.

[14] "MIMO System Simulation Methodology," *tech. rep.,European 3GPP TSG R1-02-0142*, 2002.

[15] T.S. Rappaport, *Wireless Communications*, Prentice Hall PTR, 1996.

[16] M.G. Markes and L.M. Correia, "A Wideband Directional Channel Model for UMTS Micro-cells," *12th IEEE International Symposium on Personal, Indoor and Mobile Radio Communications*, vol. 1, no. 1, pp. B–122–B–126, 2001.

[17] L. Herault, "Wideband Directional Channel Model and Measurement Campaign," *Asilum Public Deliverable D2.1*, 2002.

[18] D. Chizhik, F.R. Farrokhi, J. Ling, and A. Lozano, "Effect of Antenna Separation on the Capacity of BLAST in Correlated Channels," *IEEE Communication Letters*, vol. 4, pp. 337 – 339, 2000.

[19] K.I. Pedersen, P.E. Mogensen, and B.H. Fleury, "Spatial Channel Characteristics in Outdoor Environments and Their Impact on bs Antenna System Performance," *IEEE Proceed. on Vehicular Technology*, vol. 2, pp. 719–723, 1998.

[20] G.D. Durgin and T.S. Rappaport, "Effects of Multipath Angular Spread on the Spatial Cross-Correlation of the Received Voltage Envelope," *IEEE Proceed. on Vehicular Technology*, vol. 2, no. 2, pp. 996 – 1000, 1999.

[21] L.M. Correia, *Wireless Flexible Personalized Communications*, Wiley, 2001.

[22] A.F. Naguib and A. Paulraj, "Performance Enhancement and Tradeoffs of Smart Antennas in CDMA Cellular Networks," *IEEE Proceed. on Vehicular Technology*, vol. 1, pp. 40 – 44, 1995.

[23] A.G. Kogiantis, "Uplink Capacity Studies for Adaptive Antenna Arrays in Third Generation CDMA," *IEEE Wireless Communications and Networking Conference*, vol. 2, pp. 679 – 683, 1999.

[24] K. Yao, "Error Probability of Asynchronous Spread-Spectrum Multiple Access Communication Systems," *IEEE Trans. on Communications*, vol. 25, pp. 803–809, 1977.

[25] T. Eng and L.B. Milstein, "Coherent DS-CDMA Performance in Nakagami Multipath Fading," *IEEE Trans. on Communications*, vol. 43, no. 2-4, pp. 1134–1143, 1995.

[26] K.I. Pedersen, *Channel Modelling and Receiver-Design for DS-CDMA Systems*, Ph.D. thesis, Aalborg University, January 2000.

[27] P. van Rooyen and M.P. Lotter, "Performance of DS-CDMA systems with Antenna Arrays in Non-uniform Propagation Environments," *IEEE Intern. Conf. on Pesonal Wireless Communication*, pp. 165–169, 1999.

[28] A.F. Naguib, A. Paulraj, and T. Kailath, "Capacity Improvement with Base Station Antenna Arrays in Cellular CDMA," *IEEE Trans. on Vehicular Technology*, vol. 43, no. 3, pp. 691–698, 1994.

[29] L.C. Godara, "Application of Antenna Arrays to Mobile Communications, Part II: Beam-forming and Angle-of-Arrival Considerations," *IEEE Proceedings*, vol. 85, no. 8, pp. 1195–1245, 1997.

[30] P. Rooyen, M. Lotter, and D. Wyk, *Space-Time Processing for CDMA Mobile Communications*, Kluwer Academic Publishers, 2001.

[31] T.D. Pham, "Statistical Behaviour and Performance of Adaptive Antennas in Multipath Environments," *IEEE Trans. on Microwave Theory and Techniques*, vol. 47, no. 6, pp. 727–731, 1999.

[32] R. Price and P.E. Green, "A Communication Technique of Multiple Channels," *IRE proceedings*, vol. 46, pp. 555–570, 1958.

[33] K.I. Pedersen and P.E. Mogensen, "Performance Comparison of Vector-Rake Receivers Using Different Combining Schemes and Antenna Topologies," *IEEE Trans. on Communications*, vol. 1, pp. 233–237, 1999.

[34] J.H. Winters, "Optimum Combining in Digital Mobile Radio with Cochannel Iinterference," *IEEE Trans. on Communications*, vol. 2, no. 4, pp. 528–539, 1984.

[35] R. Prasad, J.S. Dasilva, and B.A. Fernandez, "Air Interface Access Schemes for Wireless Communications (Part 1)," *IEEE Commun. Magazine*, vol. 37, pp. 104–138, 1999.

[36] M.P. Lotter and P. van Rooyen, "Space Division Multiple Access for Cellular CDMA," *IEEE Intern. Symp. on Spread Spectrum Techniques and Applications*, vol. 3, pp. 959–964, 1998.

[37] G.P. Efthymoglou, V.A. Aalo, and H. Helmken, "Performance Analysis of Coherent DS-CDMA Systems in a Nakagami Fading Channel with Arbitrary Parameters," *IEEE Trans. on Vehicular Technology*, vol. 46, no. 2, pp. 289–297, 1997.

[38] M.B. Pursley, "Performance Evaluation for Phase-Coded Spread-Spectrum Multiple-Access Communication-Part I: System Analysis," *IEEE Trans. on Communications*, vol. 25, no. 8, pp. 795–799, 1977.

[39] H.F.A. Roefs and M.B. Pursley, "Correlation Parameters of Random Sequences and Maximal Length Sequences for Spread-Spectrum Multiple-Access Communication," *IEEE Canadian Communications and Power Conference*, pp. 141–143, 1976.

[40] G.A.J. van Dooren, *A Deterministic Approach to the Modelling of Electromagnetic Wave Propagation in Urban Environments*, Ph.D. thesis, Eindhoven University of Technology, March 1994.

[41] M.G.J.J. Klassen and A. Mawira, "A Deterministic Model for the Planning of Microcellular Mobile Radio Communication Systems," *IEEE Int. Symp. Personal, Indoor and Mobile Radio Communications*, pp. 389–395, 1994.

[42] M.H.J.L. Koelen, *Measurements and Modelling of Transmission of Radiowaves through Buildings*, MSc thesis, Eindhoven University of Technology, 2000.

[43] J.C. Liberti and T.S. Rappaport, "A Geometrically Based Model for Line-of-Sight Multipath Radio Channels," *IEEE Proceed. on Vehicular Technology*, vol. 2, pp. 844–848, 1996.

[44] M.G. Marques, *A Wideband Directional Model for Micro-Cells in UMTS*, MSc thesis, Technical University of Lisbon, 2001.

[45] R.H. Clarke, "A Communication Technique of Multiple Channels," *Bell Labs System Technology Journal*, vol. 47, pp. 957–1000, 1968.

[46] J. Salz and J.H. Winters, "Effects of Fading Correlation on Adaptive Array in Digital Wireless Communications," *IEEE International Conference on Communications*, vol. 3, pp. 1768–1774, 1993.

[47] J.S. Bendat and A.G. Piersol, *Random Data: Analysis and Measurement Procedures*, Wiley-Interscience, 1971.

[48] M. Cheol, M. Choi, and H. Park, "Performance of 2-D Rake Receiver in a Correlated Frequency Selective Nakagami Fading," *IEEE Trans. on Vehicular Technology*, vol. 50, no. 5, pp. 1312–1317, 2001.

[49] J.S. Hammerschmidt, *Adaptive Space and Space-Time Signal Processing for High-Rate Mobile Data Receivers*, Ph.D. thesis, TUM/LIS, June 2000.

[50] P. Sprent, *Applied Nonparametric Statistical Methods*, Chapman and Hall, 1993.

[51] M. Jevrosimović, D. Matić, L. Jorgušeski, M.H.A.J. Herben, and G. Brussaard, "Analysis of SINR for UMTS Rake Receiver Smart Antenna Processing Using two Modelling Approaches," *IEEE Proceed. on Vehicular Technology*, vol. 1, pp. 60–64, 2003.

[52] A. Shah and A.M. Haimovich, "Performance Analysis of Maximal Ratio Combining and Comparison with Optimum Combining for Mobile Radio Communications with Cochannel Interference," *IEEE Proceed. on Vehicular Technology*, vol. 49, no. 4, pp. 1454 – 1463, 2000.

[53] S.A. Grandhi, R. Vijayan, D.J. Goodman, and J. Zander, "Centralized Power Control in Cellular Radio Systems," *IEEE Trans. on Vehicular Technology*, vol. 42, no. 4, pp. 466–468, 1993.

[54] C.D. Mayer, *Matrix analysis and applied linear algebra*, Society for Industrial and Applied Math, 2000.

[55] G.J. Foschini and Z. Miljanić, "A Simple Distributed Autonomous Power Control Algorithm and its Convergence," *IEEE Trans. on Vehicular Technology*, vol. 42, no. 4, pp. 641–646, 1993.

[56] F. Rashid-Farrokhi, L. Tassiulas, and K.J. Ray Liu, "Joint Optimal Power Control and Beamforming in Wireless Networks Using Antenna Arrays," *IEEE Trans. on Vehicular Technology*, vol. 46, no. 10, pp. 1313–1323, 1998.

[57] M. Jevrosimović, E.R. Fledderus, L. Jorgušeski, M.H.A.J. Herben, and G. Brussaard, "Power Control with Antenna Array Processing for UMTS," *IEEE Proceed. on Vehicular Technology*, vol. 1, pp. 181–185, 2004.

[58] Y.L.C. de Jong and M.H.A.J. Herben, "Prediction of Local Mean Power Using 2-D ray-tracing-based Propagation Models," *IEEE Trans. on Vehicular Technology*, vol. 50, no. 1, pp. 325–331, 2001.

[59] W.C. Jakes, *Microwave Mobile Communications*, Wiley, 1974.

[60] G.H. Bryant, R.J.C. Bultitude, and M.J. Neve, "A Spatial Field Model for Mobile Radio," *Proceed. URSI Symposium on Wave Propagation and Remote Sensing*, pp. 220–223, 1998.

[61] C.Y.W. Lee, "The Proper Statistical Nature of Measuring and Estimating," *IEEE Trans. on Communications*, vol. 1, pp. 753–756, 1999.

Acknowledgments

I would like to thank everyone who contributed to the completion of this thesis. To begin with, I express deepest gratitude to people in the Radiocommunication group for creating a pleasant environment where mutual help and understanding were inevitable parts of everyday university life.

I thank my daily supervisor Matti Herben, who guided my work from the very beginning and was always there for discussions and advise whenever necessary. He took care that things run smoothly even at the most difficult times. His natural optimism was the main driving force.

I am grateful to my two promoters Erik Fledderus and Gert Brussaard, who helped giving this thesis a proper form, always ready to introduce interesting ideas. Erik particularly devoted a significant amount of time for meticulous proof-reading of the complete work collected in the thesis, including my other papers and reports. Gert would always highlight the good sides of my work, which kept me believe that I was on a good track.

I am indebted to Yvo de Jong, who not only created the ray-tracing tool I extensively used for my research, but who also gave me good starting guidelines.

I express my gratitude to TNO Information and Communication Technology (ICT), former KPN research, for sponsoring my work within the B4 project. Special thanks go to Dusan Matic and Ljupco Jorguseski from TNO ICT for providing practical perspectives on the cell planning and UMTS system operating issues. I particularly enjoyed exchanging some informal words in my mother language after meetings. I am grateful to Bi Mawira for keeping his interest in my work and for taking part in useful discussions on a regular basis.

I thank Ewart Martijn for giving a lot of technical assistance, which made it possible for me to spend maximum time on the research. He also took part in regular brainstorming on various subjects, which proved very useful in defining my research path. I would also like to thank the students I supervised, Luciano Colin and Rodrigo Mendes, for contribution to this thesis via their intership projects.

I am thankful to Tim Schenk, who provided invaluable help in many different aspects: exchanging ideas and providing knowledge as a peer colleague working on a related research subject, but also helping out with numerous Latex problems. He kept me up to date with a wide range of issues impor-

tant for the research, often on his own initiative for which I am particularly grateful.

I would like to thank Luis Correia from the Technical University of Lisbon, Portugal, for his warm hospitality, for devoting his time to discussions and reading of my thesis and particularly for letting me use the stochastic channel model developed in his group. I thank João Gill, Filipe Cardoso and Lucio Ferreira for giving instructions on the proper use of the model, which brought results that formed the basis of this thesis. I am also very grateful to people from Center for PersonKommunikation at the Technical University of Aalborg, Denmark, namely Ramjee Prasad for organising my visit and Lars Berger, Troels Sorensen, Wim Kotterman, Istvan Kovacs and Patrick Eggers for useful discussions on system and propagation subjects.

Special thanks to Klaus Pedersen and Jochen Hammerschmidt for providing a good insight and advise on the key issues of my research work: modelling aspects of UMTS and antenna array processing principles. I thank all members of my PhD committee for the proof-reading of my thesis and for their comments which improved its quality.

I am grateful to Susan de Leeuw, Els Gerritsen, Yvonne van Bokhoven and Pleun Bazen, for their patience in assisting me with all administrative requirements, that were quite abundant for me as a foreign PhD researcher.

I am very grateful to my other colleagues, just to name a few, Robert van Poppel, Iwan Akkermans, Haibing Yang, Maurice Kwakkernaat, Peter Smulders and Jaap Swijghuisen for their assistance in many little things on a daily basis and for their laughs and jokes during coffee breaks. I also thank all colleagues who participated in the B4 project for helping me place the work into a broader picture by exchanging experience and relating it to other systems and application areas. I am thankful to all of my friends for sharing the good and bad times with me.

Finally, I will always be grateful to my parents for giving me proper upbringing and support to tackle problems as an independent individual, which was essential for the successful completion of my thesis. I dedicate this thesis to them.

Samenvatting

In dit proefschrift wordt het effect gepresenteerd van realistische radiogolf-voortplanting in een stedelijke microcel omgeving op de prestatie van smart antennes voor het UMTS systeem. De belangrijkste zaken die aan de orde komen zijn de eisen die gesteld worden aan de kanaalmodellering voor de prestatieanalyse van smart antennes en de identificatie van de meest dominante systeem- en propagatiefactoren voor deze analyse.

Er wordt een nieuw resultaat gepresenteerd betreffende het verschil tussen deterministische en stochastische propagatiemodellering voor de voorspelling van de prestatie van smart antennes. Aangetoond wordt dat in stochastische modellen de correlatie tussen de gebruikers in de antennestelselruimte niet juist wordt verdisconteerd, wat een belangrijke invloed kan hebben op de nauwkeurigheid van de resultaten, in het bijzonder voor de UMTS-uplink.

Een nieuwe modeleringsmethode wordt voorgesteld die gebruik maakt van vereenvoudigde aspecten van het UMTS systeem op basis van deterministische propagatiedata. Het voordeel van het gebruik van een smart antenne in een UMTS systeem met power control, met betrekking tot het aantal gebruikers dat bediend kan worden en de optimale zendvermogens, wordt geanalyseerd. Een nieuwe analyse wordt gepresenteerd voor het bepalen van de propagatiefactoren in een microcel omgeving die de belangrijkste beperkingen opleggen aan de systeemprestatie voor twee representatieve methodes van antenneprocessing: optimum combining en maximum ratio combining.

De belangrijkste voordelen van het gebruik van optimum combining ten opzichte van maximum ratio combining zijn het grotere aantal gebruikers dat bediend kan worden in het UMTS systeem en de betere dekking. Er kan ook een aanzienlijke reductie van het zendvermogen bereikt worden, maar dat is sterk afhankelijk van het type lokale verstrooiers nabij het basisstation in een bepaalde omgeving. Snelle signaaldemping blijkt kritisch te zijn voor lage tot gematigde snelheden van de gebruiker bij de UMTS frequentie van 2 GHz, waar de hoekspreiding aan de kant van het mobiele station de meest invloedrijke propagatieparameter is die gerelateerd is aan dit systeemaspect. Voor gematigde hoekspreidingen manifesteren de snelle dempingseffecten zich als een aanzienlijke toename van het optimale zendvermogensniveau met toenemende snelheid van de mobiele terminal en een duidelijker verschil tussen de twee antenneprocessing procedures in de mogelijkheid tot het volgen van de

kanaalveranderingen.

Ten slotte wordt er een nieuwe methode gepresenteerd om de hoeveelheid benodigde deterministische data te minimaliseren. De kern van de methode bestaat uit de berekening van de kanaalcompositie voor het centrum van een pixel met het deterministische model en het karakteriseren van het kanaal voor ieder punt binnen de pixel op basis van die informatie. De hoofdgedachte is om de rekenlast voor trajectberekeningen te reduceren door de afmeting van de pixel te vergroten. Het probleem van het vinden van de optimale pixelgrootte met een voldoende grote nauwkeurigheid wordt vanuit systeemoogpunt behandeld. De belangrijkste beperkingen van de voorgestelde methode met betrekking tot de ruimtelijke veranderingen in de propagatiecondities worden geanalyseerd. Het verkregen resultaat voor de pixelgrootte toont aan dat het mogelijk is om de rekentijd die nodig is voor deterministische modellering aanzienlijk te verkleinen.

Curriculum Vitae

Marija Jevrosimović was born on June 11, 1975 in Belgrade, Serbia and Montenegro. She received the Dipl.Ing. degree in electrical engineering, department of telecommunications, electronics and control (major: telecommunications) from the Faculty of Electrical Engineering, University of Belgrade in 1999. After graduation she worked on electrical installations design projects at the Institute of Transportations in Belgrade, department of telecommunications, until 2001.

From 2001 to 2005, she worked on a PhD project in the Radiocommunications group at the Faculty of Electrical Engineering at the Eindhoven University of Technology, The Netherlands, under the supervision of dr.ir. M.H.A.J.Herben, prof.dr.ir. G. Brussaard and prof.dr.ir. E.R. Fledderus. The research work from this period was conducted as part of the Radio@Hand project within the BraBantBreedBand (B4) programme and is presented in this dissertation.